



THE HONG KONG
POLYTECHNIC UNIVERSITY

香港理工大學

Pao Yue-kong Library

包玉剛圖書館

Copyright Undertaking

This thesis is protected by copyright, with all rights reserved.

By reading and using the thesis, the reader understands and agrees to the following terms:

1. The reader will abide by the rules and legal ordinances governing copyright regarding the use of the thesis.
2. The reader will use the thesis for the purpose of research or private study only and not for distribution or further reproduction or any other purpose.
3. The reader agrees to indemnify and hold the University harmless from and against any loss, damage, cost, liability or expenses arising from copyright infringement or unauthorized usage.

IMPORTANT

If you have reasons to believe that any materials in this thesis are deemed not suitable to be distributed in this form, or a copyright owner having difficulty with the material being included in our database, please contact lbsys@polyu.edu.hk providing details. The Library will look into your claim and consider taking remedial action upon receipt of the written requests.

**FACILE FABRICATION OF METAL-
ORGANIC FRAMEWORK/FIBER
COMPOSITE FOR HAZARDOUS
CHEMICAL REMOVAL**

MA KAIKAI

PhD

The Hong Kong Polytechnic University

2020

**THE HONG KONG POLYTECHNIC UNIVERSITY
INSTITUTE OF TEXTILES AND CLOTHING**

**Facile Fabrication of Metal-Organic
Framework/fiber Composite for Hazardous
Chemical Removal**

MA Kaikai

**A Thesis Submitted in Partial Fulfillment of the Requirements
for the Degree of Doctor of Philosophy
February 2020**

CERTIFICATE OF ORIGINALITY

I hereby declare that this thesis is my own work and that, to the best of my knowledge and belief, it reproduces no material previously published or written, nor material that has been accepted for the award of any other degree or diploma, except where due acknowledgement has been made in the text.

_____ (Signed)

MA Kaikai (Name of student)

Abstract

Porous metal–organic framework (MOFs) with high chemical and structural complexities are gaining great interests from academia and industry for their versatility in a multitude of areas, however their poor processability hinders their potential in practical application. Design and fabrication of MOF-based composites, with intact functionality of MOFs and good processability, has attracted widespread attention in both industrial and academic areas for its importance in boosting the practical values of MOFs. Highly accessible textile fiber with high flexibility is a promising substrate to support the functional MOF coating layer for various application such as heterogeneous catalysis, chemical sensing, pollutant removal, and drug release. Although reported MOF coating fabrication methods are encouraging, coating of MOFs on fiber surface remains challenging in many aspects, including the need for expensive coating materials and equipment, low mass loading and coverage on the fiber surface, and poor method generalizability to thermo-sensitive fiber. In this thesis, the author aims to design facile fabrication methods of MOF/fiber composites, which could combine the processability of fiber substrate and functionality of MOF coating.

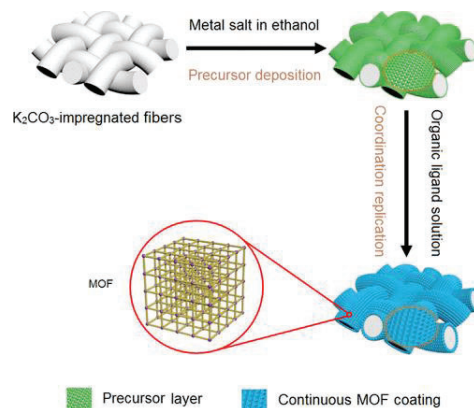
In this thesis, previously reported MOF/fiber fabrication methods and mechanisms was reviewed to understand the underlying techniques and target certain areas for further development. Following the literature review, this study demonstrated the development of three facile MOF/fiber composite synthesis methods, including coordination replication method, hydrothermal growth method, and dip-coating method, with the generalizability to different MOFs and fiber substrates. Importantly, the designed fabrication methods only need the use of common equipment widely available in materials industries, making these

methods highly desirable for their scalability. Moreover, in methods, surface chemical modification and atomic layer deposition (ALD) were not needed to improve the MOF nucleation and growth on fiber surface. The prepared flexible MOF/textile composites maintained the flexibility of fiber substrates and the functional properties of MOFs. Furthermore, these composites could be cut or tailored into different shapes, increasing their potential for mounting these materials into industrial equipment, such as adsorption devices and protective gears.

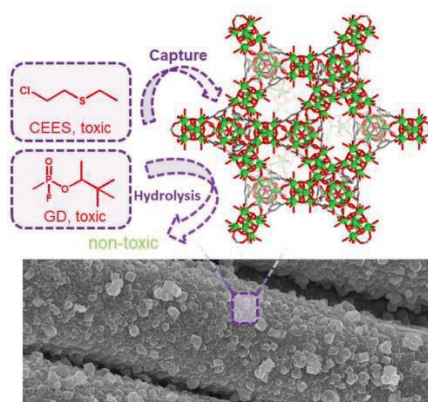
Following fabrication, the application of MOF/fiber composites in important relevant fields such as pollutant control and human protection against ultra-toxic warfare agents was explored. Firstly, the HKUST-1/cotton composite, prepared using a coordination replication method, was used as a filter for removal of organosulfur compound from simulated gasoline and toxic ammonia adsorption. The MOF coating had excellent accessibility for capture these harmful chemicals. Secondly, the Zr-MOF/polyester composite prepared via an eco-friendly aqueous synthesis approach was employed as a heterogeneous catalyst for nerve agent hydrolysis in an alkaline buffer solution. The prepared composite showed the fastest degradation efficiency against nerve agent and related simulant. Thirdly, a ternary MOF-808/polymeric buffer/cotton composite was developed using a simple dipping-coating method and showed excellent solid-phase catalytic performance in nerve agent degradation under ambient conditions, which is a significant step forward for the destruction of these harmful chemicals in practical environments. The MOF/fiber composites integrating the advantages of functionality and processability could dramatically enhance their potential industrial applications.

Publications Arising from the Thesis

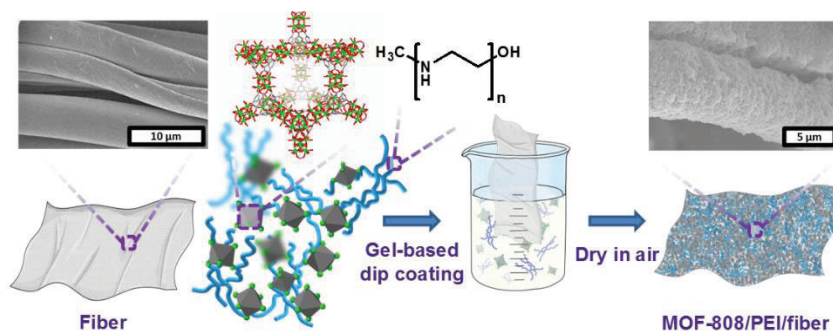
1. **Ma, K.;** Wang, Y., Chen, Z., Islamoglu, T., Lai, L., Wang, X., Fei, B., Farha, O. K., Xin, J. H. Facile and Scalable Coating of Metal–Organic Frameworks on Fibrous Substrates by a Coordination Replication Method at Room Temperature. *ACS Appl. Mater. Interfaces* **2019**, 11, 22714



2. **Ma, K.;** Islamoglu, T.; Chen, Z.; Li, P.; Wasson, M. C.; Chen, Y.; Wang, Y.; Peterson, G. W.; Xin, J. H.; Farha, O. K. Scalable and Template-Free Aqueous Synthesis of Zirconium-Based Metal–Organic Framework Coating on Textile Fiber. *J. Am. Chem. Soc.* **2019**, 141, 15626-15633.



3. Chen, Z.; **Ma, K.;** Mahle, J.J.; Wang, H.; Syed, Z.H.; Atilgan, A., Chen, Y.; Xin, J. H.; Peterson, G. W.; Islamoglu, T.; Peterson, G. W.; Farha, O. K. Integration of Metal–Organic Frameworks on Protective Layers for Destruction of Nerve Agents under Relevant Conditions. *J. Am. Chem. Soc.* **2019**, 141, 20016-20021.



4. Wang, Y.; **Ma, K.**; Xin, J. H., Stimuli-Responsive Bioinspired Materials for Controllable Liquid Manipulation: Principles, Fabrication, and Applications. *Advanced Functional Materials*, 2018, 28, 1705128.
5. Wang, Y.; Qian, B.; Lai, C.; Wang, X.; **Ma, K.**; Guo, Y.; Zhu, X.; Fei, B.; Xin, J. H*, Flexible Slippery Nanofiber Membrane to Manipulate Droplet Coalescence and Sliding, and Its Practicability in Wind-Resistant Water Collection. *ACS Applied Materials & Interfaces* 2017, 9 (29), 24428-24432.
6. Wang, Y.; Lai, C.; Wang, X.; Liu, Y.; Hu, H.; Guo, Y.; **Ma, K.**; Fei, B.; Xin, J. H., Beads-on-String Structured Nanofibers for Smart and Reversible Oil/Water Separation with Outstanding Antifouling Property. *ACS Applied Materials & Interfaces* 2016, 8 (38), 25612-25620.

List of Abbreviations

MOF	metal–organic framework
PXRD	powdered X-ray diffraction
SEM	scanning electron microscopy
BET	Brunauer-Emmett-Teller
PVDF	polyvinylidene fluoride
PET	polyester
PAN	polyacrylonitrile
PS	polystyrene
PP	polypropylene
DMF	dimethyl formamide
DMSO	dimethylsulfoxide
DI	water deionized water
HCl	hydrochloric acid
NaOH	sodium hydroxide
DBT	dibenzothiophene
BTCA	Benzene-1,3,5-tricarboxylic acid
H ₄ TBAPy	1,3,6,8-tetrakis(p-benzoic acid)pyrene
BDCA-NH ₂	2-aminoterephthalic acid
BDCA	1,4-benzenedioic acid
2-MIM	2-methylimidazole
LHS	layered hydroxide salt

CHN copper hydroxide nitrate

ZHA zinc hydroxy acetate

CHC cobalt hydroxy carbonate

CEES 2-chloroethyl ethyl sulfide

DIFP diisopropylfluorophosphate

DMMP dimethylmethylphosphonate

DMNP destroy dimethyl-4-nitrophenyl phosphate

EDX Energy-dispersive X-ray spectroscopy

FT-IR Fourier transform infrared

ALD atomic layer deposition

LbL layer-by-layer

ICP-AES inductively coupled plasma atomic emission spectroscopy

NMR nuclear magnetic resonance

UV ultraviolet

PSM Post-synthetic modification

PVP polyvinylpyrrolidone

HMDA hexamethylenediamine

PA polyamide

PU polyurethane

PEG polyethylene glycol

ESF electrospun silk nanofiber

EtOAc ethyl acetate

TGA thermogravimetric analysis

β -CD β -cyclodextrin

CTAB cetyltrimethylammonium bromide

1 D one dimensional

2 D two dimensional

3 D three dimensional

SAM self-assembled monolayers

MMM mixed matrix membrane

NO nitric oxide

PEI polyethylenimine

VX O-ethyl S-[2-(diisopropylamino)ethyl] methylphosphonothioate

DESH 2-(diisopropylamino)ethanethiol

PMPA pinacolyl methylphosphonic acid

CWA chemical warfare agent

RH relative humidity

EMPA ethyl methyl phosphonic acid

GD O-Pinacolyl methylphosphonofluoridate

Table of contents

Abstract.....	i
Publications Arising from the Thesis.....	iii
List of Abbreviations	v
Table of contents.....	viii
Acknowledgements.....	xii
Chapter 1.....	1
Introduction.....	1
1.1 Research background	1
1.2 Research objectives	5
1.3 Overall methodology.....	6
1.4 Framework of Thesis.....	7
Chapter 2.....	9
Literature Review.....	9
2.1 Synthesis methods of MOF/fiber composite.....	9
2.1.1 Doping during Electrospinning	9
2.1.2 Post-synthetic polymerization method	11
2.1.3 Covalent immobilization coating method.....	13
2.1.4 Directed supramolecular assembly.....	15
2.1.5 Direct solvothermal growth	15
2.1.6 Biomineralization inspired synthesis.....	18
2.1.7 Coordination replication from solid precursor	20
2.1.8 Atomic layer deposited metal oxide directed growth.....	23
2.1.9 Layer-by-Layer growth method.....	26
2.1.10 Solvent-free hot-pressing method.....	29

2.1.11 Inject printing method	31
2.2 Application of MOF/fiber composite.....	32
2.2.1 Particulate matters pollutant removal.....	32
2.2.2 Hazardous gases removal	34
2.2.3 Destruction of Chemical Warfare Agents	37
2.2.4 Catalytic NO Release.....	39
2.2.5 Water purification.....	40
Chapter 3.....	43
Facile and Scalable Coating of Metal–Organic Frameworks on Fibrous Substrates by a Coordination Replication Method at Room Temperature	43
3.1 Introduction	44
3.2 Experimental section.....	46
3.2.1 Materials	46
3.2.2 Characterization and Instruments.....	46
3.2.3 Predeposition of CHN on Cotton Textile	47
3.2.4 Fabrication of an HKUST-1 Coating on a Cotton Textile.....	47
3.2.5 Synthesis of powered HKUST-1 from copper hydroxide nitrate (CHN).....	48
3.2.6 Coating HKUST-1 on electrospun nanofibers and commercial polyester microfibers.....	48
3.2.7 Coating Cu-BDC on cotton textile	49
3.2.8 Coating ZIF-8 on cotton textile	49
3.2.9 Coating ZIF-67 on cotton textile	49
3.2.10 Patterning HKUST-1 on cotton textile.....	50
3.2.11 Scaled-up MOF/cotton samples fabrication	50
3.2.12 Mass loading determination based on ICP-OES	50

3.2.13 Desulfurization Test	51
3.2.14 Regeneration of the MOF/Fiber Adsorbent.....	52
3.3 Results and discussion.....	52
3.4 Conclusions	80
Chapter 4.....	81
Scalable and Template-Free Aqueous Synthesis of Zirconium-Based Metal–Organic Framework Coating on Textile Fiber.....	81
4.1 Introduction	82
4.2 Experimental section	85
4.2.1 Materials	85
4.2.2 Instrumentation	85
4.2.3 Synthesis of MOF-808 coating on fiber	86
4.2.4 Scale-up synthesis of MOF-808 coating on fiber.....	86
4.2.5 Synthesis of UiO-66-NH ₂ coating on fiber.....	87
4.2.6 Sample digestion for NMR test	87
4.2.7 Mass loading determination.....	87
4.2.8 Catalytic hydrolysis test of DMNP	88
4.2.9 Reusability and stability test.....	89
4.2.10 Catalytic hydrolysis test of GD	89
4.2.11 CEES permeation test	89
4.3 Results and discussion.....	90
4.4 Conclusion.....	112
Chapter 5.....	113
Dip-Coating Method for Fabrication of Metal-Organic Frameworks/Polymeric Buffer/Fiber Composite for Catalytic hydrolysis of Nerve Agents under Ambient Conditions.....	113

5.1 Introduction	114
5.2 Experimental section	115
5.2.1 Materials	115
5.2.2 Instrumentation.....	115
5.2.3 Synthesis of NU-1000	117
5.2.4 Synthesis of UiO-66	117
5.2.5 Synthesis of UiO-66-NH ₂	118
5.2.6 Synthesis of MOF-808 microcrystals	118
5.2.7 Synthesis of MOF-808 nanoparticles	119
5.2.8 Preparation of PEI/fiber composite as control.....	119
5.2.9 Preparation of MOF-808/fiber composite as control.....	120
5.2.10 Hydrolysis of DMNP with MOFs/PEI composite under ambient humidity.	120
5.2.11 Preparation of MOF-808/PEI/fiber composite.	120
5.2.12 Hydrolysis of DMNP with MOF-808/PEI/fiber under ambient humidity. ..	121
5.2.13 Hydrolysis of Soman (GD) with MOF-808/PEI/fiber under ambient humidity.	121
5.2.14 Stability test on MOF-808/PEI/fiber composite.....	121
5.2.15 Scaled up coating MOF-808/PEI composite layer on fiber.....	122
5.3 Results and discussions	123
5.4 Conclusion.....	140
Chapter 6.....	142
Conclusions and Suggestions for Future Work	142
6.1 Conclusions	142
6.2 Suggestions for future work	144
References.....	146

Acknowledgements

During my PhD study period, there are a lot of people supplying great support and help to my daily life and research study throughout the three years, which should be appreciated sincerely.

First of all, I would like to show my great gratitude to my chief supervisor, Prof. John H. Xin, who offered me the scholarship to support my three years' study. He always provides me insightful guidance and inspiring discussions to my research projects. I am encouraged by Prof. John H. Xin to try new unexplored research topics, and his professional advices and guidance were very helpful to solve critical problems for many times. I was supported by him for a one year visiting to Northwestern University, USA, which vastly opened my horizon in research. I would like to appreciate my co-supervisor, Dr. Bin Fei, who has supplied his useful advices in the group meeting and my confirmation report. I also would like to thank my host co-supervisor, Prof. Omar Farha, in Northwestern University for offering great resources to do my research during my visiting there. I also thank the technical assistants of Northwestern University's Atomic and Nanoscale Characterization Experimental Center (NUANCE) for their help in my sample characterization.

I am very grateful to my collaborators, Dr. Yuanfeng Wang, Dr. Chuilin Lai, Dr. Xiaowen Wang, Dr. Baitai Qian, and Dr. Yujuan Guo, who gave me lots of help in experiment operation and thesis writing. My sincere appreciation also goes to my colleagues Dr. Huawen Hu, Dr. Yang Liu, Chang Gao, Sha Li, Suju Fan, Dr. Liang He, Yanxia Han, and Eelin Ng for their help in my daily work. I also want to show my gratitude to Pengpeng Yao, Yadie Yang, Qian Wang, and Xue Luo, who offered me company and help during my PhD study. The appreciations are also sent to Ms. Megan Wasson, Dr. Xuan Zhang,

Dr. Peng Li, Dr. Zhijie Chen, and Dr. Timur Islamoglu during my visiting for the assistance in experiment design and paper writing. Sincerely thank my new friends, Yongwei Chen, Yijun Liao, Xingjie Wang, Yuanyuan Zhang, Fenfen Wang, and Karam Idress at Northwestern University, because they gave lots of supports in both life and study. Last but not least, I would like to greatly appreciate my family for their endless love, support and encouragement.

Chapter 1

Introduction

1.1 Research background

Metal–organic frameworks (MOFs), also termed as porous coordination polymers (PCPs), are a promising class of porous crystalline frameworks, built from the coordination of inorganic metal ions/nodes and organic ligands, as shown in Figure 1 for some representative MOF structures.¹⁻⁵ The chemical and morphological diversity of MOFs are highly tunable and designable for versatile functionalities. As key structural features, the ultrahigh porosity of MOFs is up to 90% free volume, and surprisingly high internal surface areas of MOFs exceed $8000 \text{ m}^2 \text{ g}^{-1}$.⁶ These tailorable porous MOFs materials have showed great attraction for the applications such as gas storage and separation,⁷⁻¹² catalysis,¹³⁻¹⁶ pollutant control,¹⁷⁻²⁰ and sensing.²¹⁻²⁴

Through general synthesis methods, MOFs are obtained as fine powdered materials. As the fragile property of the MOF powders, they could not be engineered and shaped by pelleting under pressure. Poor mechanical stability and bad processability may decrease the performance of MOFs in industrial applications. Fortunately, integrating functional MOFs with a supporting material has been developed recently to tackle the challenges in practical application.²⁵⁻²⁸ The researchers have demonstrated several impressive strategies to prepare high-performance MOF based composites with better processability. The MOF components have been successfully immobilized onto a series of substrates, such as carbon nanotube,²⁹ plastic film,³⁰ form,³¹ ceramic,³² metal,³³ and textile fiber.³⁴⁻⁵¹ In MOF based composites, the functional properties of both MOF component (chemical diversity, high porosity, and

crystallinity) and supporting substrates (flexibility, robustness, and processability) can be combined ingeniously, and therefore, improved mechanical properties and functionalities, not obtainable by powdered MOF material, may be accessible. Consequently, the integrated advantages of composites resulting from the rational combination of both MOF particles and the supporting substrates make them practical for a wide range of industrial applications.

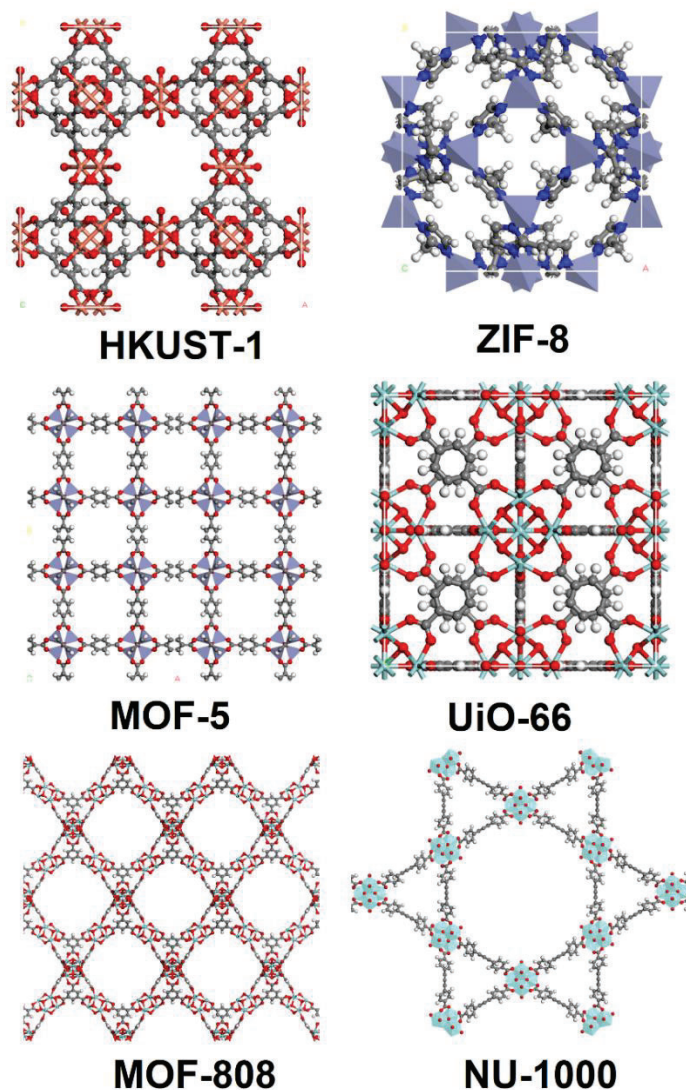


Figure 1. Representative MOFs structure: HKUST-1, ZIF-8, MOF-5, UiO-66, MOF-808, NU-1000.

Flexible textile fibers are inexpensive and easily available supporting substrates to prepare MOF based materials. Textile substrate properties can be tuned include polymer kind, thickness, permeability, porosity, and flexural rigidity. To date, MOF particles have been successfully coated onto natural fiber, such as cotton³⁴ and silk,³⁵ and synthetic commercial fiber, including nylon,³⁶⁻³⁷ polyester (PET),³⁸ polypropylene (PP),^{39,43} polyacrylonitrile (PAN),^{40,43} and polystyrene (PS),⁴¹ resulting in integrated properties and performance compared with individual component. Especially, the MOF/fiber composites offer the great advantage in flexible shape engineering, which could be easily tailored, folded, and rolled into different types for various valuable fields, for example, for the applications in liquid or air phase.

A variety of MOF/fiber composites fabrication strategies have been developed in the past two decades, and prepared MOF/fiber composites have also been explored for the applications in toxic gas adsorption,⁴⁰⁻⁴² water purification,⁴³⁻⁴⁴ catalytic degradation of warfare agent,^{36,37,46,47} and biomedical applications.⁴⁸ However, there are several limitations of previously reported approaches for production MOF/fiber composites, hindering the practical applications. For example, commonly used solvothermal synthesis methods are not friendly to fiber substrates. MOFs are typically synthesized at high temperature often exceeding 100 °C in toxic organic solvents such as DMF, DEF and DMSO. These demanding conditions challenge the integration of MOF coating layers on a range of polymeric fiber materials, and many of which possess lower stability in hot solvent. For example, polyacrylonitrile (PAN), a widely used synthetic fiber of appreciable interest for preparing MOF/fiber composites, dissolves in DMF under MOF synthesis conditions. Beside *in situ* growth coating methods, an alternative route to fabricate MOF/PAN

composite is by direct doping during electrospinning, while this method results in lower yield, it is relatively inexpensive.⁴¹

Usually, the textile fiber surfaces are chemically inert, which is adverse for MOF nucleation and growth during coating synthesis. In some reported coating methods, an ALD oxide layer or surface modification was conducted to facilitate the MOF deposition, however dramatically increased cost is not favorable for scaled-up production. Unfortunately, the most widely used solvothermal reported methods showed a very low efficiency in coating MOF on fiber, yielding 5–20 times more free MOF particles in reaction media compared with the amount that coated onto the fiber's surface.⁵² Therefore, more efficient methods are highly desired to lower the cost of production and minimize the environmental impact. Toxic solvent, including DMSO and dimethylformamide (DMF), the most common solvent used in MOF synthesis, can be trapped in the MOFs porosities during coating synthesis, leading to potential risk when the composites are used in human protection gear. Moreover, it is quite infeasible to safely synthesize bulk MOF/fiber composite using high temperatures and highly flammable organic solvents in industrial settings. The MOF/fiber composite synthesis may be more industrial operable at room temperature in eco-friendly solvent, such as water.

Besides, these prepared binary MOF/fiber composites only contain pure MOF layer and a fiber substrate, which may limit their applications in multitask fields. Polybasic composites, which introduce polymers, metal nanoparticles, bio-macromolecules into MOF/fiber composite system, may be helpful to get synergetic and enhanced functional materials. However, there is only few studies about fabrication of polybasic MOF-based composites.

1.2 Research objectives

Coating of Metal–organic frameworks (MOFs) with rich structural and chemical diversity on flexible and inexpensive fiber substrates is a critical technology in various application fields. However, the most of reported coating methods have the limitations, such as needing expensive engineering equipment, low precursor utilization, and poor feasibility to sensitive polymer fiber. The goals of the study in this thesis is to design facile and scalable fabrication method for various MOFs coating on flexible textile fiber surface, and to explore the applications of the prepared MOF/fiber composite materials. The detailed research objectives of this thesis are described as follows:

- (i) To develop a room temperature and scalable method for coating copper, zinc, and cobalt-based MOF coating on textile fiber via a coordination replication method, in which the MOF coating is transformed from a pre-deposited solid precursor layer.
- (ii) To study the growth mechanism of the solid precursor derived MOF coating and explore the resulted materials' application in liquid and gas adsorption of pollutants.
- (iii) To develop a scale and template-free aqueous synthesis method for coating zirconium-based MOFs on textile fiber.
- (iv) To explore the nucleation mechanism of the zirconium-based MOFs on fiber surface and study the MOF/fiber composite's application in catalytic degradation of nerve agent in aqueous alkaline buffer solution and adsorption capture of mustard gas simulant.
- (v) To fabricate a composited coating of zirconium MOFs and polymeric buffer using a facile and scalable gel-based dip-coating method.

- (vi) To investigate the solid-state catalytic performance of the as-prepared ternary composite material in nerve agent hydrolysis degradation hydrolysis under real-world service conditions, namely ambient conditions.

All of the research objectives are not carried out by other researchers before this study in this thesis, indicating the innovation of this research proposal. These objectives are achieved based on the study in this thesis.

1.3 Overall methodology

In this thesis, the facile and scalable fabrication methods of MOF/fiber composites and applications were investigated. Inexpensive fibrous substrates, such as cotton fiber and polyester fiber, were chosen as the fiber substrates, and physical or chemical modification on fiber surface was not necessary in all methods developed here. Three coating methods were involved, including coordination replication method, hydrothermal growth method, and dip-coating method, in this study to fabricate MOF/fiber composites. After preparation, detailed characterizations have been conducted to explore the properties of the MOF/fiber composites. The surface morphologies of the MOF coating were studied by scanning electron microscopy (SEM) and the crystallinities of the composites were tested by powdered X-ray diffraction (PXRD). Mass loadings of the MOF coating were evaluated by inductively coupled plasma atomic emission spectroscopy (ICP-AES) after digestion of the composite, and porosities of the composites were investigated using nitrogen sorption isotherms. Fourier transform infrared (FT-IR), proton nuclear magnetic resonance (^1H NMR) and energy dispersive X-ray analysis (EDX) were employed as supplementary techniques to study the distribution and surface chemical compositions of the composites. The breaking strength and elongation of the fibrous composites were tested according to a

grab test method [ASTM D5034—09(2017)]. Ammonia sorption experiments on HKUST-1/cotton composites were performed on a 3Flex (Micromeritics) multiport surface characterization instrument. The desulfurization performance of the HKUST-1/cotton composites were analyzed by measuring the remaining dibenzothiophene in simulated gasoline (*n*-heptane) by UV–visible spectroscopy. The mechanical stabilities of MOF coating on fiber substrates were evaluated by SEM observation and ICP-AES test after stirring for 24 h. The Zr-MOFs/fiber composites were used in the catalytic hydrolysis of nerve agent GD (O-Pinacolyl methylphosphonofluoridate) and low toxic simulant, and the conversion and selection of reaction were monitored by ³¹P NMR spectroscopy. In order to demonstrate the barrier properties of porous Zr-MOF/fiber composites, the permeation rates were measured using a mustard gas simulant as the analyte in accordance with ASTM F739-12.

1.4 Framework of Thesis

The thesis contains six chapters.

Chapter 1 introduces the background, research objectives, overall methodologies, and frameworks of this study.

Chapter 2 reviews the typical works for coating MOF on surface, especially on textile fiber surface. The fabrication methods and related applications were summarized.

Chapter 3 focuses on the fabrication, characterization, and growth mechanism study of a room temperature synthesized MOF coating on textile fiber using pre-deposited solid precursor, followed by the applications in continuous removal of the organosulfur compound from simulated gasoline and ammonia capture.

Chapter 4 presents the fabrication, characterization, and growth mechanism study of an aqueous synthesized zirconium MOF coating on fiber surface. Generality and scalability of the method was studied. The MOF coating's application in catalytic degradation of nerve agent and adsorption capture of a mustard gas simulant was also explored.

Chapter 5 concentrates on the development of a facile and scalable gel-based dip-coating method for MOF/polyethyleneimine coating on textile fiber. The material's application in catalytic hydrolysis of nerve agent under ambient conditions was studied. The catalytic activities under various surrounding challenges, such as sweat, atmospheric CO₂, and heavy contaminants (i.e. octane) from vehicles, were also investigated.

Chapter 6 draws a conclusion based on this thesis and gives several suggestions and research directions for future work.

Chapter 2

Literature Review

2.1 Synthesis methods of MOF/fiber composite

2.1.1 Doping during Electrospinning

As a facile and direct method, electrospinning approach was used to fabricate MOF/fiber composites by spinning the blending suspension of the MOF nanoparticles and polymers under a high voltage.^{41,46,47,55} The method is adaptable to the polymer substrates which are dissolved in polar organic solvents, such as dimethylformamide (DMF). Many types of polymers, including polyacrylonitrile (PAN),^{41,53} polystyrene (PS),⁴¹ polyvinylpyrrolidone (PVP),^{41,53} and polyvinylidene difluoride (PVDF),⁴⁷ have been utilized as the substrates in electrospinning method for fabrication MOF/nanofiber composite. Wang's group showed the generalizability of this fabrication strategy to different polymer substrates, including PAN, PS and PVP, and the various MOFs nanoparticles (as shown in Figure 2.1).⁴¹ Very high MOF mass loading (up to 60 wt %) and excellent MOF particles dispersion behaviour in composite were achieved by this method. Encouragingly, the porosity and the surface area of MOF nanoparticle were intact after doping in the fibrous composite. The composites were highly flexible, however lacked structural strength. To improve the practicality, other supporting substrates, such as metal mesh or nonwoven fabric, were used to enhance the structural robustness of the MOF/nanofiber composite. However, electrospinning is a low yield technology, which may hinder its practical application for its high cost and poor scalability. Also, the prepared MOF/fiber composites usually could not

be used in polar solvent in applications, such as heterogeneous catalyst, because of the solubility of the polymer substrates.

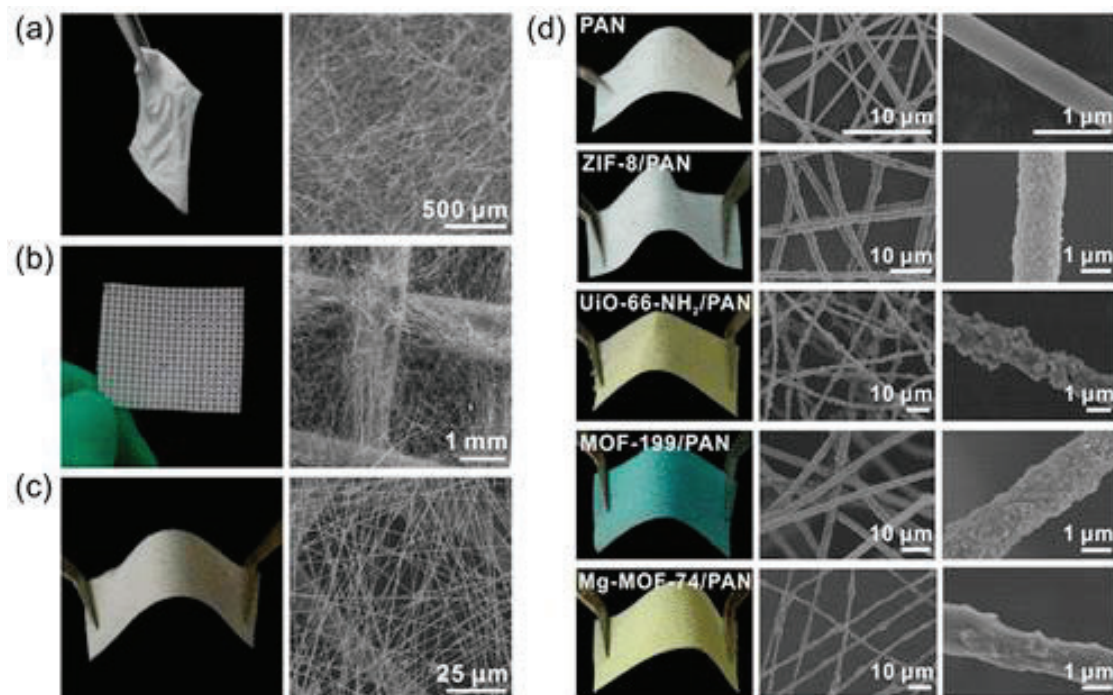


Figure 2.1 Photograph and SEM images of (a) free-standing ZIF-8/PAN nanofiber composite, (b) ZIF-8/PAN nanofiber composite supported on a metal mesh and (c) nonwoven textile. (d) Photographs and SEM images of MOF/PAN nanofiber composites supported on a nonwoven fabric piece.⁴¹

As a rarely used method for doping nanofiber during electrospinning, López-Maya et al. developed a process strategy to introduce MOF nanoparticles onto silk nanofiber substrates by spray drying.⁴⁶ UiO-66 suspension was atomized and sprayed over the silk nanofiber substrate during the electrospinning process. The MOF nanoparticles were captured in the void of silk nanofiber substrate to form a UiO-66/nanofiber composite material. Though this method could also achieve high MOF mass loading (above 60%) in the composite, the

MOF nanoparticles may be not so stable, because of its weak interaction with fiber surface. The leaching of the functional MOF nanoparticle may reduce the validity of the material in real industrial applications.

2.1.2 Post-synthetic polymerization method

The physical doping of polymeric fiber by functional MOFs brings great possibility to practical application, while the covalent combination of MOFs and polymer substrates is still challenging. Cohen's group reported a simple, scalable, post-synthetic polymerization (PSP) method to fabricate covalently combined MOF/nylon composite as shown in Figure 2.2a.³⁷ Post-synthetic modification (PSM) of UiO-66-NH₂ was conducted firstly through the reaction with adipoyl chloride to introduce reactive acyl chloride groups on the ligands of MOF. The functionalized UiO-66-int (int=intermediate) and ten equivalents of adipoyl chloride in ethyl acetate (EtOAc) were carefully poured on top of a water solution of hexamethylenediamine (HMDA). Copolymerization only occurred at the interface of the two phases, during which UiO-66-int component was covalently bonded into PA-66 polymer chain, and the resulted PA-66-UiO-66-NH₂ hybrid could be engineered into flexible fiber by a simple stretching (Figure 2.2b). The introduction of the UiO-66-NH₂ MOF particles in the composite fiber was verified by powder X-ray diffraction (PXRD) and scanning electron microscopy (SEM) (Figure 2.2c). The reaction of the modified UiO-66-NH₂ MOF component with the precursors of nylon polymer during the interfacial polymerization gave a composite material with a mass loading about 29%. The covalently combined UiO-66-NH₂/PA-66 fiber composite showed nearly an order of magnitude improvement in the catalytic performance for the hydrolysis of a nerve agent simulant (dimethyl-4-nitrophenyl phosphate, DMNP) compared to MOFs these physically

embedded in nylon substrates. While there several demerits for this method, for example, the diameter of prepared fiber was too large, making it different to be weaved or knitted for further application. Some MOF particles were entrapped in the inner space in the fiber, which may reduce their functionality.

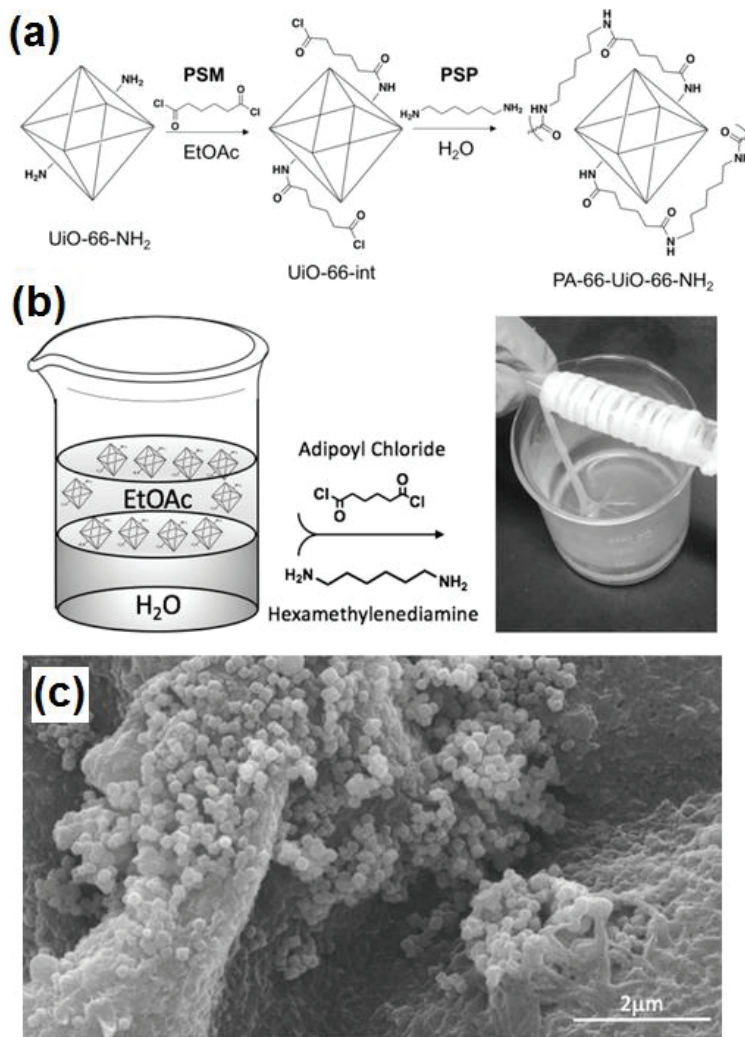


Figure 2.2. (a) Reaction route of the postsynthetic polymerization for introducing UiO-66-NH₂ into PA-66 polymer (b) Illustration of interfacial fabrication method for UiO-66-NH₂/PA-66 fiber composite. (c) SEM image of UiO-66-NH₂/PA-66 fiber composite.³⁷

2.1.3 Covalent immobilization coating method

Direct coating of MOF on commercial fiber substrates could be more attractive for large-scale applications because of the poor processability of the MOF/fiber composites prepared from electrospinning or copolymerization. Li et al. reported an eco-friendly coating method for the covalent immobilization of MIL-101(Cr) on nylon fiber by γ -ray initiated co-graft polymerization with 2-hydroxyethyl acrylate (Figure 2.3a).⁴⁹ Briefly, a mixture of 2-hydroxyethyl acrylate monomer and MIL-101(Cr) nanoparticles in ethanol was casted onto the nylon fabric, which was then irradiated by a ^{60}Co γ -ray source at room temperature to initiate the copolymerization. Free radicals were generated on nylon and MOF surface under γ -ray irradiation, which promote the graft polymerization with 2-hydroxyethyl acrylate to form a network for covalently tethering MIL-101 nanoparticles on fiber surface. SEM showed the presence of MOF particle on nylon fiber surface after the γ -ray radiation induced co-graft polymerization, and X-ray diffraction (XRD) demonstrated that the crystalline structure of the MIL-101(Cr) particles was intact. The MOF coating layer was proved as an efficient aroma carrier for the textile, which could supply sustained release of aroma. Together with the added the function from MOF coating, the textile was colored as green (Figure 2.3b), which may reduce the severe pollution from the conventional dyeing processes. The MIL-101(Cr)/nylon composite exhibited excellent dry laundering durability. No obvious fading was noticeable, and MIL-101 coating was retained on fiber surface as confirmed by SEM and TGA (thermogravimetric analysis) even after 30 h dry laundering (Figure 2.3c-d).

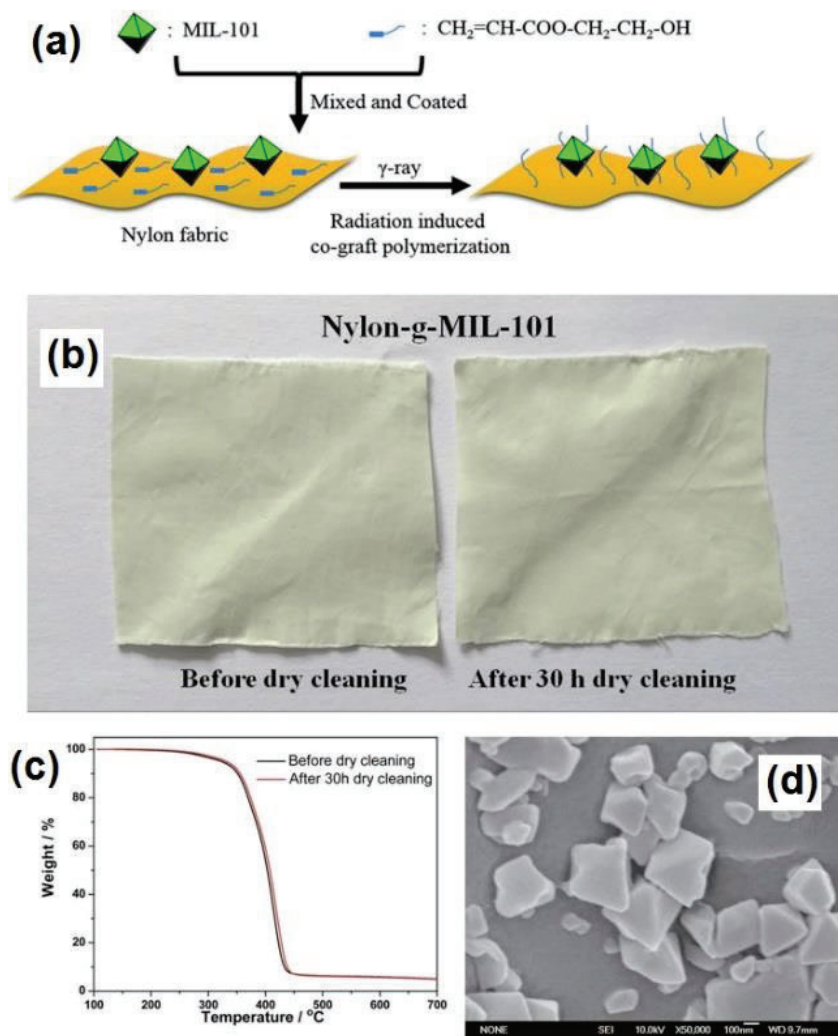


Figure 2.3. (a) Illustration of the fabrication of MOF/fiber composite by γ -ray initiated graft polymerization. (b) Photograph Images of MIL-101/nylon composite before and after 30 h dry washing. (c) TGA curves of MIL-101/nylon composite before and after 30 h dry washing. (d) SEM image of MIL-101/nylon composite after 30 h dry washing.⁴⁹

2.1.4 Directed supramolecular assembly

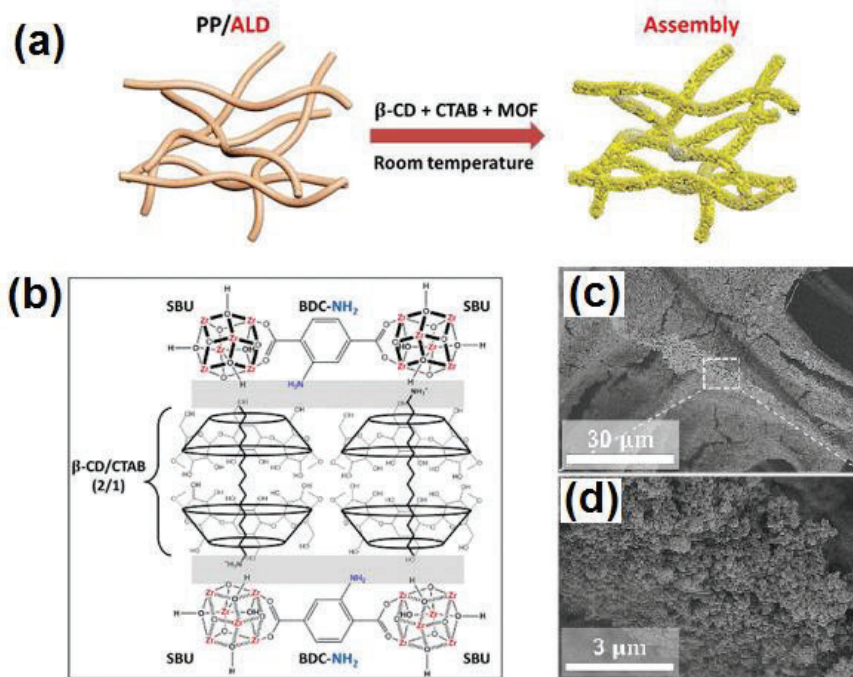


Figure 2.4. (a) Illustration of the supramolecular directed assembly strategy for UiO-66-NH₂/PP composite fabrication. (b) Schematic of expected interactions between MOF and the supramolecular complex (β -CD + CTAB). (c-d) SEM images of UiO-66-NH₂/PP composite by supramolecular directed assembly.⁵⁰

Lee et al. reported a facile assemble route to coat pre-synthesized UiO-66-NH₂ nanocrystals onto nonwoven polypropylene (PP) textile (Figure 2.4a).⁵⁰ The assembly is chemically directed by β -cyclodextrin (β -CD) and cetyltrimethylammonium bromide (CTAB) as surfactant assembly agents, which could rapidly self-assemble on the MOF nanocrystal surface to promote the MOF nanocrystals adhesion onto fiber surface, while simultaneously avoiding the nanocrystals agglomeration during the assembly (Figure 2.5b-d). Moreover, they found that metal oxide thin layers, including Al₂O₃, TiO₂, and ZnO, by

atomic layer deposition (ALD) supplied a hydrophilic surface further improved assembly uniformity and MOF coverage, resulting a UiO-66-NH₂ mass loading as high as 40 wt % and a BET surface area above 200 m²/g. The adhesion stability of the assembled UiO-66-NH₂ nanocrystals on the textile surface was evaluated by vigorous stirring at 500 rpm for one day. Mass loading measurement showed that less than 0.1% coating was lost, indicating very strong bonding between MOF nanocrystals and fiber surface. A brushing test on the UiO-66-NH₂/PP composite was also conducted for further investigation of the mechanical stability of the coating. After 30 manual brushing cycles, no MOF particles stained on the brush, and the original yellow color of the composite was intact, indicating strong adhesion of the MOF coating on fiber surface against brushing force.

2.1.5 Direct solvothermal growth

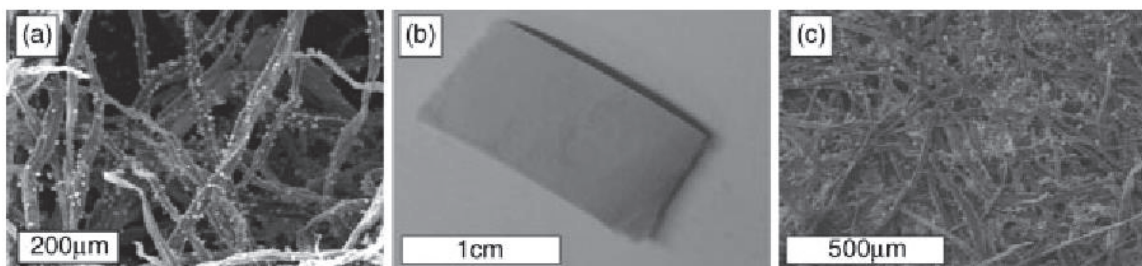


Figure 2.5. (a) SEM image of HKUST-1 coated pulp fibers, (b) photograph image of HKUST-1 coated paper sheet, and (c) SEM image of the HKUST-1 coated paper sheet.⁵¹

Küsgens et al. were among the first research groups trying to coat MOF on fiber substrate. Several kraft pulp fibers and paper sheet were chosen the substrate for HKUST-1 growth using a direct solvothermal synthesis method.⁵¹ The fibers were directly added in precursors solution for HKUST-1 growth under heating, and rare MOF particles were obtained on fiber surface (Figure 2.5). They found that the pulp fibers with higher lignin

content achieved a higher HKUST-1 loading, because the presence of carboxylic groups on lignin, while, these carboxylic groups were limited to induce dense MOF coating formation (Figure 2.5). As a result, the HKUST-1 mass loading and the coverage of coating on the pulp fiber surface were both low. Through SEM observation, the HKUST-1 particles were loosely bonded on fiber surface, implying the poor stability of coating. In the direct solvothermal synthesis, most of the MOF nucleation occurs in solvent, resulting serious waste of reactants. The MOF mass loading on the composite from direct solvothermal usually very low, limiting the capacity in practical application.

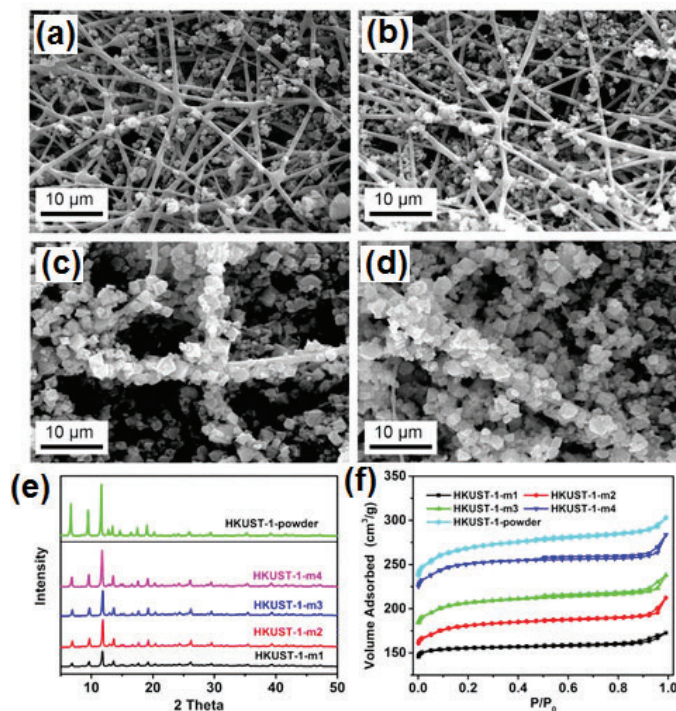


Figure 2.6. SEM images of (a) HKUST-1 coated nanofiber after 1 (a), 2 (b), 3(c) and 4 (d) synthesis cycles; (e) PXRD patterns and (f) N₂ sorption isotherms of HKUST-1/nanofiber composites after different growth cycles.⁵⁴

Wu and Morlay etc. reported the coating of four kinds of MOFs on electrospun nanofiber substrates using direct solvothermal synthesis methods by adding fibrous substrates into precursor solution.⁵⁴ A ternary nanofiber composite composed of polyacrylic acid, polyvinyl alcohol and SiO₂ was prepared by electrospinning method and used as the substrate for MOF growth. HKUST-1 and MIL-53(Al) were coated onto fiber substrates via a common solvothermal coating method, while ZIF-8 and MIL-88B(Fe) were deposited via microwave-assisted solvothermal synthesis. The obtained coating after one cycle solvothermal synthesis was tenuous, despite having many functional groups (-OH and -COOH) on fiber surface. To improve the mass loading, the solvothermal synthesis procedure was repeated for extra one to three cycles. For example, composite samples termed as HKUST-1-m1, HKUST-1-m2, HKUST-1-m3, and HKUST-1-m4 were prepared after 1 to 4 synthesis cycles as shown in Figure 2.6. The intensity of PXRD patterns belonging to HKUST-1 increased with the repetition of the growth cycles due to more MOF crystals were coated onto fiber surface, consisting well with the SEM observation. The N₂ sorption isotherms revealed that porosities on the composites were improved correspondingly.

2.1.6 Biomineralization inspired synthesis

Biomineralization is the process in biochemistry to generate biomineral shells and skeleton tissues, in which biomolecules not only accelerate the mineralization process of the inorganic materials, but also supply an anchoring surface for the biomineral to form robust biomolecules-mineral composites. Inspired by biomineralization, Yang and Fu et al. proposed the preparation of MOF/fiber composite employing electrospun silk nanofiber (ESF) mate as biomacromolecules substrate.⁴⁴ Two zeolitic imidazole frameworks (ZIF-8 and ZIF-67) were

chosen for coating. The silk nanofiber substrates were immersed in precursors mixture and incubated in mild condition at 38 °C for ZIF-8 coating and 80 °C for ZIF-67 for 1 h. In both cases, silk nanofiber composite presented surface densely covered crystalline coating (Figure 2.7a-c), which were proven to be ZIFs by PXRD verification. The SEM image of sectional views demonstrated a core-shell structure. Interestingly, a clear intergrown morphology was observed on the MOF coating, which implied the better stability and higher of the coating. They also chose two synthetic polymer nanofiber substrates, polyacrylonitrile (PAN) and polyurethane (PU), for comparison in the deposition of MOF layer. However, resulted coating presented a loose coating structure on the fibers with poor uniformity (Figure 2.7d-g), which implied the importance of the chemical structure of silk bio-substrates for inducing MOF nucleation and growth.

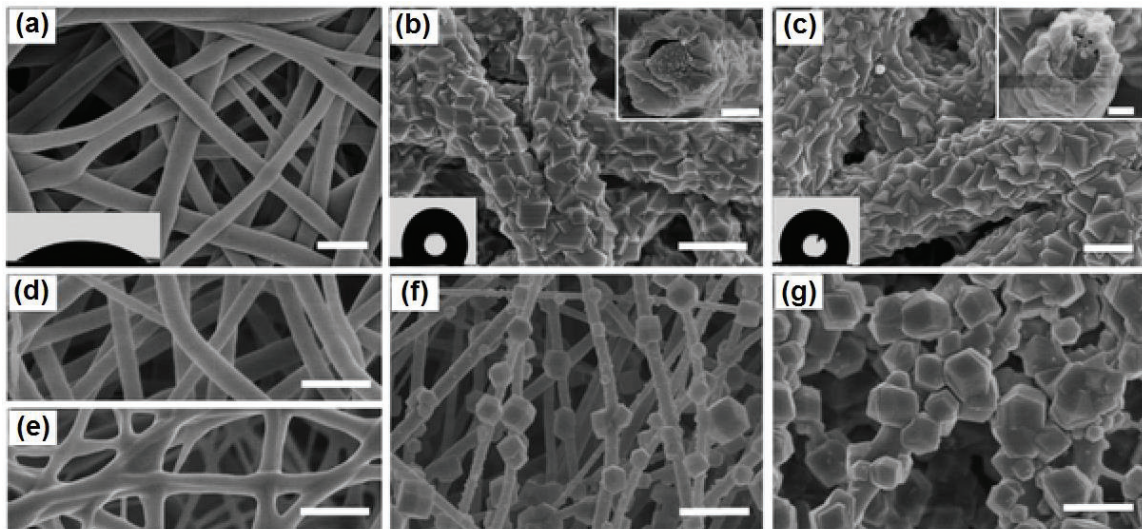


Figure 2.7. SEM images of ESF (a) ZIF-8/ESF with the sectional section view the top inset , (b) ZIF-67/ESF with the sectional section view in the top inset, (c) PAN nanofiber, (d) PU nanofiber, (e) ZIF-8/PAN, (f) and (g) ZIF-8/PU composite.⁴⁴

2.1.7 Coordination replication from solid precursor

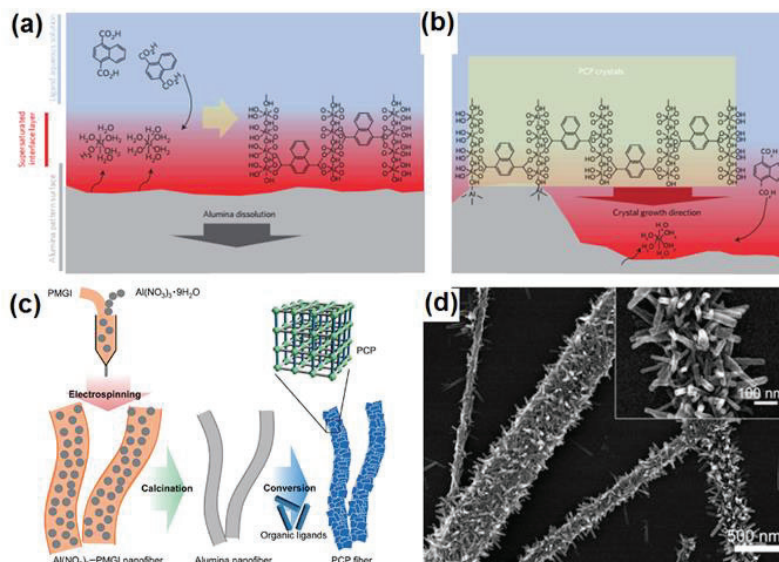


Figure 2.8 (a-b) Schematic illustration of the coordination replication mechanism proposed by Kitagawa’s group. (c) Fabrication of aluminum MOF nanofiber by coordination replication from alumina nanofiber precursor. (d) SEM image of [Al(OH)(bdc)]_n/alumina nanofiber composite by coordination replication of solid precursor.^{55,56}

Coordination replication from solid ligands precursor was also used for MOF/fiber composite. An advantage of the method is to use cheap insoluble precursor directly. Inspiring works in this field were firstly proposed by Kitagawa’s group as shown in Figure 2.8ab.⁵⁵ The authors found a versatile synthetic strategy for the morphologic replacement of a shaped sacrificial metal oxide (Al₂O₃), acting as both a metal ion source and an “architecture-directing agent”, by a well-structured MOF architecture. Al-MOF based 1D nanofiber, as well as the 2D pattern and 3D mesoscopic architecture, were obtained by using this pseudomorphic replication approach.^{55,56} Fabrication of precursor template was a critical

step for this method, a facile solution-processed method was used to prepare alumina nanofiber as a solid precursor for 1-D Al-MOF nanofiber synthesis,⁵⁶ while polymeric beads templated method was employed to prepare the ordered 2D and 3D precursor structures.⁵⁵ This team proposed a coupled ‘dissolution–reprecipitation’ mechanism for the explanation of liquid–solid interfacial reaction. The dissolved precursor forms an interface layer filled with aluminum ions. A fast coordination reaction between dissolved cations and ligands generates MOF happens on substrate surface. As the consumption of metal ion, the interface layer is recharged with freshly released metal ions, which feed the MOF crystal growth, together with the pre-dissolved organic ligand (Figure 2.8a). Contrasting to the slow kinetics of oxide dissolution, fast MOF crystallization kinetics result in a localized supersaturated metal ion layer only at the interface between the substrate surface and the ligand solution (Figure 2.8b). Hence MOF crystals are precisely positioned at the solid/liquid interface that enables the formation of continuous MOF film when sufficient precursors are supplied. Based on this mechanism, aluminum MOF, including $[\text{Al}(\text{OH})(\text{bdc})]_n$ or $[\text{Al}(\text{OH})(\text{ndc})]_n$, was deposited onto alumina nanofiber. As shown in Figure 2.8c, the $\text{Al}(\text{NO}_3)_3$ was introduced into poly(methylglutarimide) (PMGI) nanofiber by electrospinning, which was calcined to get self-standing alumina nanofiber. The obtained alumina nanofiber substrate was then heated at 180 °C for 1 min under microwave irradiation in a water solution of H_2ndc or H_2bdc to generate the corresponding Al-MOF with a conversion around 10% (Figure 2.8d).⁵⁶ The overall composite was fragile and poorly processable because the MOF layer was supported on unreacted alumina nanofiber substrates, hindering its further application.

Majano et al. found that solvent insoluble precursor, $\text{Cu}(\text{OH})_2$, can be rapidly transformed into HKUST-1 at room temperature (rt) through reaction with BTCA ligand ethanol solution.⁵⁷ The self-sourced coordination replication strategy was developed subsequently to converse copper hydroxide into HKUST-1 coating and pattern on copper mesh, wire and grid.⁵⁸ However, undesired impurity, such as CuO , was introduced into the MOF coating, because of the unstable $\text{Cu}(\text{OH})_2$ precursor. To extend the application fields, facile coating of MOF on non-copper based flexible polymeric fiber surface is highly desired.

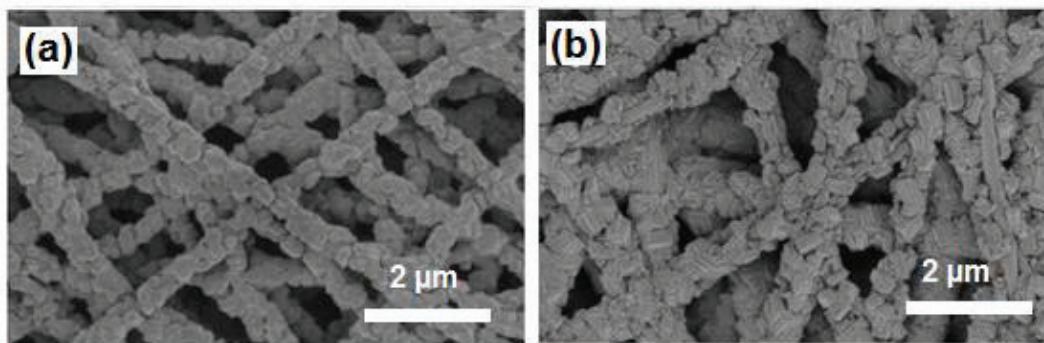


Figure 2.9 ZIF-8/PAN and MIL-53-NH₂(Al) nanofiber composite through the conversion from ALD metal oxide thin films.⁴⁰

Precoating of the solid precursor layer is the critical step for this strategy, Bechelany et al. reported the synthesis of ZIF-8 and MIL-53-NH₂(Al) coating on PAN nanofibers through conversion from ALD deposited zinc oxide or alumina as shown in Figure 2.9.⁴⁰ The conversions were triggered by microwave-assisted heating at 100 °C in 2-methylimidazole and 2-aminoterephthalic acid solution, respectively. This group also found that a conventional heating produced a coating with poor uniformity and coverage, which further indicated the importance role of microwave-assisted heating in fast coordination replication conversion.

2.1.8 Atomic layer deposited metal oxide directed growth

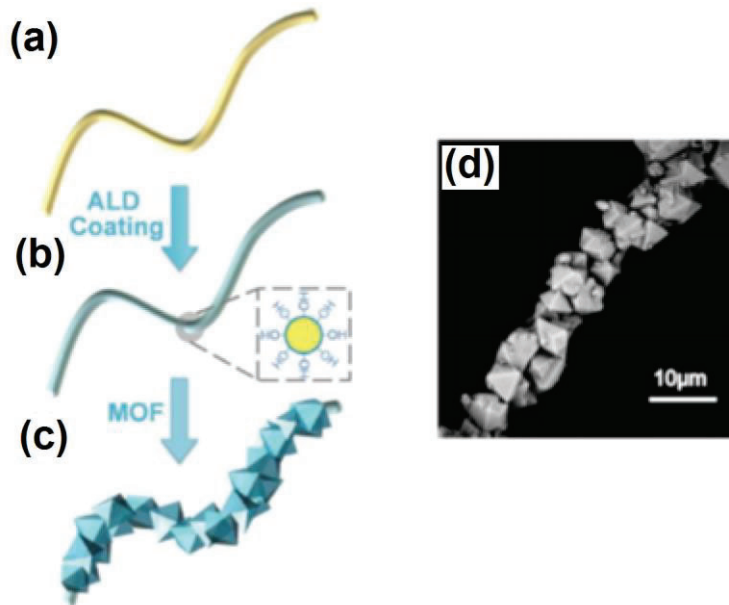


Figure 2.10 (a-c) Illustration of ALD metal oxide directed thermal growth of MOF coating on fiber surface. (d) SEM image of HKUST-1 coating on ALD alumina deposited PP fiber.³⁹

From the works on growing MOF film on inorganic substrates, researchers found that precursors could react with inorganic substrate to form a nucleation layer for further growth of MOF.^{32,59} Parson's group developed a general method to fabricate MOF/fiber composites, in which a metal oxide (ZnO , Al_2O_3 , and TiO_2) nucleation layer was deposited on polymeric fiber surface via atomic layer deposition (ALD) to facilitate the MOF nucleation and growth.^{36,39,43,52,60}

They showed that ALD Al_2O_3 (about 24 nm) thin layer deposited on polypropylene (PP) fibers enable conformal growth of dense HKUST-1 coating on the fiber surface using solvothermal synthesis as shown in Figure 2.10.³⁹ Compared to untreated PP fibers, the

HKUST-1 areal loading was increased from 9.61 mg/cm² to 14.78 mg/cm² with the ALD Al₂O₃ nucleation layer, and the MOF mass loading (75.3%) was among the highest values from the reported methods. This strategy was general to other fiber substrates, polybutylene terephthalate (PBT) and cotton fibers, and other MOF coating, including MOF-74 and UiO-66. They also explored the growth mechanism of HKUST-1 growth on different ALD metal oxides, including ZnO, Al₂O₃, and TiO₂, in the solvothermal synthesis.^{43,60} The fastest growth was only observed on ALD ZnO deposited on fiber. XRD studies revealed that ZnO template layer was more reactive to Cu(NO₃)₂ precursor to form a (Zn,Cu) hydroxy double salt intermediate, which could be transferred into HKUST-1 through fast anion exchange with ligand. This group also deposited a TiO₂ ALD nucleation layer (5 nm) onto electrospun PA-6 nanofiber and a common solvothermal synthesis was used to coat Zr-MOF on the TiO₂ coated PA-6 nanofibers (noted as PA-6@TiO₂ in this work).³⁶ Dense MOF coatings were observed on nanofiber surface by SEM and TEM tests for all the three types of Zr-based UiO-type MOF including UiO-66, UiO-66-NH₂, and UiO-67 (Figure 2.11).³⁶ The high crystallinity and porosity of the Zr-MOF coating on nanofibers were verified by PXRD and nitrogen sorption isotherm, respectively. Conformal morphology of the MOF coating was helpful to improve the robustness and the Zr-MOF coating on nanofibers were maintained after catalytic application. In a comparison study, MOF coating obtained on PA-6 without TiO₂ deposition had a poor coverage and aggregation structure. The mechanism study revealed that the role of ALD TiO₂ layer in Zr-MOF deposition was different with that in the case of HKUS-1 coating. ALD TiO₂ layer herein acted as nucleation layer for ligand attaching, rather than forming the intermediate via the

reaction with zirconium salt. Similarly, they also coated UiO-66-NH₂ MOF onto an inexpensive and easily available PP nonwoven textile using the same method.⁵²

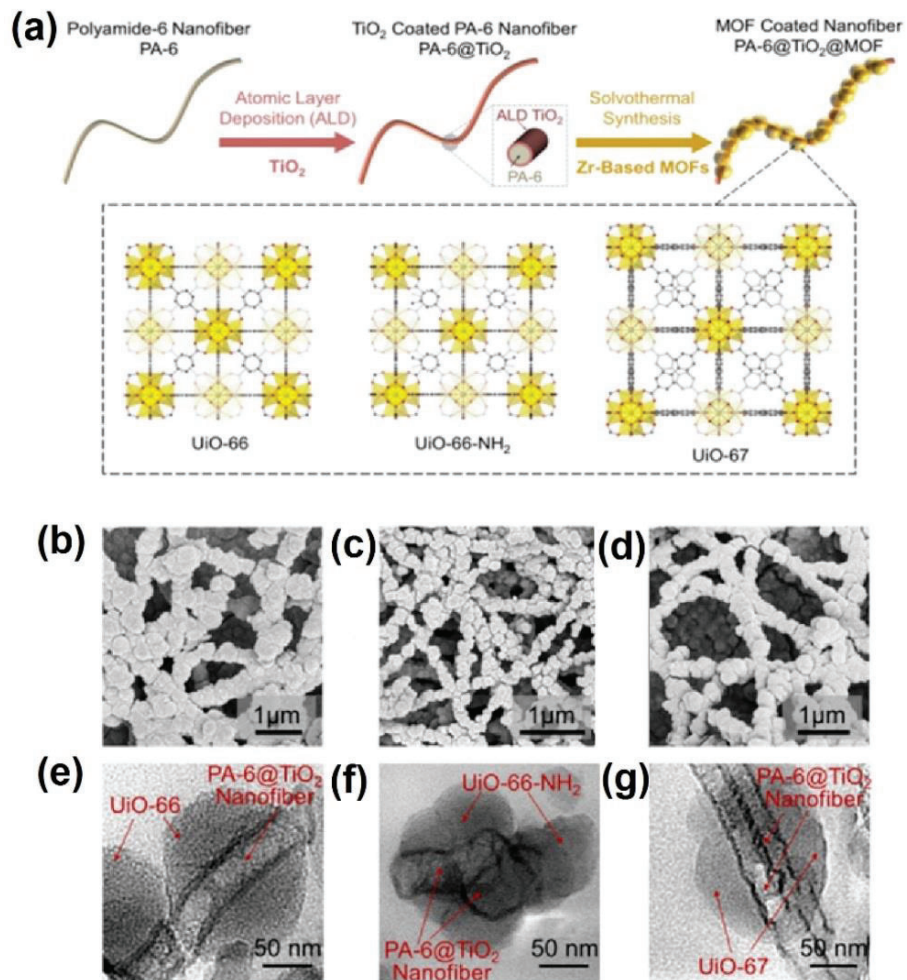


Figure 2.11. (a) Illustration of the ALD TiO₂ directed growth of Zr-MOF on PA-6 nanofiber substrates. SEM and TEM images of (b,e) UiO-66 coating on PA@TiO₂ nanofibers, (c,f) UiO-66-NH₂ coating on PA@TiO₂ nanofibers, and (f,g) UiO-67 coating on PA@TiO₂ nanofibers.³⁶

2.1.9 Layer-by-Layer growth method

Similar to direct solvothermal synthesis, layer-by-layer (LbL) growth approach was also explored in growing MOF coating on fiber substrates possessing functional groups, such as -COOH and -NH₂. Abbasi et al. investigated ultrasound treatment assisted LbL method to grow HKUST-1 and MOF-5 on silk fiber surface.^{35,61} The silk substrates were sequentially dipped in metal salt solution and organic ligand solution, with washing steps to remove unreacted precursor. Sonication treatment was found to accelerate the LbL growth reaction and improve the uniformity of MOF coatings on silk fibers in both cases, however prepared MOF/silk composites failed to get a coating with high mass loading and full coverage (Figure 2.12). This may be due to the lack of functional groups on untreated fiber surface for anchoring the metal ions and linkers for MOF nucleation and growth during the LbL process.

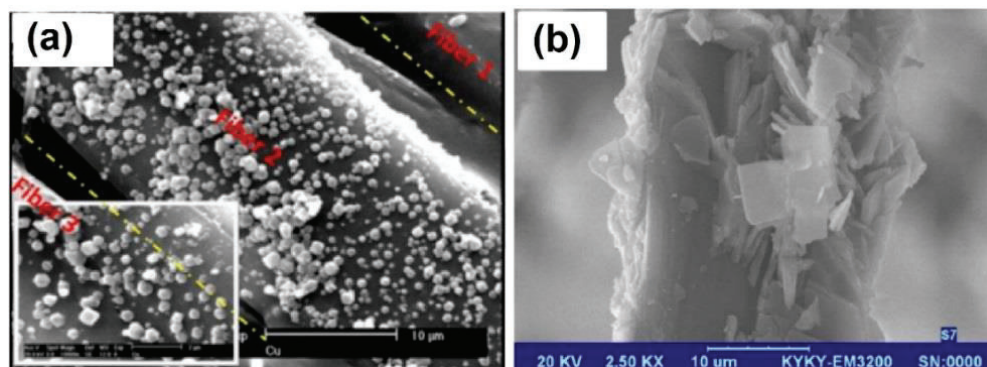


Figure 2.12 SEM images of (a) HKUST-1 and (b) MOF-5 coated silk fiber using direct LbL growth method.^{35,61}

To improve the nucleation selection of surface, chemical modification assisted growth method was developed by Biemmi and co-workers, while this method was originally designed to coat oriented MOF on hard surface, such as gold surface.⁶² This work

demonstrated a robust general strategy of nanoparticle coating and pattern, utilizing grafted 11-mercaptoundecanoic acid self-assembled monolayers (SAM) and 11-mercaptoundecanol SAM as a complex ligand. The essential step of this approach is to graft SAM layers, which act as linkers, onto substrates. Then metal ion is chemically absorbed onto SAM. Lastly, the absorbed ion is treated by specific reactants to transform them into MOF coating.

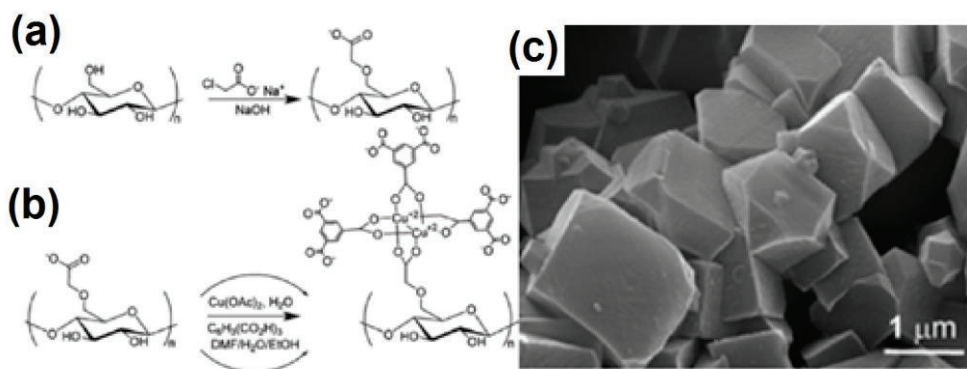


Figure 2.13. (a) Grafting of carboxymethyl groups onto cellulose and (b) a proposed mechanism of LbL method for HKUST-1 growth on cellulose fiber. (c) SEM image of HKUST-1 coated cotton fibers.⁴⁸

Neufeld et al. extended this method to coat HKUST-1 onto cotton cellulose fiber by a LbL method.⁴⁸ Carboxylate groups were firstly grafted onto the cotton cellulose, which supplied coordination site for copper ion for further HKUST-1 growth as illustrated in Figure 2.13a. After 8 LbL cycles, the cotton fiber in copper salt aqueous solution and H₃TC ligand DMF/ethanol/water (1/1/1) solution, a dense HKUST-1 coating was observed on fiber surface by SEM image (Figure 2.13c) and its crystal identity was verified as HKUST-1 by XRD test.

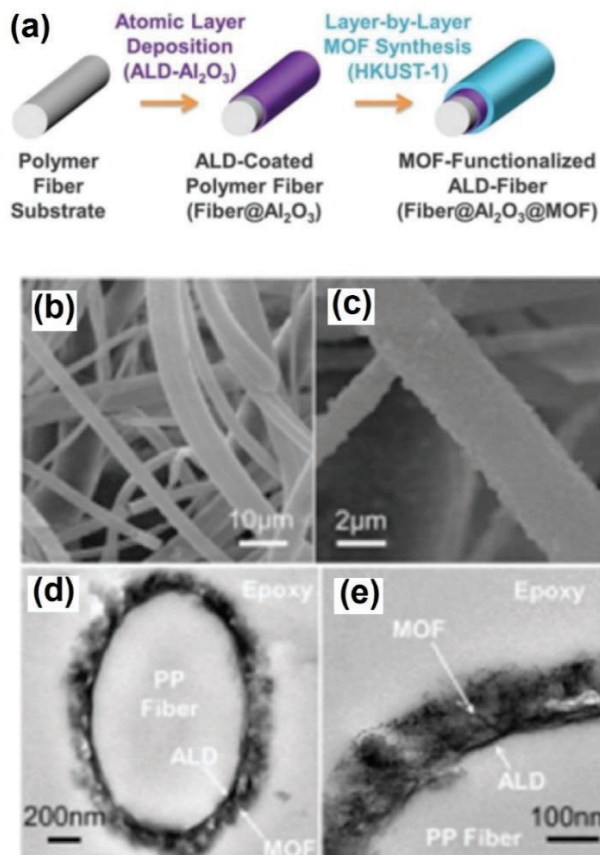


Figure 2.14 (a) Illustration of the LbL synthesis of HKUST-1 coating using ALD Al₂O₃ as nucleation layer. (b-c) SEM images of prepared HKUST-1 coating on ALD Al₂O₃ modified PP fibers. (d-e) TEM images showing the cross-sectional view of HKUST-1 coating on ALD Al₂O₃ modified PP fibers.⁴²

As ALD deposited metal oxide layers have been proved as efficient nucleation sets for direct MOF solvothermal growth on fiber surface, the LbL growth of MOF on ALD oxide deposited fiber surface was also investigated.⁴² Zhao et al. studied the ultrasound assisted growth of HKUST-1 coating on ALD Al₂O₃ deposited PP fibers as described in Figure 2.14. A conformal and uniform HKUST-1 coating was obtained after 40 LbL growth cycles, and no agglomerated HKUST-1 crystals were observed in the voids between fibers in SEM

and TEM images (Figure 2.14b-e). MOF film thickness and mass loading were found as a function of the number of LbL growth cycles, indicating the fine tunability of this method. However, the mass loading for each growth cycle is relative loading, which may be a disadvantage to get dense coatings on fiber. This synthesis method was generalized to coat HKUST-1 layer on polyethylene terephthalate and cotton fiber substrates.

2.1.10 Solvent-free hot-pressing method

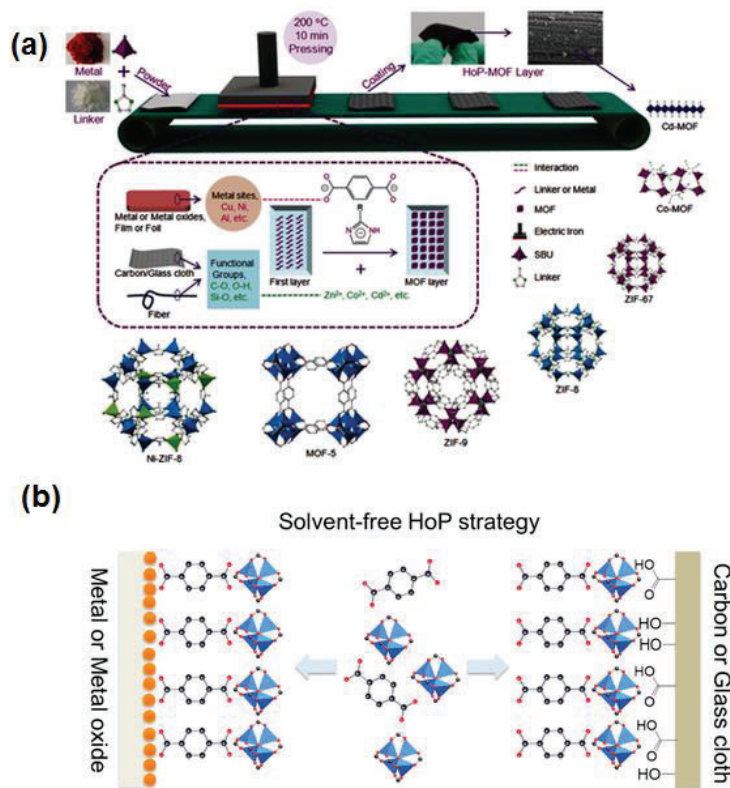


Figure 2.15. (a) Schematic illustration of the solvent-free hot-pressing (Hop) strategy and (b) the proposed interaction mechanism between precursor and fiber substrates during MOF deposition.⁶⁵

A solvent-free approach was presented by Wang etc. for producing stable MOF coatings by a hot-pressing method as illustrated in Figure 2.15a.^{45,63-65} In this general method, high

temperature and pressure are applied simultaneously using an electric iron to facilitate the rapid deposition of MOF layer onto various fibrous substrates. Two reaction steps may be involved in the hot-press process as demonstrated in Figure 2.15b. Firstly, under heating and pressure, precursors (metal ions and/or ligands) were chemically immobilized onto -OH and/or -COOH functional groups or metal sites on the substrate surfaces, such as carbon fiber and metal grid. Then, MOF nucleation and crystal growth occurred on the surface to form a stable coating.⁶⁵ A polymeric compound, polyethylene glycol, was used as a surfactant in this method to promote the diffusion of precursors, which could be removed completely by washing from MOF layers after synthesis. This strategy was proven to be applicable to carboxylate-based (such as MOF-5), imidazolate-based (ZIF-8), and mixed-metal MOF, and various fiber substrates such as carbon cloth, melamine sponge, glass fiber, and plastic mesh. Superhydrophobic and “Janus” MOF films were also obtained through layer-by-layer pressing, which brought water-proof property to the water unstable MOF composite. Interestingly, the mechanical stability of the MOF coating prepared by hot-press method was improved against abrasion resistance and stirring tests. X-ray photoelectron spectroscopy (XPS) analysis showed the strong interaction between the MOF layer and fiber substrates. Importantly, this hot-pressing method can be scaled up through a continuous roll-to-roll production and may push MOF bulk application in industrial level.⁶⁴ This method produced less pollutant to our environment, making it very eco-friendly, while heating under high temperature (200 °C) and press may cause damage to most widely used polymeric fiber matrix, such as cotton, polyester and nylon. At the same time, there are several other limitations for hot-pressing method needing to be tackled, such as the less applicability to zirconium-based and iron-based MOF and the undesired MOF

aggregation on the fiber surface. Also, the mass gain for each hot-press cycle was low, therefore multiple coatings were necessary to get a high low loading for this method, which would be time-consuming in industrial production.

2.1.11 Inject printing method

Based on the evaporation induced crystallization mechanism,^{66,67} Zhuang et al. developed a direct printing strategy for positioning MOF coatings and patterns on flexible substrates.³⁰ As the viscosity and surface tension of the precursor ink solution is critical for the inkjet printing process, they developed a printable ink formula. The ethylene glycol was used as a stabilizer of the precursor dissolved in ethanol/dimethylsulfoxide (DMSO) mixture solvents. The precursor ink was printed onto the substrates, such as polyester film, office paper and cotton fiber, using a commercial printer, and MOF patterns were obtained after a heating treatment as shown in Figure 2.16. The thickness of the MOF coating and the mass loading of the MOF layer were controlled by adjusting the printing-drying cycles. Because of the relative low yield of each printing cycle, the method here may be more attractive in exact engineering necessary field.

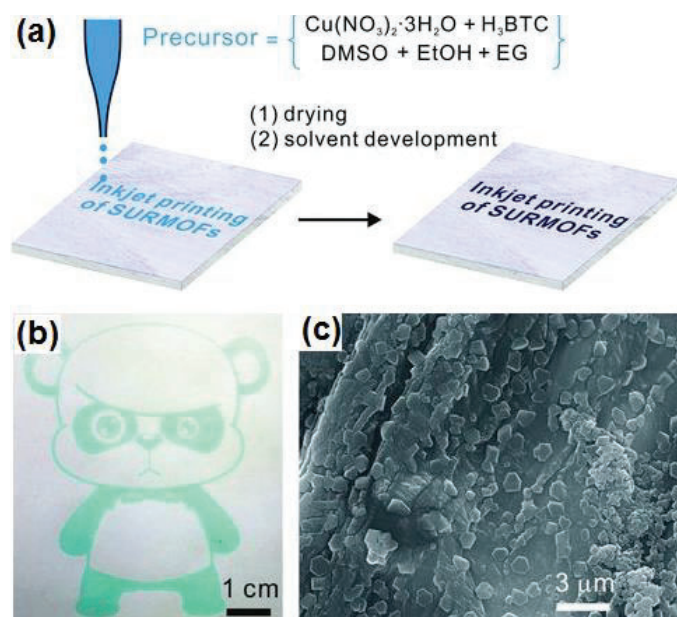


Figure 2.16. (a) Illustration of inkjet printing of HKUST-1 onto flexible substrates using precursor solution as the ink. (b) Photograph image and (c) SEM image of a HKUST-1 pattern on office paper.³⁰

2.2 Application of MOF/fiber composite

2.2.1 Particulate matters pollutant removal

Particulate matters (PM), especially these with a diameter below 2.5 μm ($\text{PM}_{2.5}$), are becoming a severe pollution problem all over the world. MOF with unsaturated metal sites and defects are usually charged on its surface, which could capture the highly polar PM through electrostatic interactions. Wang's group explored the potential of MOF/filter composite for efficient PM capture as shown in Figure 2.17.⁴¹ They studied the PM filtration efficiency of their electrospun MOF/nanofiber composites in a simulated and the real smoggy atmosphere in Beijing. In a comparison study, the prepared four composite all with PAN as a polymeric substrate, while the functional MOF in the composite were varying from MOF-199, UIO-66-NH₂, Mg-MOF-74, and ZIF-8. Under the real hazy

condition ($PM_{2.5}$: $350 \mu\text{g m}^{-3}$, PM_{10} : $720 \mu\text{g m}^{-3}$, relative humidity: 58.6%, and temperature: $23.5 \text{ }^\circ\text{C}$), their MOF/nanofiber composite all showed superior performance in PM removal compared with pure PAN nanofiber. They found the positive correlations between the removal efficiency and zeta potential of the MOFs used in composites. For example, ZIF-8 has the highest zeta potential value among the four MOFs, and its composites achieved the best performance in PM removal, with about 90% of the PM removed. The removal efficiency of ZIF-8/PAN nanofiber composite didn't show obvious degradation after 48 h exposure in above hazy atmosphere. And it had a very high removal capacity of 29.5 g m^{-2} or 0.037 g g^{-1} .⁴¹ Similarly, excellent PM removal performance was obtained for the roll-to-roll hot pressing method prepared MOF/fiber composites. Interesting, they found the removal efficiency could be fully recovered after a sample tap water washing and drying.⁶⁴

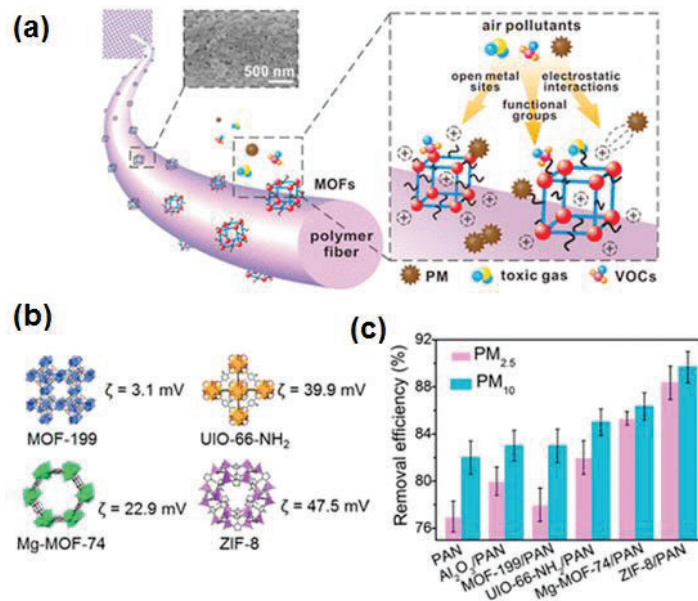


Figure 2.17. (a) Schematic illustration of air pollutants removal mechanism using the MOF/fiber composite. (b) Zeta potentials (ζ) of MOFs used for nanofiber doping and (c) PM removal efficiency comparison using different nanofiber-based filter.⁴¹

2.2.2 Hazardous gases removal

Since MOFs have a large amount of bonding site for adsorption of toxic industrial gases, such as NH_3 , SO_2 , HCl and H_2S ,¹⁹⁻²¹ MOF/fiber composites are drawing great attention from researchers for fabricating protective gear against these toxic gases.^{30,39,41-43}

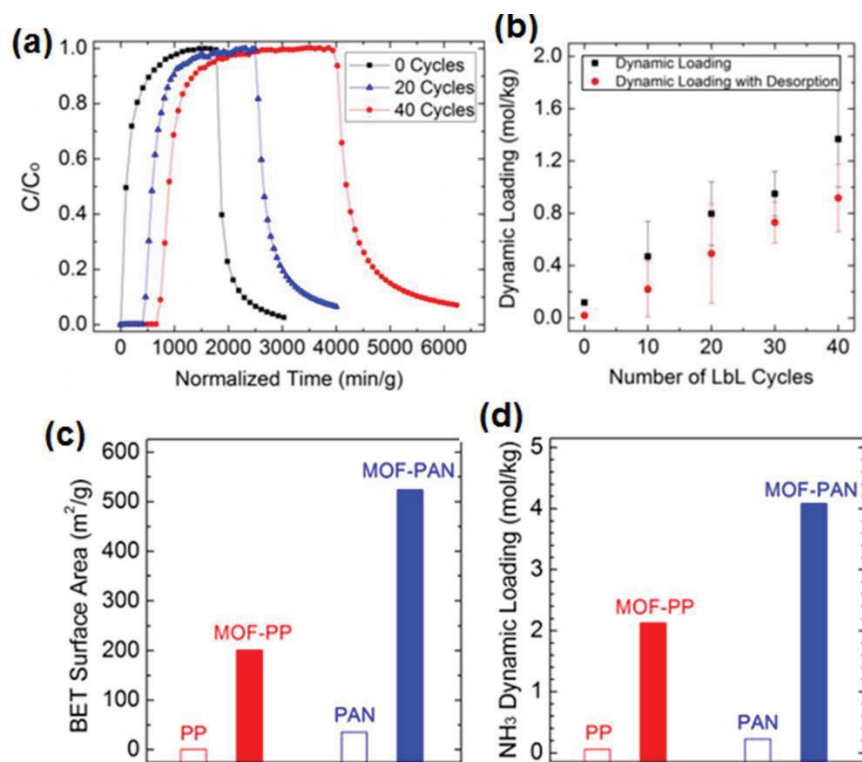


Figure 2.18. (a) NH_3 breakthrough curves and (b) NH_3 dynamic loading of ALD deposited PP microfiber after different HKUST-1 LbL growth cycles.⁴² (C) BET surface area and (D) NH_3 dynamic loading of PP microfiber and PAN nanofiber with or without HKUST-1 coating.⁴³

Parsons's group investigated the NH_3 and H_2S removal performance of their HKUST-1/fiber composites, which were precoated with an ALD zinc oxide to facilitate the MOF growth.^{42,43} The HKUST-1 was coated onto PP with an ALD zinc oxide layer by a LbL dipping method. NH_3 adsorption capacities were improved with the increasement of LbL

cycles (Figure 2.18a-b). After 40 LbL cycles, the HKUST-1/PP composite with a mass loading of 17% showed an ammonia dynamic adsorption capacity of 1.37 mol NH₃/kg composite (normalized as 7.63 mol NH₃/kg MOF) and a H₂S dynamic loading of 1.49 mol H₂S/kg composite (normalized as 9.46 mol H₂S/kg MOF). As an obvious demerit, multiple dippings were needed for this method, while the obtained mass loading was relatively low. They also prepared HKUST-1 coating on PAN nanofibers and PP microfiber via a one-step synthesis strategy using a dense ALD zinc oxide template. In this method, the dense zinc oxide layer reacted with the copper salt firstly to form a double hydroxyl salts, which could be converted into HKUST-1 rapidly. Compared with HKUST-1 coated PP microfibers from same approach, HKUST-1/PAN nanofiber composite showed a much higher NH₃ adsorption capacity, because of its higher MOF mass loading (Figure 2.18c-d). The high dynamic loadings of NH₃ as well as H₂S on these MOF-functionalized fiber mats suggest that these composites are very promising for gas filtration and protective suites.⁴³

In addition, Zhuang et al. printed HKUST-1 pattern on cotton textile fiber and reported the color change as a sensor of toxic gas exposure. After exposure to NH₃, HCl and H₂S atmosphere, the turquoise blue color of HKUST-1 pattern became dark blue, yellow and brown, respectively. At the same time as an efficient adsorbent, the HKUST-1/fiber composite could also act as an indicator of the presence of hazardous gas.³⁰

SO₂ is another most harmful pollutant gases which could threaten human health and cause environmental problems, such as acid rain. Several studies had been conducted to remove the toxic SO₂ using MOF/fiber composites. Wang's group measured the capture performance of their electrospun MOF/fiber composite using a dynamic adsorption test method.⁴¹ With feed SO₂ concentration of 100 ppm and a flow rate of 50 mL min⁻¹, the

HKUST-1/PAN nanofiber composites and UiO-66-NH₂/PAN nanofiber composites showed a higher adsorption capacity of SO₂ compared with the pure PAN nanofiber without MOFs doping, because of the open copper sites or amino groups on ligands in the MOF/fiber composite. In addition, the pressure drop in the MOF/fiber composite was relatively small, below 20 Pa at the flow rate of 50 mL min⁻¹ in test (Figure 2.19a). Interestingly, UiO-66-NH₂/PAN maintained a fine capture capacity toward SO₂ after several adsorption cycles, possible due to its chemical robustness (Figure 2.19a).⁴¹

Together with the chemical adsorption of toxic gases, the catalytic degradation of toxic gases is another promising application. Ozone (O₃) gas is an in-door air pollutant, especially in confined working places, such as printing room and office. Wang's group found that MIL-100(Fe), possessing ultra-high BET surface area and abundant Fe cluster active sites, showed efficient catalytic activity for continuous decomposition of ozone.⁶⁸ They prepared a fibrous composite by hot-pressing the pre-synthesized MIL-100(Fe) nanoparticle onto a nonwoven fabric. The catalytic activity was fully maintained after coating process (Figure 2.19b). The ozone with a concentration of 200 ppb could be totally degraded by the MOF/fiber composite under the flow rate of 1000 mL min⁻¹ and 45% relative humidity. The composites with excellent catalytic performance had great potential in production of personnel protective devices, such as mask filter, against ozone pollution.

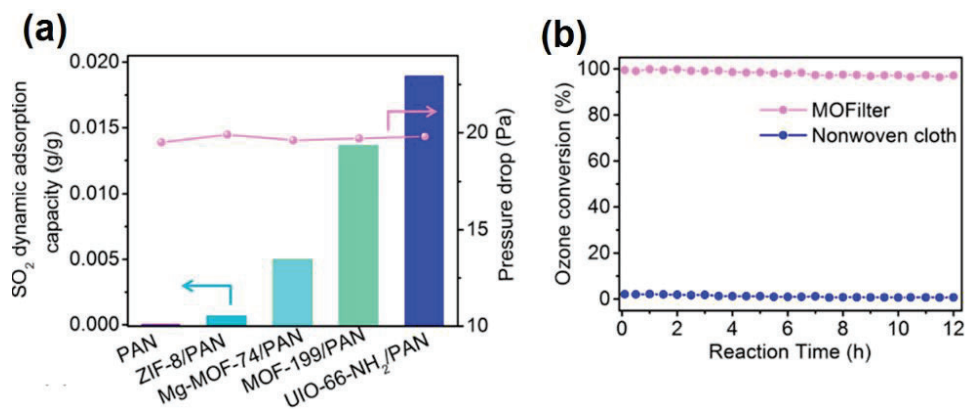


Figure 2.19. (a) SO₂ dynamic adsorption capacity and pressure drop of PAN nanofiber and MOF/PAN composite.⁴¹ (b) Catalytic decomposition of ozone (200 ppb) using MIL-100(Fe)/fiber composite.⁶⁸

2.2.3 Destruction of Chemical Warfare Agents

The application of MOF as a heterogeneous catalyst in the ultra-toxic warfare agents is becoming a new research focus. Though few zirconium MOFs have showed excellent catalytic activity in hydrolysis of warfare agents or their related simulant, the real application is hindered by the poor processability of powdered MOFs.⁶⁹⁻⁷² Introducing catalytic Zr-MOFs onto flexible fiber substrate is a promising strategy to produce protective clothes, which could be potentially widely used for protecting soldiers, first-responders, and the public against nerve agent threat.^{36,37,46,47,50}

López-Maya et al. investigated the catalytic degradation of nerve agent simulants using UiO-66/silk composite catalysts. MOF nanoparticles were firstly introduced onto the silk nanofiber mate by spray and further chemically modified with LiO*t*Bu.⁴⁶ Low toxic diisopropylfluorophosphate (DIFP) and dimethylmethylphosphonate (DMMP) were used as the nerve agent simulant, while 2-chloroethylethylsulfide (CEES) was used the mustard

gas simulant. The half-lives of DIFP, DMNP and CEES were 20 min, 50 min and 8 min, respectively. The heterogeneous nature of these composite catalysts was verified by a filter test.

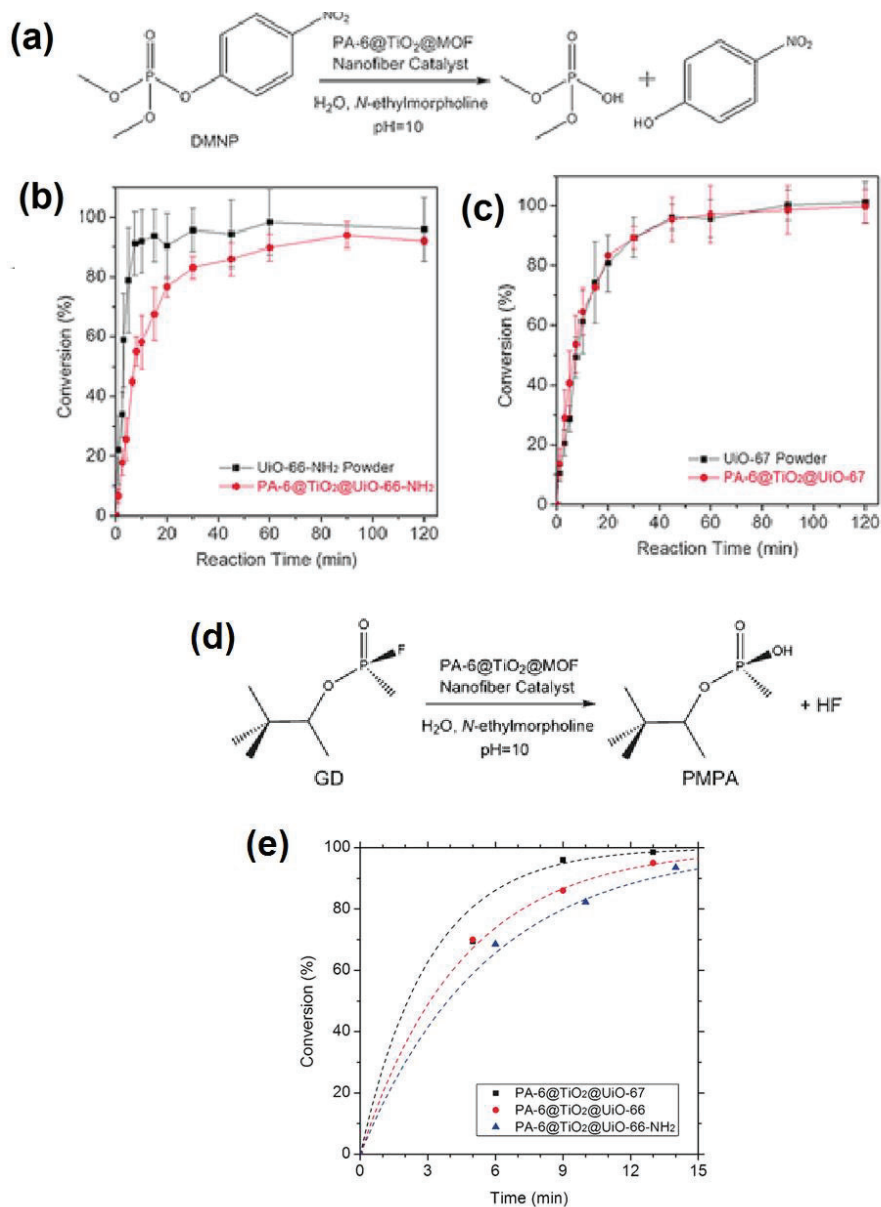


Figure 2.20. (a) Catalytic DMNP hydrolysis reaction and (b-c) kinetics using MOF nanoparticles or Zr-MOF coated nanofiber. (d) Catalytic GD hydrolysis reaction and (e) kinetics using Zr-MOF/nanoparticles composite.³⁶

Parsons's group synthesized conformal Zr-based MOF coating, including UiO-66, UiO-66-NH₂ and UiO-67, on electrospun PA-6 nanofibers, which were pre-coated with an ALD TiO₂ layer as the nucleation facilitator.³⁶ The prepared composites were used in catalytic hydrolysis of a nerve agent simulant (DMNP) and a real nerve agent Soman, also known as GD. Catalytic hydrolysis reaction of DMNP in an aqueous buffer solution (pH = 10) was evaluated with Zr-MOF coated nanofiber catalysts and free Zr-MOF nanoparticles. UiO-66-NH₂ and UiO-67 coating on PA-6 nanofiber demonstrated ultra-fast catalytic reaction rates for DMNP hydrolysis with half-lives less than 8 min (shown in Figure 2.20a-c). Importantly, the MOFs bonded onto fibrous substrate showed comparable catalytic activity compared with free MOF nanoparticle, while the PA-6 nanofiber with TiO₂ ALD coating, showed a half-life of about 20 h, verifying the catalytic activity of MOF layer. Catalytic degradation of a real nerve agent, GD, was also explored using UiO-66-NH₂ coated PA-6 fiber. The half-lives for GD were 3.0 min with UiO-66 coated PA-6, 3.7 min with UiO-66-NH₂ coated PA-6, and 2.3 min with UiO-67 coated PA-6 (Figure 2.20d-e). This work was the first demonstration for catalytic degradation of a real nerve agent (GD) using MOF/fiber composite.

2.2.4 Catalytic NO Release

The controlled release of nitric oxide (NO) is important in biomedical field because of its bioactivity in antiplatelet aggregation, antibacterial and anti-inflammatory effects, while it is still under challenge.⁷³⁻⁷⁵ Reynolds etc. have found a copper-based MOF, HKUST-1, showed effective catalytic property for generation of NO from S-nitrosocysteine precursor,⁷⁶ and they developed HKUST-1/cotton composite for the heterogeneous catalyst for NO release (Figure 2.21).⁴⁸ HKUST-1 coated cotton fiber showed the catalytic activity

to trigger the efficient generation of NO ($7.1 \pm 1.2 \mu\text{mol NO /mg MOF}$) over a long release period. It was also found that HKUST-1 coating on cotton fiber exhibited a shorter induction period compared to mixed matrix membrane (MMM) with the same amount of HKUST-1, indicating higher availability of the catalytic site on substrate surface for the diffusion precursor. They also proved the stability of the coating using diffuse reflectance UV-Vis spectra and ICP-AES tests after the catalytic reaction. The excellent catalytic performance made the HKUST-1/cotton composite a promising catalyst for controlled NO release.

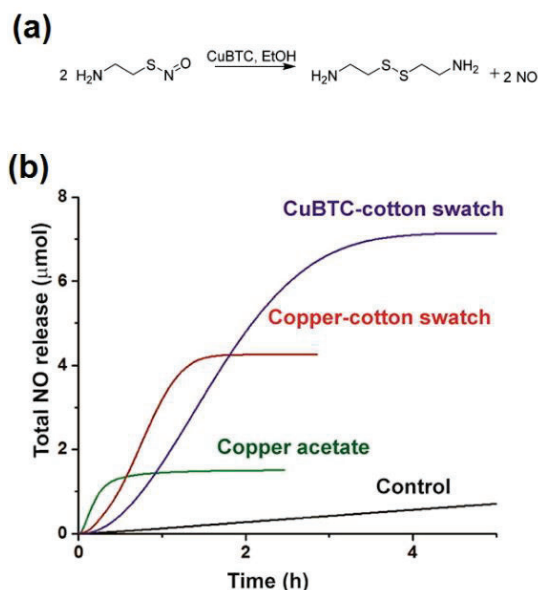


Figure 2.21. (a) Catalytic release NO from S-nitrosocysteamine precursor and (b) NO release kinetics using different catalyst.⁴⁸

2.2.5 Water purification

Taking advantage of the good processability and the maintained high porosity, MOF/fiber composites present attractive potential in pollutant removal from water. Moreover, the fibrous composites could be more easily recovered compared with powdered MOF absorbent in water

purification application. Fu et al explored the MOF/nanofiber composites' application in removal of toxic heavy metal ions and organic dyes (Figure 2.22).⁴³ In that study, electrospun silk nanofiber mate was used the substrate for MOF growth. Encouragingly, the MOF coating on fiber achieved the same uptake capability of that of free MOF powders, indicating the high accessibility of the active site in the MOF coating For example, the ZIF-67 coating component on the component had a normalized malachite green adsorption of 2124 mg g⁻¹, which very close to the uptake capacity of the free MOF powder. The MOF/fiber composites showed nearly 100% removal performance of two kinds of heavy metal ion (As(v) and Cr (VI)) and organic dyes (rhodamine B and malachite green). A filtration device using the as the functional filter was also assembled for continuous adsorption of malachite green, and a removal efficiency of about 100% was obtained in one round. The blue color of simulated polluted water turned almost colorless after the filtration using the ZIF-67/silk nanofiber composite filter (Figure 2.22 b).

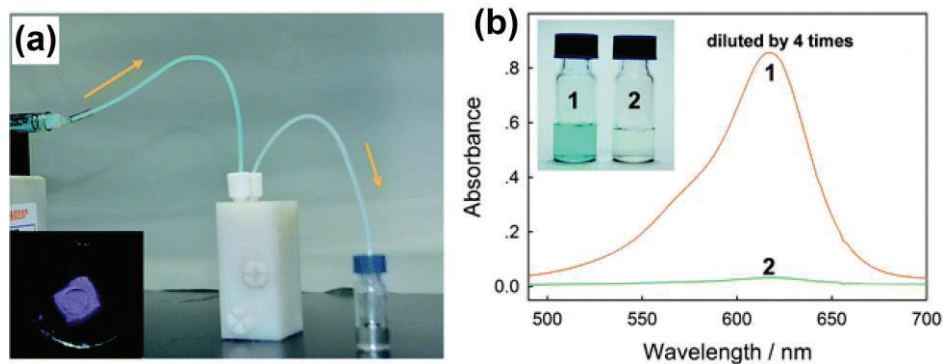


Figure 2.22 (a) Photograph image of a filtration device using ZIF-67/fiber composite (insert) as the filler. (b) The UV-visible spectra and the photograph image of malachite green solution before (1) and after (2) filtration.⁴⁴

Wang's group built a filtration device employing the MOF/carbon fiber composites, which were prepared using the hot-pressing method, as the filter filler for continuous adsorption of high toxic As^V ion from water.⁴⁴ ZIF-8/carbon fiber composite, ZIF-9/carbon fiber composite, and ZIF-67/carbon fiber composite demonstrated good uptake capacities of 27.2, 53.1 and 32.6 mg g⁻¹ m⁻², respectively, while uncoated carbon fiber cloth only showed an insignificant capacity of 4.3 mg m⁻².

Chapter 3

Facile and Scalable Coating of Metal–Organic Frameworks on Fibrous Substrates by a Coordination Replication Method at Room Temperature

Coating of metal–organic frameworks (MOFs) on flexible substrates is a crucial technology for applications such as purification/separation, sensing, and catalysis. In this chapter, a facile coordination replication strategy was developed to coat various MOFs onto flexible fibrous materials where a dense layer of an insoluble precursor template, such as a layered hydroxide salt, was first deposited onto a fiber substrate via a mild interfacial reaction and then rapidly transformed into a MOF coating in a ligand solution at room temperature. Spatiotemporal harmonization of solid precursor dissolution and MOF crystallization enabled precise replication of the precursor layer morphology to form a continuous MOF coating composed of intergrown crystals. The resulting flexible, highly robust, and processable fibrous MOF/textile composites demonstrated tremendous potential for industrially relevant applications such as continuous removal of the organosulfur compound dibenzothiophene from simulated gasoline and ammonia capture. This rapid, versatile, eco-friendly, and scalable MOF coating process at room temperature gives rise to new possibilities for preparing MOF-coated functional materials.

3.1 Introduction

Metal–organic frameworks (MOFs) with extremely high surface area and rich structural and chemical diversity have drawn a considerable amount of attention from researchers in various fields.¹⁻¹⁰ Despite the fact that MOFs possess tremendous value in numerous fields, their practical applications are hampered because powdered MOFs are typically poorly processable; thus, stable MOF coatings on various substrates are needed for practical applications.^{25,77-79} Flexible and tailorable fibrous materials, such as textiles, sponges, and meshes,^{34-40,80-83} are inexpensive and readily available substrates for supporting MOFs in various applications including pollutant adsorption,^{30,43} gas separation,^{82,83} catalysis,⁵⁸ protective devices,^{36,37} and particulate matter removal.⁶⁴ Ink-jet printing,³⁰ hot pressing,^{45,64} and chemical vapor deposition-assisted coating^{36,39,42} have been developed for coating of MOFs on fibrous and flexible surfaces. However, the previously reported methods usually have one or more of the following limitations, requiring sophisticated equipment or harsh reaction conditions, resulting in low loading efficiency, or not being compatible with thermally sensitive fibrous materials.

In this chapter, a facile and scalable strategy for the fabrication MOF coatings was developed by coordination replication of a predeposited insoluble precursor template. Deposition of the precursor was conducted via a mild solid/liquid interfacial reaction between potassium carbonate (K_2CO_3) impregnated in the substrate fibers and a metal salt solution in ethanol. An insoluble layered hydroxide salt (LHS), such as copper hydroxide nitrate (CHN), was predeposited on the target fiber surface and served as both the metal ion precursor and a template (ca. nucleation site) for MOF growth. When the template-coated fibrous material was treated with an organic ligand solution, a fast coordination

replication reaction occurs at the interfacial layer between the solid precursor and the ligand solution, replicating the precursor layer morphology and positioning the MOFs on the fiber surface (Figure 3.1).⁵⁵ In this chapter, the coating of HKUST-1 on the cotton fiber was chosen as a model system for demonstrating the proposed coordination replication coating process.

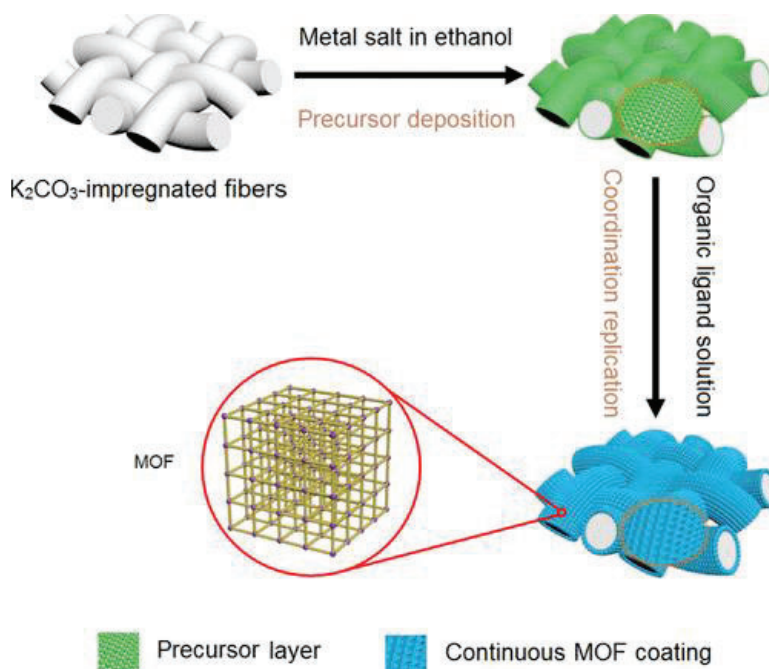


Figure 3.1. Schematic illustration of the fabrication of a MOF coating on a fibrous substrate by coordination replication of a predeposited metal ion precursor template. This approach mainly includes two steps: (i) deposition of an insoluble metal ion precursor through an interfacial reaction between a slightly soluble inorganic base (K_2CO_3) impregnated in the substrate fibers and a metal salt dissolved in ethanol. (ii) Coordination replication of the metastable precursor layer (represented as a green layer) by more stable MOF crystals (blue layer). The continuous morphology of the precursor layer is effectively replicated in the MOF layer

3.2 Experimental section

3.2.1 Materials

A cotton fabric with an areal density of 277 g m^{-2} was provided by China Dye Ltd., Hong Kong. Before use, all cotton samples were scoured in a boiling aqueous 3% NaOH solution for 0.5 h to remove impurities. A polyester (PET) microfiber fabric with an areal density of 268 g m^{-2} was purchased from Weifang Tricol Textile Co. Ltd., China. A polyacrylonitrile (PAN) nanofiber with an areal density of 60 g m^{-2} was prepared by electrospinning at 10 kV with a tip-to-collector distance of 15 cm. A 10% solution of PAN dissolved in *N,N*-dimethylformamide (DMF) was used as the electrospinning solution. $\text{Cu}(\text{NO}_3)_2 \cdot 2.5\text{H}_2\text{O}$ (99%), $\text{Zn}(\text{CH}_3\text{CO}_2)_2 \cdot 2\text{H}_2\text{O}$ (99%), $\text{Co}(\text{Cl})_2 \cdot 6\text{H}_2\text{O}$ (98%), dibenzothiophene (DBT, 99%), carboxymethylcellulose sodium salt (molecular weight: 250 000; degree of substitution: 0.9), all solvents, and metal standard solution were purchased from Sigma-Aldrich. Benzene-1,3,5-tricarboxylic acid (BTCA, 98%), 1,4-benzenedioic acid (BDCA, 99%), 2-methylimidazole (2-MIM, 99%), DMF (99.8%), ethanol (99.8%), K_2CO_3 (99%), and NaOH (99%) were purchased from Acros Organics. The water used in this chapter was deionized. All reagents were used as received without any further purification.

3.2.2 Characterization and Instruments

Morphological images of all samples were taken with a scanning electron microscope (Vega 3 Tescan) at an accelerating voltage of 20.0 kV. Powder X-ray diffraction (PXRD) experiments were carried out using a Rigaku SmartLab diffractometer with $\text{Cu K}\alpha$ radiation ($\lambda = 1.5406 \text{ \AA}$). The metal content on the MOF/fiber composite samples was measured by inductively coupled plasma optical emission spectrometry (ICP-OES)

(Agilent 5100). Fourier transform infrared (FTIR) spectra of all samples were recorded on a FTIR spectrometer (PerkinElmer System 2000) in the attenuated total reflection mode. UV–visible reflectance spectra were collected on a Datacolor 650 spectrophotometer. Nitrogen adsorption–desorption isotherms and Brunauer–Emmett–Teller (BET) surface area data were collected on Quantachrome Instruments (surface area and pore size analyzer NOVA touch LX (4) at 77 K. The breaking strength and elongation of the textile samples along the warp direction were tested according to a grab test method [ASTM D5034—09(2017)] on a tensile strength tester (Instron 4411). Five replicates were tested for the breaking strength and breaking elongation, and the average values were reported. Ammonia sorption experiments were performed on a 3Flex (Micromeritics) multiport surface characterization instrument.

3.2.3 Predeposition of CHN on Cotton Textile

Four pieces of cotton fabric (4 cm × 4 cm) were immersed in 50 mL of a K₂CO₃ aqueous solution with a weight concentration ranging from 10 to 50% for 30 min. After the removal from the bath solution, the fabrics were rolled through a laboratory padder at a nip pressure of 2 kg cm⁻² with a rotation speed of 5 rpm and dried at 60 °C for 30 min to remove water. To form the CHN deposition layer, the K₂CO₃-containing fabrics were immersed in 100 mL of a 0.5 M Cu(NO₃)₂·2.5H₂O ethanol solution for 24 h. After washing with deionized water, the grass-green fabrics were dried in air at room temperature.

3.2.4 Fabrication of an HKUST-1 Coating on a Cotton Textile

The CNT/cotton fabric samples were immersed in 100 mL of a 0.1 M BTCA ethanol/water solution for 1 h, washed with 100 mL of ethanol three times, dried in a vacuum oven at 100 °C for 24 h, and stored under vacuum until characterization. To investigate the process

of MOF growth from the predeposited CHN layer, the CHN/cotton textile samples prepared from 20% K₂CO₃ were immersed in a BTCA solution and periodically characterized by several techniques. Unless otherwise indicated, the water volume percentage in the BTCA ligand solution was 10%.

3.2.5 Synthesis of powered HKUST-1 from copper hydroxide nitrate (CHN)

CHN powder was prepared by mixing 60 mL of a 0.5 M K₂CO₃ aqueous solution and 400 mL of a 0.5 M Cu(NO₃)₂·2.5H₂O ethanol solution and vigorously stirring for 30 min. After filtration, the green powder was rinsed with deionized water and dried in air. The equation for the transformation of Cu(NO₃)₂ to 2Cu₂(OH)₃NO₃ is as follows:



In the next step, 10 mmol CHN was added into 100 mL of a water/ethanol (1/2: v/v) solution containing 15 mmol BTCA and agitated by vigorous magnetic stirring at room temperature. The colour of the mixture quickly turned to turquoise from green within several seconds. After 2 min, the blue powder was quickly removed by filtration through a polypropylene membrane (0.2 μm pore size, CHMLAB Group) and washed with 100 mL of ethanol from 3 times. A total of 3.7 g of product was obtained after drying in a vacuum oven at 120 °C for 24 h. The sample was stored under vacuum until characterization. The space-time-yield (STY) of the reaction was 2.66 x 10⁴ kg m⁻³ d⁻¹.

3.2.6 Coating HKUST-1 on electrospun nanofibers and commercial polyester microfibers.

The electrospun nanofiber and commercial polyester microfiber substrates were dipped into 20% K₂CO₃ aqueous solution for 30 min, padded through a lab padder at a nip pressure

of 2 kg cm^{-2} and dried at $60 \text{ }^\circ\text{C}$ for 30 min to remove water. The subsequent procedures of precursor deposition and conversion into MOFs were the same as those for cotton textile outlined above.

3.2.7 Coating Cu-BDC on cotton textile

Similar processes were performed to coat Cu-BDC on cotton textile. CHN-deposited cotton fabrics were soaked in 100 mL of a 0.1 M BDCA DMF/water (9/1 v/v) solution for 4 h to form a MOF coating, washed with 100 mL of DMF 3 times, and dried in a vacuum oven at $100 \text{ }^\circ\text{C}$ for 24 h before characterization.

3.2.8 Coating ZIF-8 on cotton textile

Textile samples (4 cm x 4 cm) treated with a 20% K_2CO_3 solution were first immersed in 100 mL of a 0.2 M $\text{Zn}(\text{acetate})_2 \cdot 2\text{H}_2\text{O}$ in ethanol for 24 h to deposit an insoluble zinc hydroxy acetate (ZHA) precursor layer, washed with deionized water, and dried at room temperature. Then, the fabrics were soaked in 100 mL of a 0.1 M 2-MIM in ethanol/water (9/1 v/v) solution for 4 h to form a MOF coating, washed with 100 mL of ethanol 3 times, and dried in a vacuum oven at $100 \text{ }^\circ\text{C}$ for 24 h before characterization.

3.2.9 Coating ZIF-67 on cotton textile

Textile samples (4 cm x 4 cm) treated with a 20% K_2CO_3 solution were first immersed in 100 mL of a 0.2 M $\text{Co}(\text{Cl})_2 \cdot 6\text{H}_2\text{O}$ in ethanol for 24 h to deposit an insoluble cobalt hydroxy carbonate (CHC) precursor layer, washed with deionized water, and dried at room temperature. Then, the fabrics were soaked in 100 mL of a 0.1 M 2-MIM in an ethanol/water (9/1 v/v) solution for 4 h to form a MOF coating, washed with 100 mL of ethanol 3 times, and dried in a vacuum oven at $100 \text{ }^\circ\text{C}$ for 24 h before characterization.

3.2.10 Patterning HKUST-1 on cotton textile.

A 40% K₂CO₃ aqueous solution containing 2% carboxymethylcellulose sodium salt was preprinted in the logo of The Hong Kong Polytechnic University on cotton textile by screen printing. The subsequent procedures were the same as those for the textile coating outlined above. Note that the addition of sodium alginate as a thickening agent was necessary to produce a precise pattern. Without the thickening agent, the pattern edge became blurred.

3.2.11 Scaled-up MOF/cotton samples fabrication

Scaled-up batches of HKUST-1/cotton, ZIF-8/cotton, and ZIF-67/cotton samples (12 cm x 54 cm) were also prepared according to a similar protocol. The volumes of the metal salt and ligand solutions used in precursor deposition and coordination replication were 2000 mL, and the other parameters were the same as those in the small-scale processes outlined above.

3.2.12 Mass loading determination based on ICP-OES

Mass loading of MOFs on fiber was calculated based on ICP-OES. All samples before ICP-OES test were dried under vacuum oven overnight at 100 °C, and 100 mg sample quickly weighted and cut into tiny pieces. After being digested in 10 mL HNO₃, 100 uL of the solution is diluted into 10 mL using Milli-Q water for ICP-OES test. The mass loading (ML) is calculated as following equation:

$$ML = (C \times 100 \times 0.01 \text{ L}) / (100 \text{ mg} \times W_{\text{Metal}}) \times 100\%$$

where C is the concentration of metal in the diluted acid solution measured by ICP-OES, mg/L. 100 is the dilution factor, and 0.01 L is the volume of concentrated HNO₃ used in

digestion of fiber composite. W_{Metal} is the mass percentage in MOFs: 31.7% for HKUST-1, 28.1% for Cu-BDC, 28.7% for ZIF-8, and 26.7% for ZIF-67.

3.2.13 Desulfurization Test

For continuous flow desulfurization, HKUST-1/cotton samples were cut into circles with a diameter of 2.5 cm and activated at 100 °C under vacuum for 24 h. Four layers of the round cotton pieces were placed in a filter unit with an inner diameter of 2.5 cm. The filter was linked to a syringe pump to form a continuous adsorption device, as shown. Before the desulfurization test, the filter was wetted by 5 mL of pure *n*-heptane with a flow rate of 0.5 mL min⁻¹. Simulated gasoline (*n*-heptane) contaminated with 4000 ppmw DBT (695 ppmw sulfur) was pumped through the filter unit using a syringe pump with a flow rate of 0.1 mL min⁻¹. The simulated gasoline flow was periodically analyzed by UV–visible spectroscopy until saturation was reached. The remaining sulfur concentration in the gasoline flow was calculated based on the calibration curve method. The sulfur saturation adsorption capacity of the HKUST-1/fiber adsorbent was calculated with the following equation

$$q_s = \frac{v\rho x_i}{m} \int_0^{t_s} \left(1 - \frac{c_t}{c_i}\right) dt \times 100\%$$

where q_s is the saturation sulfur capacity per unit weight of the MOF/fiber adsorbent, %, v is the flow rate of simulated gasoline, mL min⁻¹, ρ is the simulated gasoline density, g mL⁻³, c_i is the initial sulfur concentration, ppmw, c_t is the sulfur concentration of the simulated gasoline at time t , ppmw, m is the weight of the adsorbent in the filter unit, g, x_i is the concentration of sulfur in the simulated gasoline, %, and t_s is the saturation time when $c_t/c_i = 1$, min.

3.2.14 Regeneration of the MOF/Fiber Adsorbent

The used MOF/fiber adsorbent was immersed in 100 mL of pure methanol for 24 h at room temperature, followed by drying at 100 °C under vacuum for 24 h. The desulfurization performance of the regenerated sample was evaluated according to the protocol described above.

3.3 Results and discussion

When immersing K_2CO_3 -impregnated cotton fabrics in an alcoholic solution of cupric nitrate (0.5 M), a deposition reaction tends to preferentially occur at the interface between the fiber and the solution to form an insoluble CHN layer, as illustrated in Figure 3.1.

Compared to a smooth pristine cotton fiber, the formation of a dense rodlike coating on the cotton fiber surface was observed by scanning electron microscopy (SEM) after 24 h of the reaction (Figure 3.2a,b) and the identity of the coating was verified by PXRD and FTIR spectroscopy experiments. The PXRD patterns of the cotton substrate after precursor deposition show new peaks at 12.8° and 25.8° (Figure 3.2g), which can be assigned to the (001) and (002) planes of CHN.⁸⁴ For the CHN-deposited cotton sample, new FTIR absorption bands were observed at approximately 1315 and 1420 cm^{-1} which can be assigned to the symmetric and asymmetric vibration stretching modes of the nitrate ions (NO_3^-) in CHN (Figure 3.2h).⁴³

To investigate the process of MOF growth from the predeposited CHN layer, the cotton textile samples were immersed in a BTCA solution (0.1 M) and periodically characterized by several techniques. SEM images revealed that small crystals with diameters below 200 nm formed on the cotton fiber surface after only 1 min of treatment in the BTCA solution. On the basis of PXRD characterization, the newly formed crystals were identified as

HKUST-1. After 5 min of reaction, the surface coverage of the fiber was near completion with submicrometer-sized HKUST-1 particles and with prolonged immersion, the octahedral HKUST-1 crystals on the fiber surface grew larger.

This observation indicates that reagents can diffuse in or out through the intercrystalline voids and/or pores of HKUST-1 which facilitates further crystal growth.^{55,85} The particles formed a stable morphology with a diameter of approximately 2 μm after 30 min of reaction because of the exhaustion of the CHN precursor. Importantly, the MOF coating is continuous, and the crystals are extensively intergrown, implying the high mechanical stability of the coating.⁸⁶ The HKUST-1 peaks in the PXRD pattern became stronger and sharper with increasing reaction time conforming the continuous growth of the HKUST-1 crystals. After 30 min, the intensity of the HKUST-1 peaks no longer increased and the peaks that correspond to the precursor disappeared. Throughout PXRD screening at different time points, no by-products, such as copper oxide, were found. The transformation of CHN to HKUST-1 was further confirmed by FTIR spectra. After exposure of the CHN-coated cotton to the ligand solution, the bands corresponding to the nitrate groups gradually disappeared, whereas new stretching vibration modes for C=O (at 1374 and 1649 cm^{-1}) and bending vibration modes for =C-H (at 762 and 730 cm^{-1}) formed and became stronger with increasing reaction time.⁴³ These prominent peaks are consistent with the pattern of the HKUST-1 powder synthesized from CHN particles dispersed in the solvent. The observed spectral changes demonstrate the replacement of the nitrate anions by the BTCA ligand.

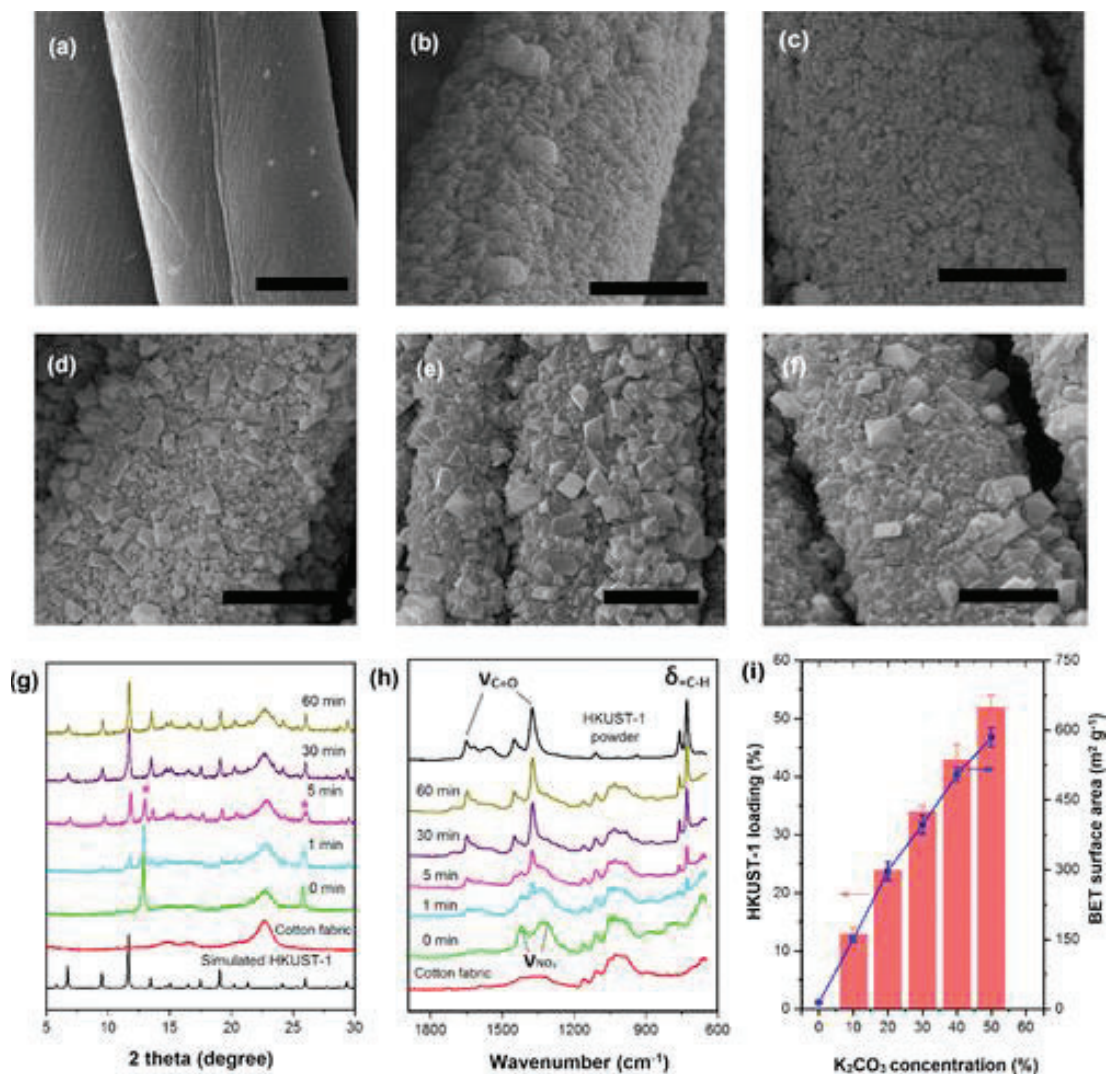


Figure 3.2. SEM images showing the changes in the cotton fiber surface: pristine cotton fiber (a) and CHN-deposited cotton fiber from 20% K_2CO_3 before (b) and after BTCA treatment for 1 (c), 5 (d), 30 (e), and 60 min (f). All scale bars are 10 μm . (g) XRD patterns and (h) FTIR spectra of the corresponding samples. The asterisks in (g) mark the XRD pattern of the CHN precursor. (i) HKUST-1 loading and S_{BET} of the MOF/cotton composites prepared from different K_2CO_3 concentrations.

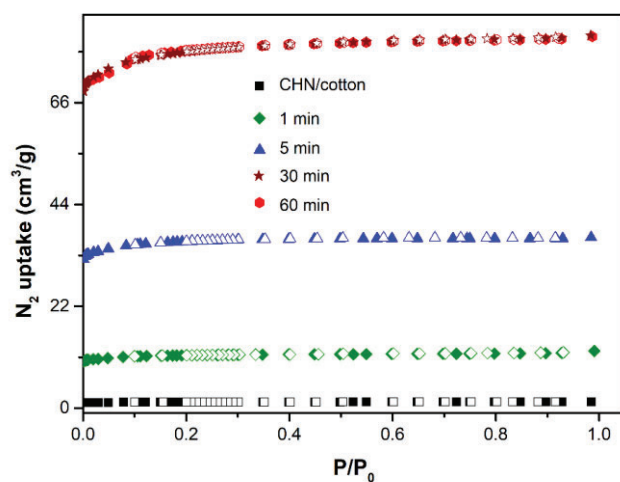


Figure 3.3. Nitrogen adsorption-desorption isotherms of the HKUST-1/cotton sample with different reaction time.

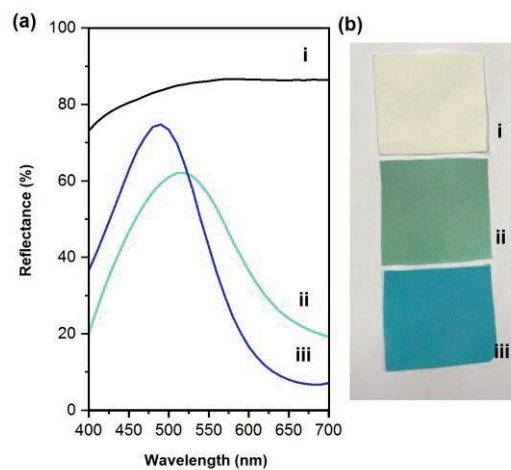


Figure 3.4. UV-vis reflection spectra (a) and photographs (b) of cotton (i), CHN/cotton (ii), and HKUST-1/cotton (iii).

Nitrogen adsorption–desorption isotherms of samples after different reaction times were also measured to monitor the progress of reaction (Figure 3.3). It is clear that N_2 uptake of the samples did not change after 30 min, indicating that the reaction is complete after 30

min, which is consistent with PXRD and FTIR measurements. The green color of the CHN-deposited cotton sample became turquoise after the reaction (Figure 3.4), giving a visual indication of HKUST-1 formation.^{30,43} The MOF mass loading on the fiber, which was calculated from the copper elemental analysis using ICP–OES, is 24.7%. The thickness of the coating is approximately 3 μm based on the observation of a crack formed after ultrasonic treatment for 10 min (Figure 3.5).

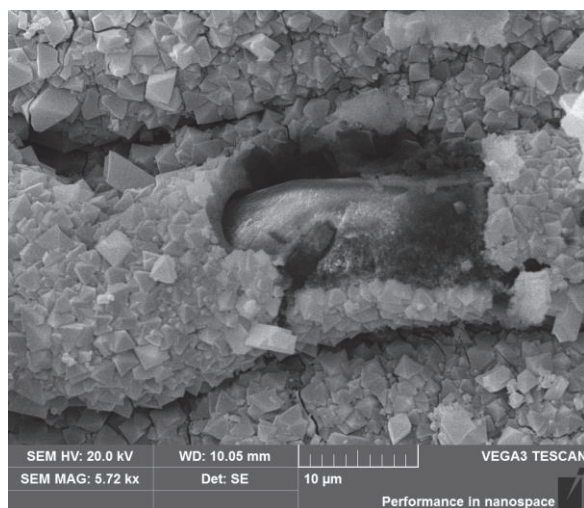


Figure 3.5. SEM image of the HKUST-1/cotton sample subjected to ultrasonic treatment for 10 min. The thickness of the coating is approximately 3 μm based on observation of the crack in the image.

The limited solubility of the inorganic base (K_2CO_3) in ethanol played a critical role in precursor deposition and the final MOF loading. When the absorbed K_2CO_3 was replaced by an equivalent amount of ethanol–soluble NaOH, very few HKUST-1 particles formed on the fiber surface and the loading was only 1.7%, as calculated from the copper elemental analysis, owing to poor precursor deposition (Figure 3.6).

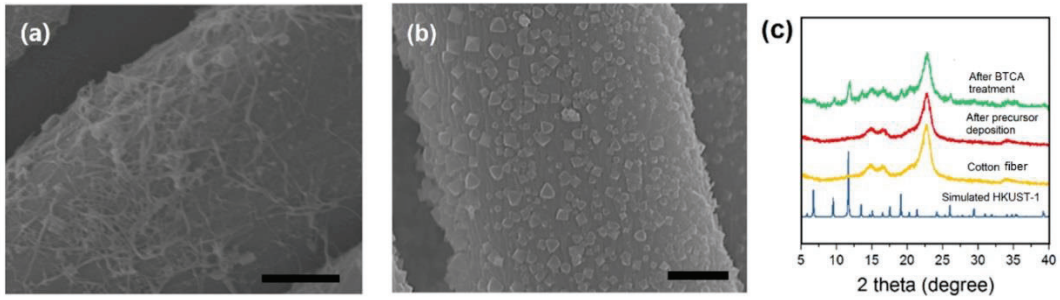


Figure 3.6. SEM images of (a) the sample after precursor deposition using an equivalent amount of NaOH as an inorganic base and (b) after BTCA treatment. All scale bars: 2 μm . (c) XRD patterns of the corresponding samples.

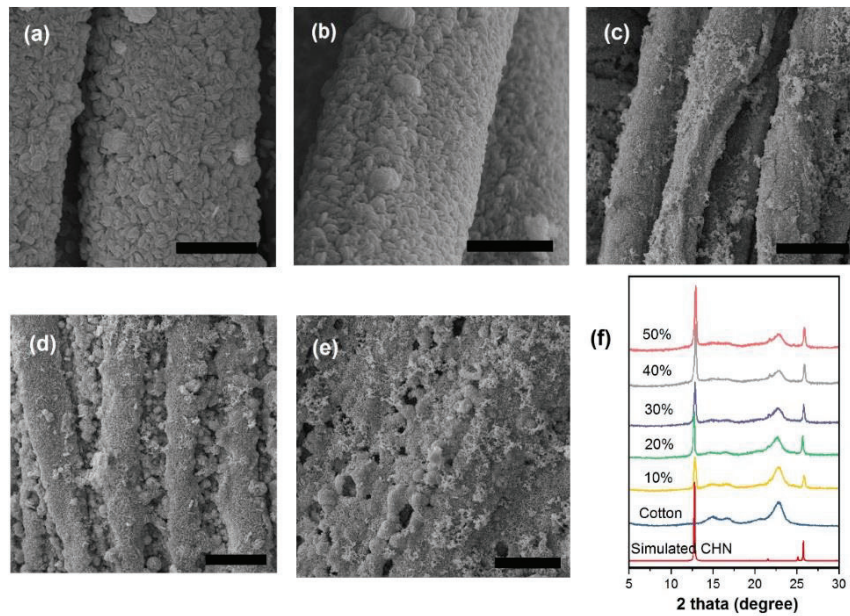


Figure 3.7. SEM images of the samples after CHN deposition from different K_2CO_3 concentrations. (a) 10%, (b) 20%, (c) 30%, (d) 40%, and (e) 50%. Scale bars: 10 μm (a, b), 20 μm (c-e). (f) XRD patterns of the corresponding samples.

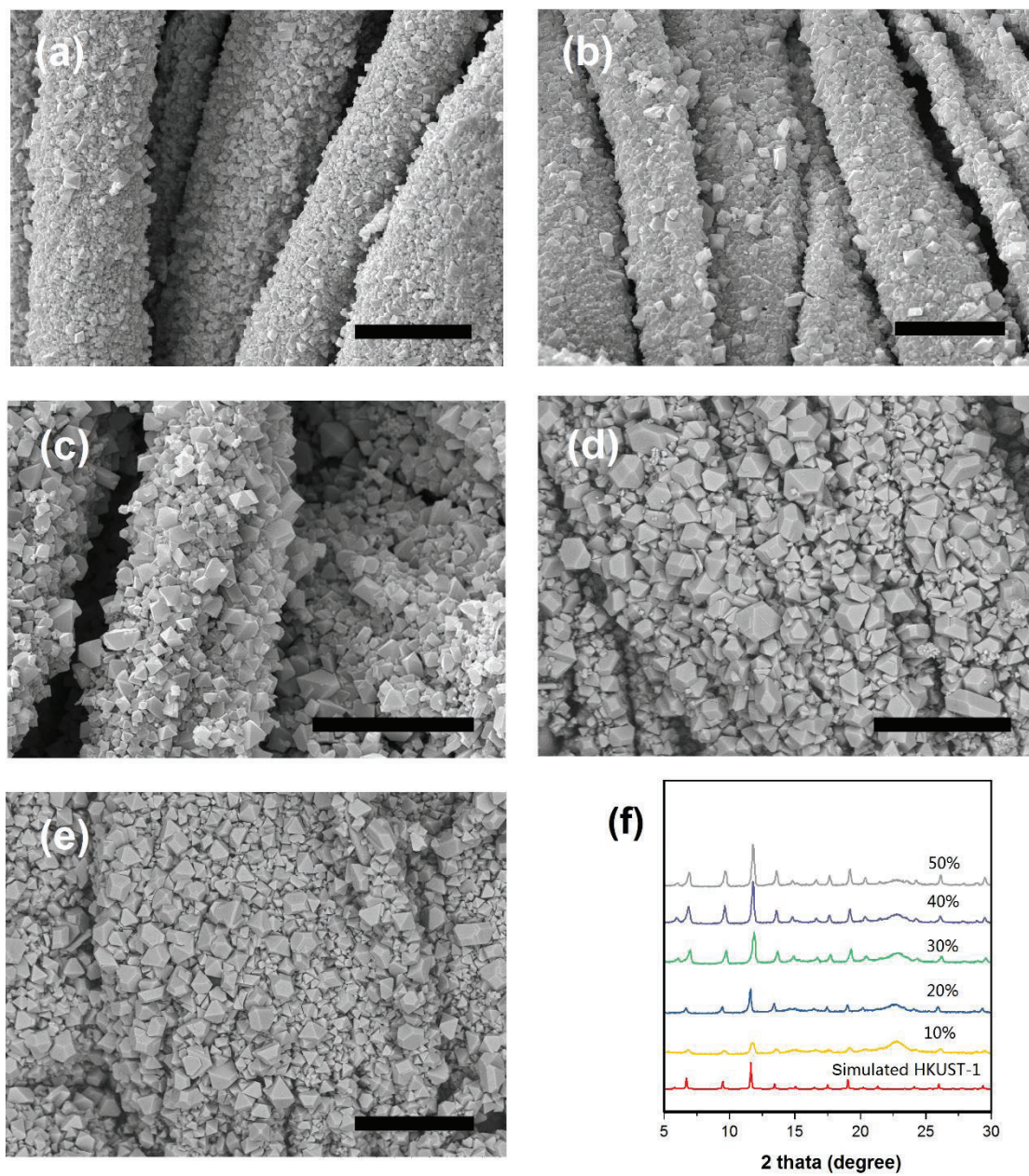


Figure 3.8. Tuning the HKUST-1 loading by adjusting the K_2CO_3 concentration. SEM images of samples obtained from different K_2CO_3 concentrations: (a) 10%, (b) 20%, (c) 30%, (d) 40%, (e) and 50%. All scale bars: 20 μm . (f) XRD patterns of the corresponding samples.

By tuning the K_2CO_3 concentration used in precursor deposition, different CHN precursor loadings on the cotton textile and corresponding HKUST-1 loadings were obtained (Figure 3.2i, Figure 3.7, and Figure 3.8). The HKUST-1 mass loading on the cotton textile increased from 13 to 54% when the K_2CO_3 concentration increased from 10 to 50%, whereas the corresponding areal MOF loading on the textile increased approximately from 43 to 320 g m^{-2} (Table 1).

For the samples with higher loadings, HKUST-1 crystals as large as $5\text{ }\mu\text{m}$ were observed because of the presence of a sufficient supply of copper precursor for continued HKUST-1 growth (Figure 3.8d,e). The complete conversion of the precursors and the high purity of the MOF crystals on the fibrous composite were confirmed by PXRD patterns (Figure 3.8 f).

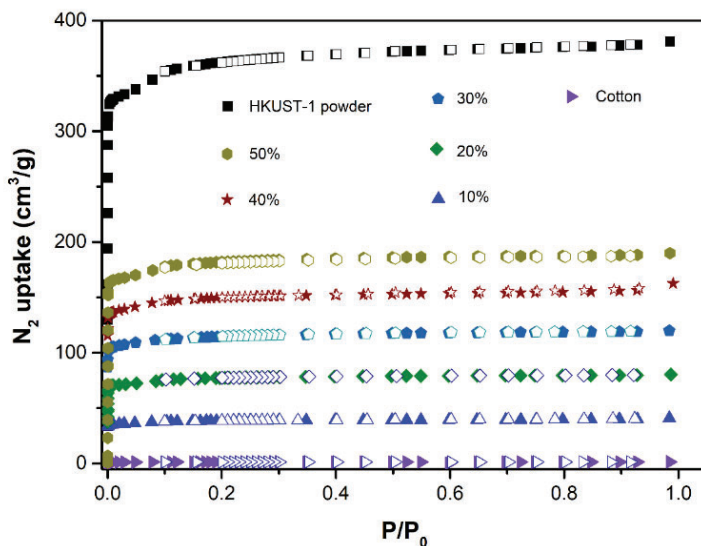


Figure 3.9. Nitrogen adsorption-desorption isotherms of the HKUST-1/cotton samples obtained from different K_2CO_3 concentrations at 77 K up to 1 bar. The solid and open markers represent adsorption and desorption points, respectively.

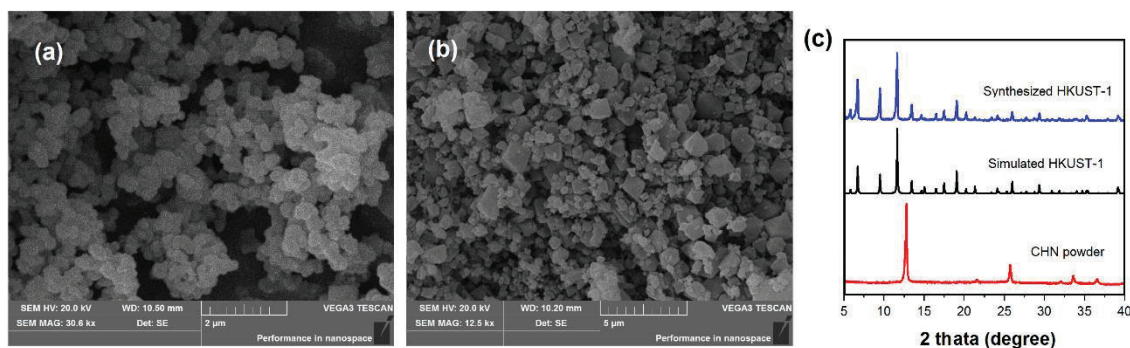


Figure 3.10. SEM images of CHN particles (a) and HKUST-1 particles (b). (c) XRD patterns of the corresponding samples.

Table 3.1. Summary of the HKUST-1 MOF loading and BET surface area (S_{BET}) results.

K_2CO_3 concentration (%)	MOF mass loading (%)	MOF areal loading (g m^{-2}) ^{a)}	S_{BET} of the composite ($\text{m}^2 \text{g}^{-1}$)	S_{BET} of the MOF component ($\text{m}^2 \text{g}^{-1}$) ^{b)}
10	13.4±1.1	42.9	151±7	1127
20	24.7±0.8	74.5	297±20	1202
30	35.0±0.9	149.2	396±22	1054
40	44.3±2.5	220.3	504±35	1145
50	53.6±2.2	320.0	584±33	1081

Note: ^{a)}MOF areal loading = MOF mass loading*277/(100% - MOF mass loading), where 277 is the areal density of cotton fabric, g m^{-2} ; ^{b)}BET surface area of HKUST-1 component = (S_{BET} of the MOF/cotton composite - S_{BET} of cotton)/MOF mass loading.

N_2 adsorption (77 K) measurements demonstrated that the MOF-modified cotton substrates possessed large porosities. Samples activated under vacuum at 100 °C for 24 h show an

apparent BET surface areas (S_{BET}) in the range of 150–580 $\text{m}^2 \text{g}^{-1}$ (Figures 3.2 i, Figure 3.9, and Table 1). On the basis of the MOF mass loading of each sample, the estimated S_{BET} of the HKUST-1 component is from 1050 to 1200 $\text{m}^2 \text{g}^{-1}$, which is in the range of the HKUST-1 powder (1360 $\text{m}^2 \text{g}^{-1}$) produced from the dispersed CHN precursor (Figure 3.10).

In this reaction, we chose an eco-friendly water/ethanol mixture as the reaction medium. The effect of the water volume percentage (v/v %) in solution on the formation of the MOF coating was investigated. If the absolute ethanol was solely used as the solvent in the reaction, small HKUST-1 crystals with sizes below 1 μm formed on the fiber surface after 1 h of reaction and PXRD patterns indicated that partial transformation of CHN to HKUST-1 occurred. When 10% v/v water was added to the solvent mixture, dense octahedral crystals with sizes of approximately 2 μm formed and PXRD patterns revealed that complete conversion of the CHN precursor to HKUST-1 had occurred after 1 h. However, when the volume percent of water in the solvent mixture was above 30%, the HKUST-1 crystal coating became much looser and the loading decreased (Figure 3.11 and Table 2)

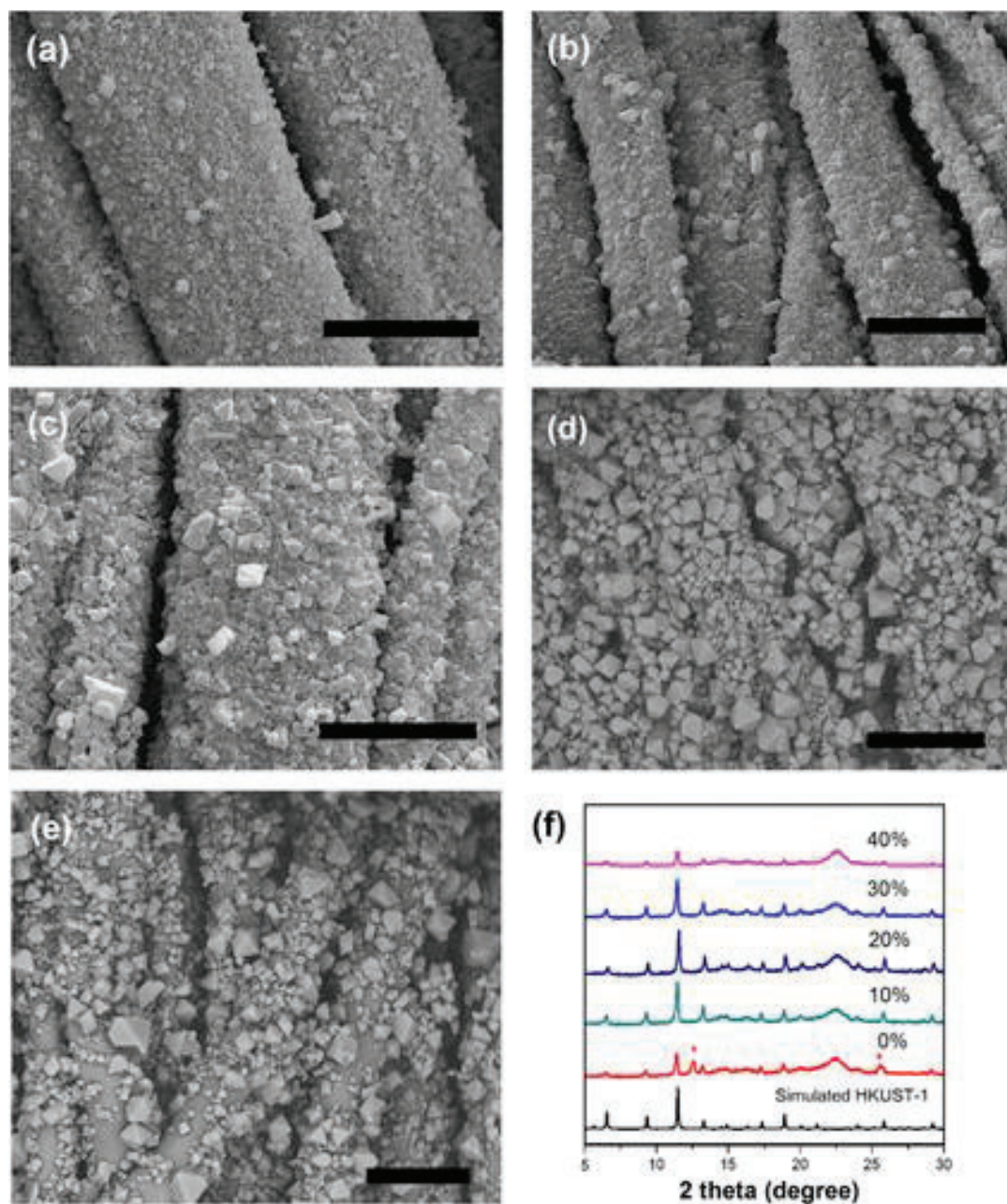


Figure 3.11. SEM images of samples prepared from ligand solutions containing different volume percentages of water: (a) 0, (b) 10, (c) 20, (d) 30, and (e) 40%. All scale bars are 20 μm . (f) PXRD patterns of the corresponding samples. The asterisks in (f) mark the pattern of the unreacted CHN precursor. All samples were treated with the ligand solution for 60 min. The asterisks in (f) mark the XRD pattern of the CHN precursor.

Table 3.2. Effect of the water volume percentage on the HKUST-1 mass loading

Water volume percentage (%)	MOF mass loading (%)
10	24.7±0.8
20	21.2±0.6
30	18.1±0.9
40	11.6±0.9

On the basis of the observations outlined above, a coupled “dissolution–reprecipitation” mechanism can be applied to explain the coordination replication reaction, as illustrated in Figure 3.12.⁵⁵ In an acidic BTCA solution with a low water percentage, a localized precursor/liquid interface layer supersaturated with cupric ions forms during the dissolution of CHN. Reaction between the dissolved cupric cations and BTCA ligands generates HKUST-1 nuclei on the fiber surface within 1 min because of the fast crystallization kinetics. As the metal ions are consumed, the interface layer is recharged with freshly released metal ions, which feed MOF crystal growth by reacting with the organic linker in the solution. By controlling the spatial localization of the heterogeneous crystallization process, the HKUST-1 crystals were nucleated at the precursor solid/liquid interface, enabling the formation of a continuous MOF coating composed of intergrown crystals when a sufficient amount of precursor is provided. The occurrence of highly localized MOF crystallization on the fiber surface was also proven by the CHN precursor utilization efficiency analysis. The copper areal density on the HKUST-1/cotton sample

prepared from the medium containing 10% (v/v) water was 23.5 g m^{-2} , which is only slightly lower than that of the CHN-deposited cotton sample (25.6 g m^{-2}). This result indicates that 91.8% of the copper ions from the CHN was transformed into the HKUST-1 coating and immobilized on the cotton fibers.

The water percentage in the ligand solution played a critical role in forming the intergrown HKUST-1 coating. The presence of a small amount of water in the reaction media could reduce the pH of the solution by deprotonating the organic ligand (BTCA), which could promote the release of cupric ions from the precursor for subsequent MOF crystal growth.^{57,58,87} The accelerated conversion of insoluble precursors to MOFs in the presence of water was also reported in other studies.^{57,87} Excess water (above 30% v/v), however, led to poor MOF loading and a scattered coating because of rapid precursor (CHN) dissolution does not allow for the formation of supersaturated ion interface layer. Similarly, Kitagawa et al. reported that the MOF crystallization kinetics must be faster than the precursor dissolution kinetics to convert pre-shaped alumina to the aluminum naphthalene dicarboxylate framework ($\text{Al}(\text{OH})(\text{ndc})$) by the coordination replication method.^{55,87} In their reports, microwave heating was utilized to accelerate the crystallization kinetics, whereas in our study, the ultrafast MOF crystallization kinetics in the room-temperature conversion of layered CHN is an innate advantage for the preparation of localized MOF coatings. Fast crystallization kinetics was also observed in the synthesis of HKUST-1 powder using dispersed CHN particles and a BTCA ligand solution (Figure 3.10), in which an exceptionally high space-time yield of $2.66 \times 10^4 \text{ kg m}^{-3} \text{ d}^{-1}$ was obtained.

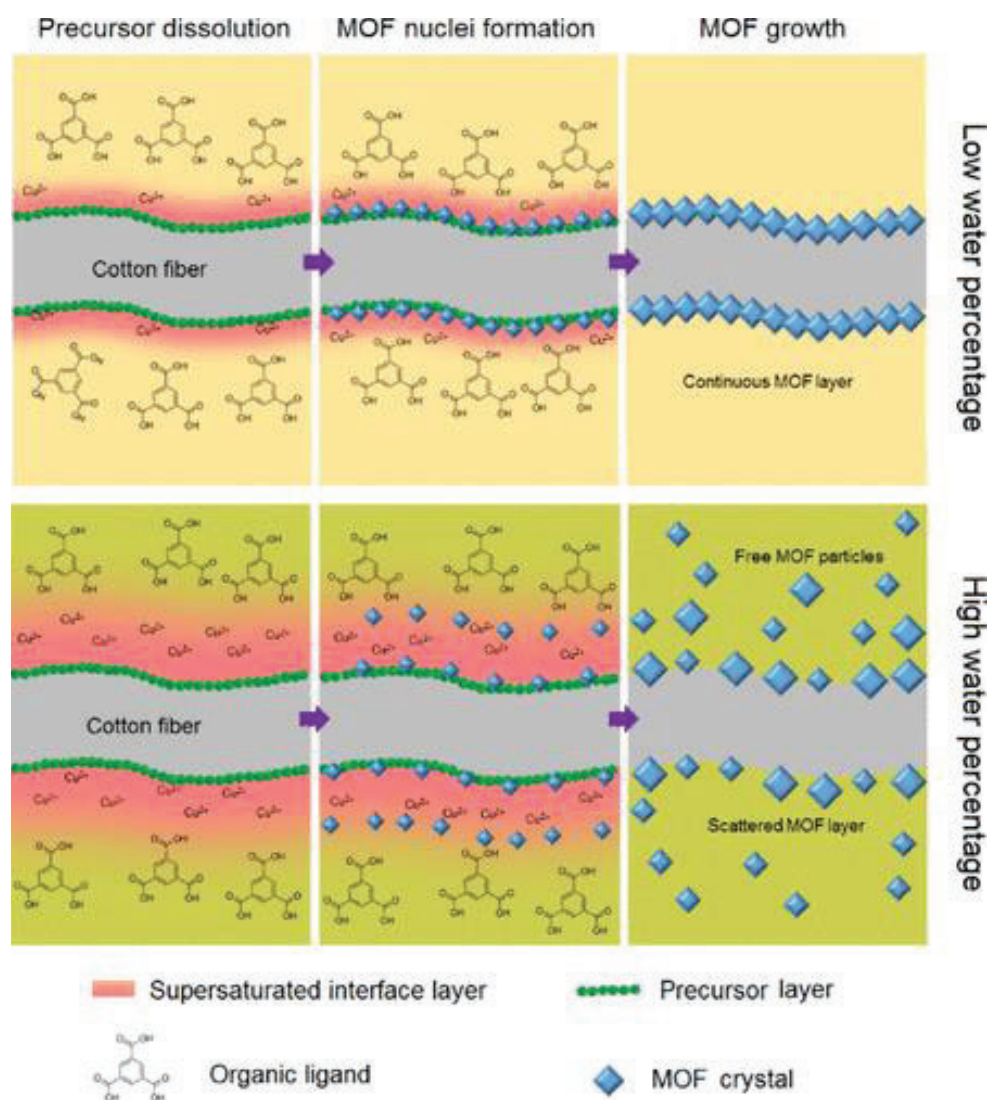


Figure 3.12. Schematic illustration of the “dissolution–reprecipitation” mechanism.

Table 3.3. Change in the HKUST-1 loading after 24 h of stirring at 500 r/min.

Water volume percentage (%)	Mass loading before stirring (%)	Mass loading after stirring (%)	Mass loading loss percentage (%)
10	24.7±0.8	22.5±0.7	8.9
30	18.1±0.9	1.4±0.2	92.0

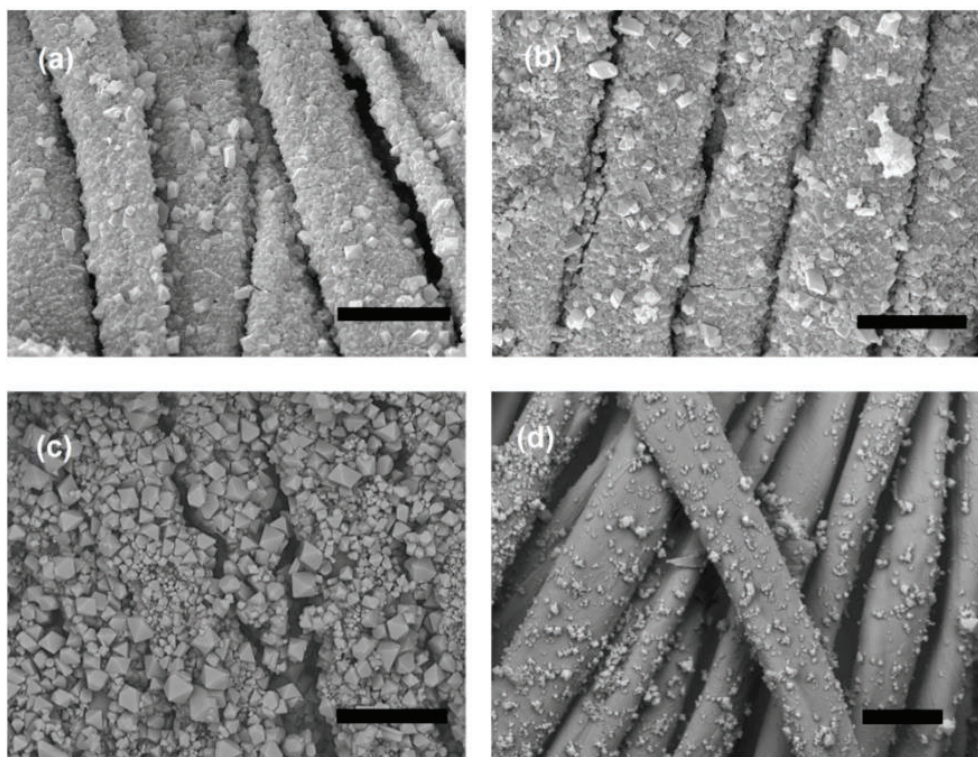


Figure 3.13. SEM images of samples synthesized from ligand solutions with 10% v/v water (a) and 30% v/v water (c) before and (b, d) after stirring for 24 h at 500 rpm. All scale bars: 20 μm .

High robustness of the MOF coating layer in the composite is an essential requirement for its practical applications, as the disintegration of loose MOF particles could reduce the lifespan of MOF-functionalized composites.³⁶⁻³⁸ The adhesion of an extensively intergrown MOF coating to a cotton fiber was tested through vigorous stirring (500 rpm) of the sample in ethanol for 24 h, and only a slight loss of particles was observed by SEM measurements (Figure 3.13). Quantitative copper analysis by ICP-OES showed that approximately 8.9% of the initial MOF coating peeled during vigorous stirring (Table 3). When a sample with a less extensively intergrown HKUST-1 coating was exposed to the

same stirring conditions, most of (92%) the particles were removed (Table 3). This result indicates that the continuous and intergrown morphology of the MOF coating layer efficiently enhances the stability of the composite materials.^{55,86}

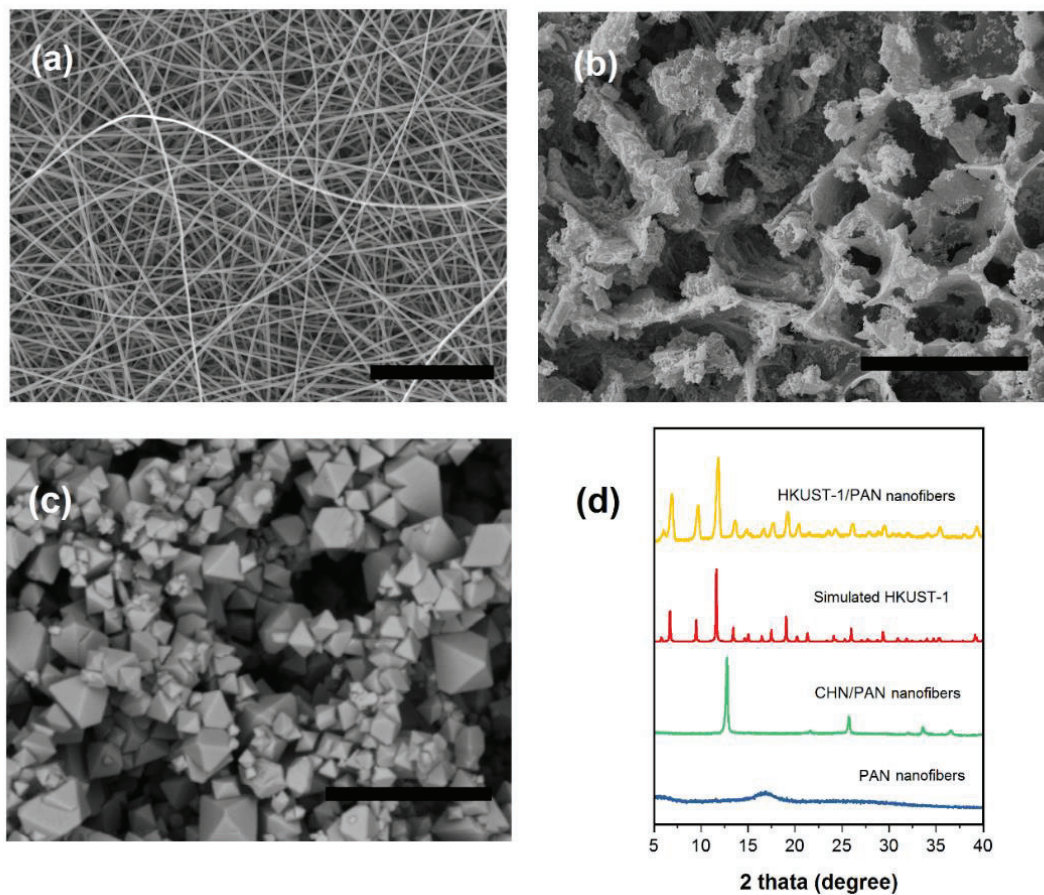


Figure 3.14. Coating HKUST-1 on PAN nanofibers. SEM images of (a) PAN nanofibers, (b) CHN-deposited PAN nanofibers, and (c) HKUST-1-coated PAN nanofibers. Scale bars: 10 μm (a) and 20 μm (b, c). (d) XRD patterns of the corresponding samples.

It is important to demonstrate transferability of our findings from HKUST-1/cotton composites to other fiber substrates because different applications require composites of different chemical, mechanical, and/or physical properties. Therefore, we prepared dense

HKUST-1 coatings on other fibrous materials, including an electrospun PAN nanofiber (500 nm) mat and a commercial PET microfiber (5 μm) textile, possessing different fiber diameters and surface properties compared to the cotton fiber (for detailed fabrication and characterization information, see Figures 3.14, Figures 3.15, Figures 3.16 and Table 4).

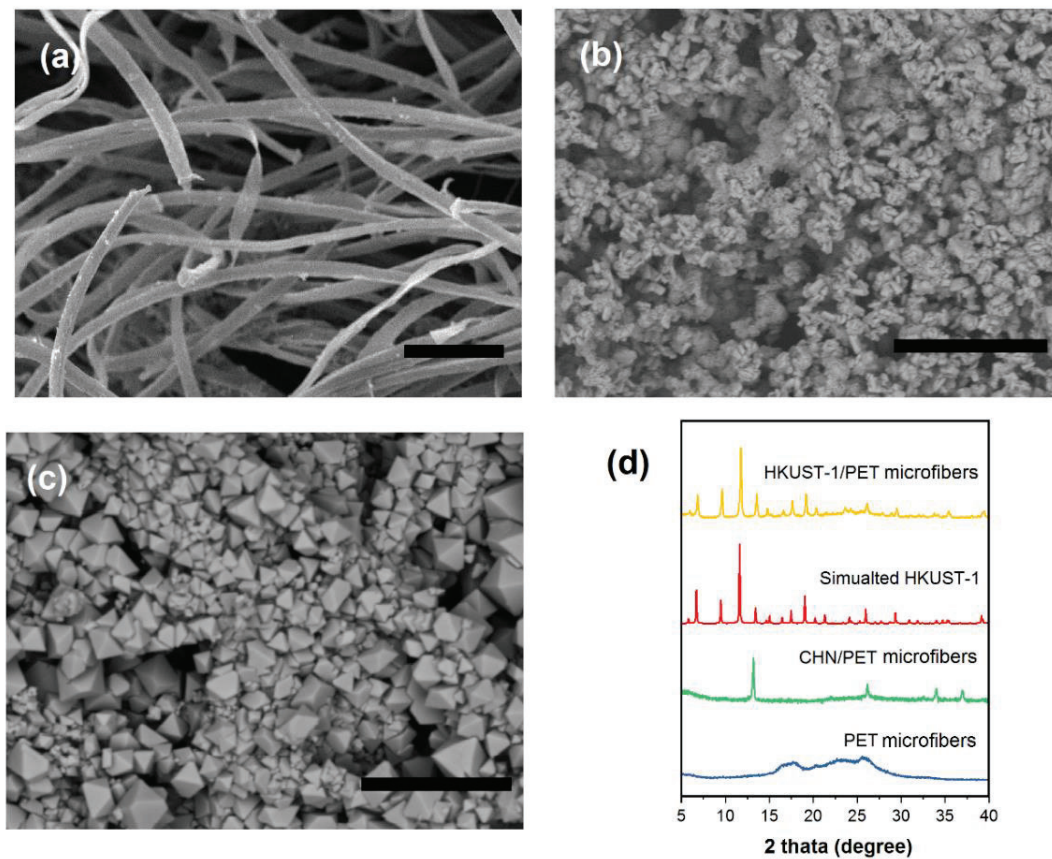


Figure 3.15. Coating HKUST-1 on PET microfibers. SEM images of (a) PET microfibers, (b) CHN-deposited PET microfibers, and (c) HKUST-1-coated PET microfibers. Scale bars: 50 μm (a) and 20 μm (b, c). (d) XRD patterns of the corresponding samples.

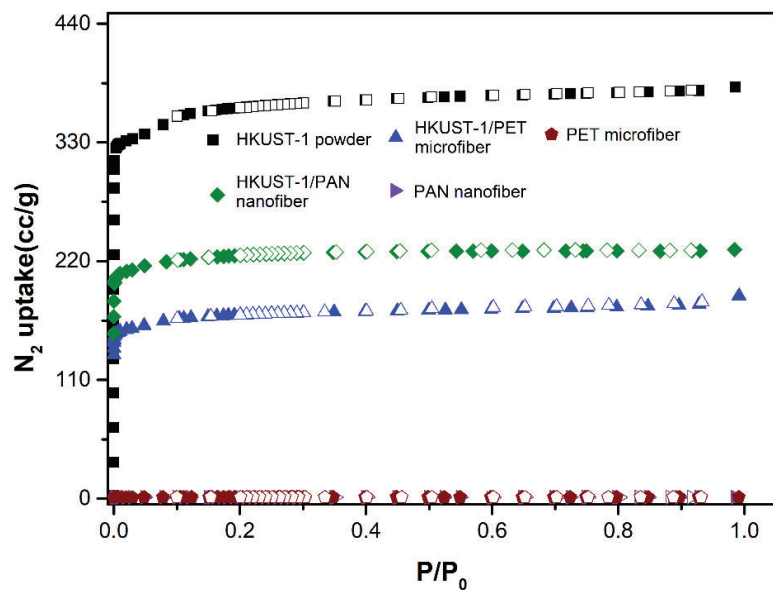


Figure 3.16. Nitrogen adsorption-desorption isotherms of the PAN nanofibers and PET microfibers before and after HKUST-1 coating at 77 K up to 1 bar. The solid and open markers represent the adsorption and desorption points, respectively.

Table 3.4. HKUST-1 loading and S_{BET} of the PAN nanofibers and PET microfibers

Fiber substrate	MOF mass loading (%)	MOF areal loading (g/m^2)	S_{BET} of the composite ($\text{m}^2 \text{g}^{-1}$)	S_{BET} of the MOF component ($\text{m}^2 \text{g}^{-1}$)
PAN nanofibers	72.9 ± 4	161.4	893 ± 91	1225
PET microfibers	64.2 ± 6	480.6	677 ± 67	1056

Additionally, several other MOFs were successfully coated onto a cotton fiber by altering the ligands and/or metal precursors besides the archetypical HKUST-1. For example, a

flower-like Cu-BDC (where BDC is 1,4-benzenedicarboxylate) coating was prepared on a cotton textile when the BTCA ligand was replaced with 1,4-benzenedicarboxylic acid (BDCA) (Figure 3.17b).^{43,89}

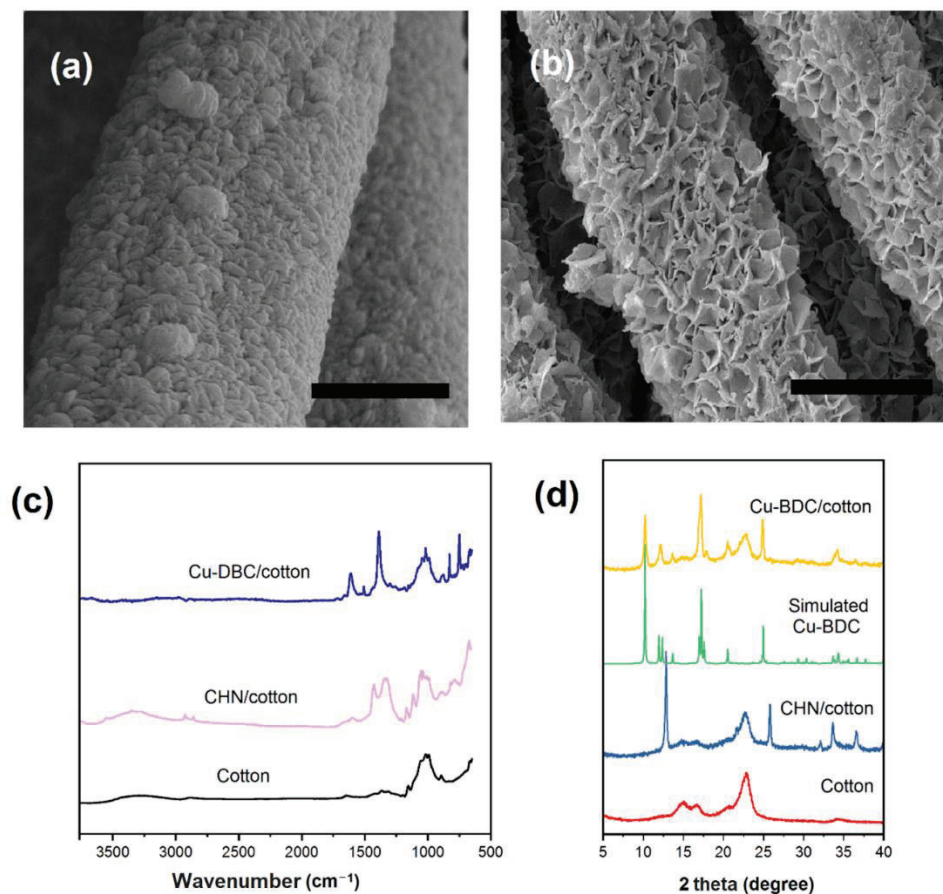


Figure 3.17. SEM images of (a) CHN-deposited cotton and (b) Cu-BDC-coated cotton.

Scale bars: 10 μm (a) and 20 μm (b). (c) FTIR spectra and (d) XRD patterns of the corresponding samples.

The CHN-deposited fiber sample showed a remarkable change in the surface morphology after treatment with the BDCA ligand solution. Specifically, a continuous flower-like coating formed on the fiber surface. The length of each flake was 3-4 μm, and the thickness

was approximately 200-300 nm. The conversion from CHN to Cu-BDC was investigated by FTIR. Similar to the case of HKUST-1, after BDCA treatment, the absorption bands at 1315 cm^{-1} and 1420 cm^{-1} assigned to the vibration stretching modes of the nitrate ions in CHN disappeared. At the same time, new stretching modes associated with C=O at 1384 cm^{-1} and 1607 cm^{-1} and the bending vibration nodes for =C-H at 829 cm^{-1} and 747 cm^{-1} were observed.⁹⁰ Additionally, the conversion was thoroughly confirmed by XRD. The newly formed XRD peaks are consistent with the peaks in the simulated Cu-BDC pattern and also agree well with those reported in the literature.

Similarly, through reactions between pre-deposited insoluble zinc and cobalt precursors with 2-methylimidazole, two kinds of zeolitic imidazolate frameworks, ZIF-8 and ZIF-67, were coated onto cotton substrates. All of these MOF coatings on fiber substrates were observed via SEM experiments, and the identities of the prepared coatings were thoroughly confirmed by PXRD, FTIR, and ICP-OES studies (Figure 3.17, Figure 3.18, Figure 3.19 and Table 5). The results indicate that different kinds of MOF coatings can be prepared on fiber substrates to meet the various needs of specific applications by utilizing coordination replication method described here.

The zinc precursor, zinc hydroxy acetate (ZHA), was deposited onto cotton fiber sample, which exhibited a rough surface morphology as shown in Figure 3.18. The identity of the precursor was verified by FTIR and XRD analysis.⁹¹ The strong bands observed at 1500 and 1382 cm^{-1} in the FTIR spectrum of the ZHA-deposited cotton sample were due to the antisymmetric and symmetric vibrations of the carboxylate groups.⁹¹ Figure 3.18d shows the XRD pattern of ZHA-deposited cotton, and the 2 theta peaks observed at 7.6° , 13° , and 20° correspond to the (001), (002), and (003) crystal planes of ZHA.⁹²

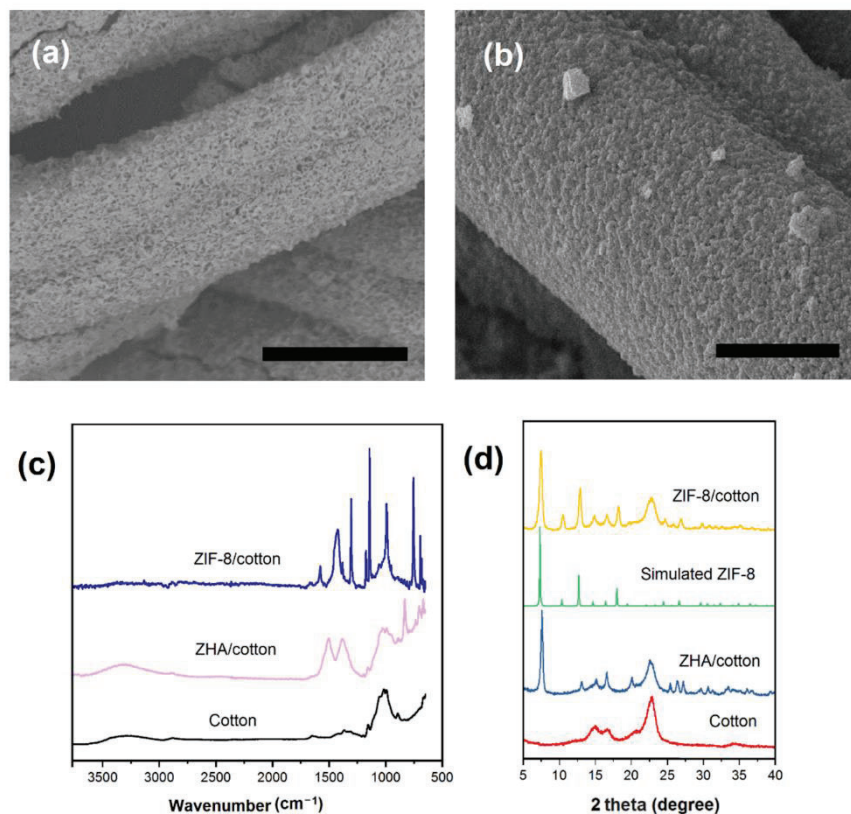


Figure 3.18. SEM images of (a) ZHA-deposited cotton and (b) ZIF-8-coated cotton.

Scale bars: 20 μm (a) and 5 μm (b). (c) FTIR spectra and (d) XRD patterns of the corresponding samples.

After treatment with the 2-methylimidazole ligand solution, dense particles with sizes of approximately 200 nm were observed on the fiber surface, composing a continuous coating. In the FTIR spectrum of the ligand-treated sample, these two bands corresponding to carboxylate vibrations decreased while new bands appeared. The peak observed at 1578 cm^{-1} resulted from the C=N stretching mode, and the intense band observed at 1424 cm^{-1} was assigned to the 2-methylimidazolate ring stretching vibration.⁹² The bands in the region of 1175–940 cm^{-1} are associated with the in-plane bending of the 2-methylimidazolate ring,

and those peaks at 754 and 693 cm^{-1} resulted from the out-of-plane bending of the ring.⁹³ Moreover, the coating was identified as ZIF-8 by XRD test.⁹³

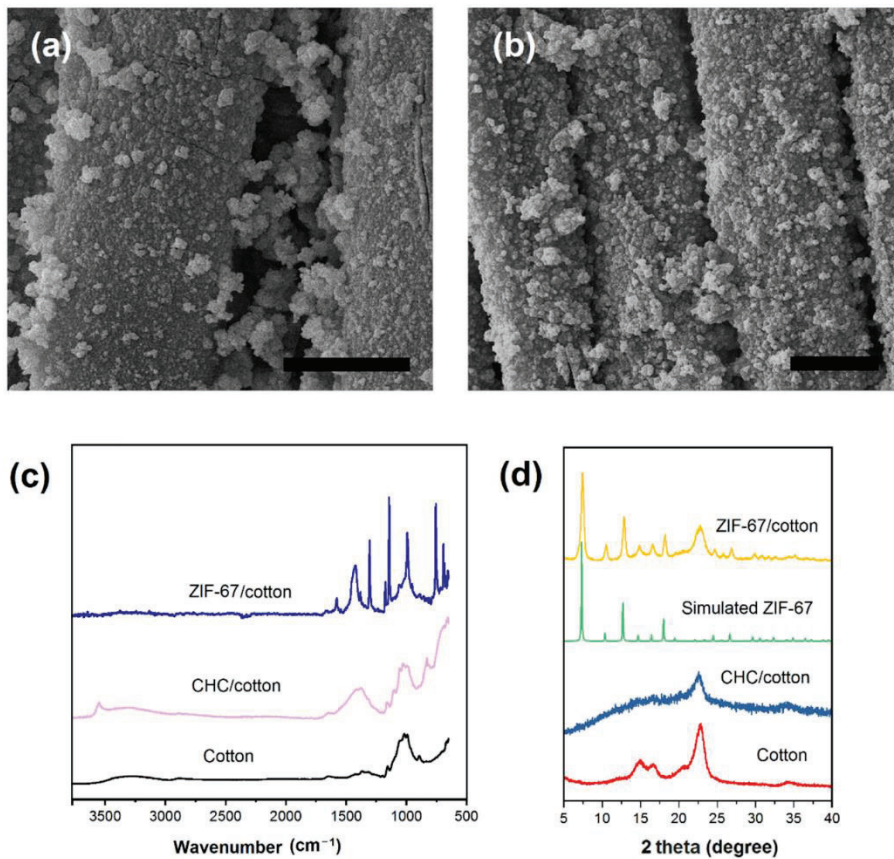


Figure 3.19. SEM images of (a) CHC-deposited cotton and (b) ZIF-67-coated cotton. All scale bars: 10 μm . (c) FTIR spectra and (d) XRD patterns of the corresponding samples.

The insoluble cobalt hydroxy carbonate (CHC) layer was deposited fiber as the cobalt precursor. After treatment with the 2-methylimidazole ligand solution, a continuous coating composed of dense particles formed on the fiber surface. The particle size was approximately 1 μm . The conversion from CHC to ZIF-67 was investigated by XRD and FTIR spectroscopy. The hydroxy group (O-H) stretching mode at 3550 cm^{-1} and the

carbonate (CO_3^{2-}) stretching vibration mode at 1418 cm^{-1} were clearly observed in the FTIR spectrum of the CHC/cotton sample.⁹⁴ After ligand treatment, these two bands vanished, while new bands corresponding to 2-methylimidazole appeared, which is very similar to the case of the ZIF-8/cotton sample.⁹³ The undefined XRD peaks of the CHC-deposited sample suggests the amorphous nature of the CHC precursor. After ligand treatment, unambiguous XRD peaks assigned as ZIF-67 were observed.⁴⁵

Table 3.5. MOF mass loading on Cu-BDC/cotton, ZIF-8/cotton, and ZIF-67/cotton

MOF	Mass loading (%)
Cu-BDC	24.3±0.5
ZIF-8	21.6±0.7
ZIF-67	22.6±0.7

By controlling the initial inorganic base position, specific MOF patterns could be obtained (Figure 3.20a and Figure 3.21). This facile MOF patterning approach offers easy access to the fabrication of flexible and wearable devices such as sensors.³⁰ Remarkably, this facile and inexpensive synthetic approach is a greener method because it is performed under ambient conditions in ethanol (as opposed to DMF) and results in high precursor utilization, making it easy to scale up for bulk production. Figure 3.20b shows large pieces of cotton fabric ($12\text{ cm} \times 54\text{ cm}$) coated with HKUST-1, ZIF-8, and ZIF-67. The scaled-up samples showed very similar MOF surface morphologies and mass loadings compared to small-scale batches (Figure 3.22 and Table 6). Under the mild operation conditions without extensive heat, the MOF-functionalized textiles preserved the mechanical properties of parent textiles. The room-temperature scaled-up MOF/cotton samples maintained 90% of

the breaking strength that of the pure cotton sample (see Figure 3.20c and Table 7), thus expanding the application scope to thermally sensitive polymeric materials.

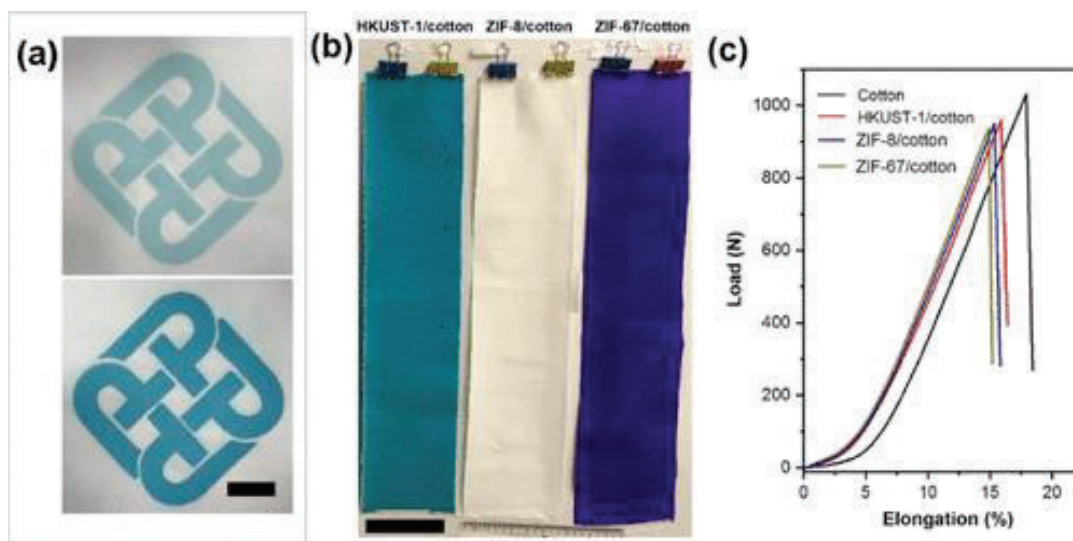


Figure 3.20. (a) CHN pattern (above) and replicated HKUST-1 pattern (below). Scale bar: 2 cm. (b) Photograph of scaled-up HKUST-1/cotton, ZIF-8/cotton, and ZIF-67/cotton samples. Scale bar: 10 cm. (c) Load-elongation curves of cotton and scaled-up MOF/cotton samples.

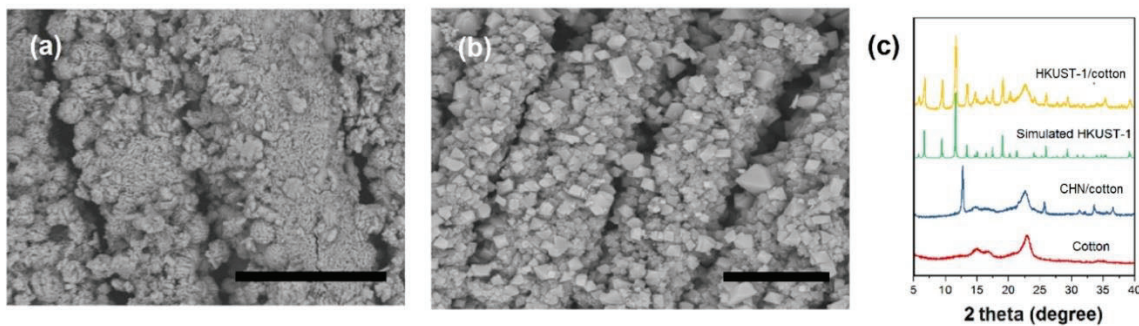


Figure 3.21. SEM images of (a) a CHN precursor patterned sample and (b) the replicated HKUST-1 patterned sample. All scale bars: 20 μm . (c) XRD patterns of the corresponding samples.

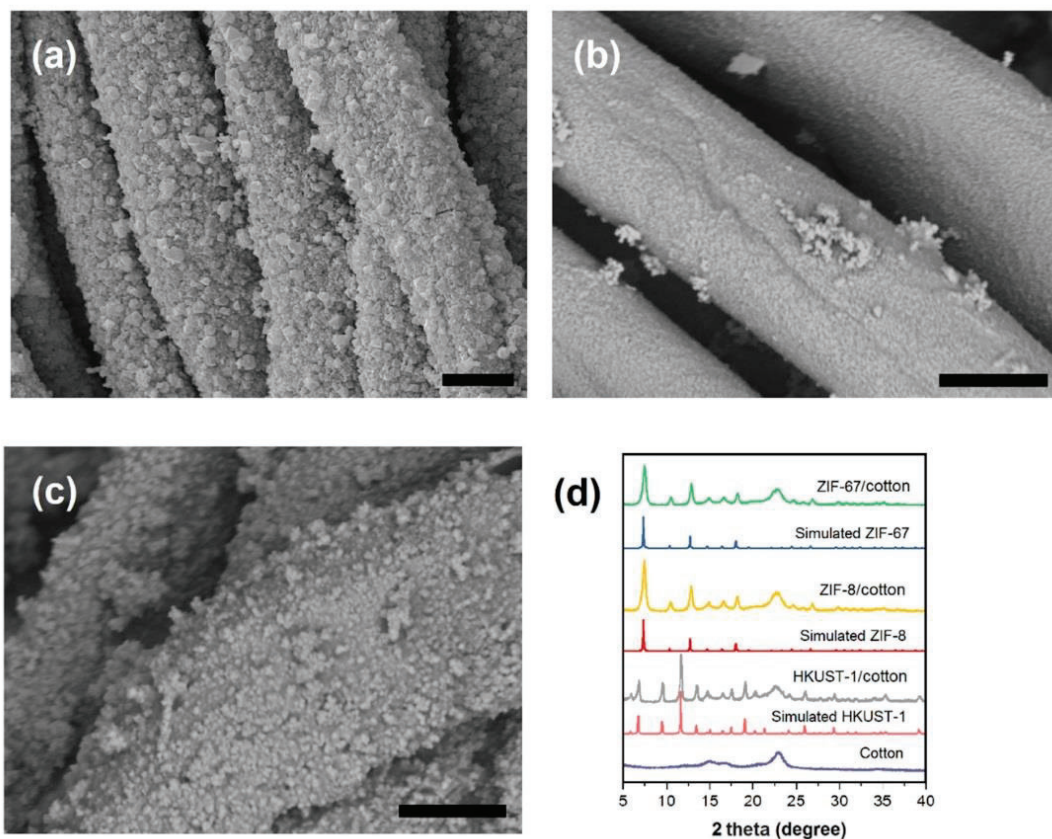


Figure 3.22. SEM images of scaled-up (a) HKUST-1/cotton, (b) ZIF-8/cotton, and (c) ZIF-67/cotton samples. All scale bars: 10 μm . (d) XRD patterns of the corresponding samples.

Table 3.6. MOF mass loadings of the scaled-up HKUST-1/cotton, ZIF-8/cotton, and ZIF-67/cotton samples

MOFs	Mass loading (%)
HKUST-1	25.3 \pm 0.8
ZIF-8	22.7 \pm 0.5
ZIF-67	24.5 \pm 0.7

Table 3.7. Mechanical properties comparison of cotton and the scaled-up samples

Sample	Breaking strength (N)	Breaking elongation (%)
Cotton	1030.9±50.3	18.1±1.8
HKUST-1/cotton	958.7±78.2	16.2±1.2
ZIF-8/cotton	947.2±46.6	15.3±0.8
ZIF-67/cotton	931.6±42.9	14.2±0.7

The superior processability of the flexible MOF/textile composites allow convenient structuring and engineering of these materials such as rolling them into a column or tailoring them to desired shapes for functional device assembly (Figure 3.23a,b). To demonstrate this, we prepared a syringe filter by packaging 4 layers of tailored HKUST-1/cotton composites and the resultant device was used for the continuous liquid-phase removal of the organosulfur compound DBT from an *n*-heptane solution as simulated gasoline.^{95,96} To test the desulfurization efficiency of our MOF/fiber composite, simulated gasoline containing 4000 parts per million weight (ppmw) DBT (or 695 ppmw sulfur) was pushed through the filter using a syringe pump and The simulated gasoline flow was periodically analyzed by UV–visible spectroscopy analysis based on the absorbance calibration curve at 232 nm (Figure 3.24). The DBT breakthrough curves for the fibrous MOF filter are recorded in Figure 3.23c. The sulfur saturation capacity of the HKUST-1_{25%}/cotton and HKUST-1_{54%}/cotton is measured to be 9 and 20 mg g⁻¹, respectively, equivalent to a 37 mg g⁻¹ adsorption capacity based on the HKUST-1 component of the composites, agreeing well with data reported for powdered HKUST-1.^{86,95} This result indicates that the interior of the HKUST-1 crystals in coating is highly accessible for

adsorbing organic sulfur compounds despite its dense packing on the fiber surface. After DBT uptake, the MOF/fiber composite was easily regenerated through immersion in methanol.⁹⁶ It is important noting that more than 95.5% of saturation uptake was retained after three cycles of DBT uptake (Table 8). The dynamic adsorption of sulfur containing compounds in gasoline demonstrated here by the MOF/fiber composite is highly desirable in industrial desulfurization applications.

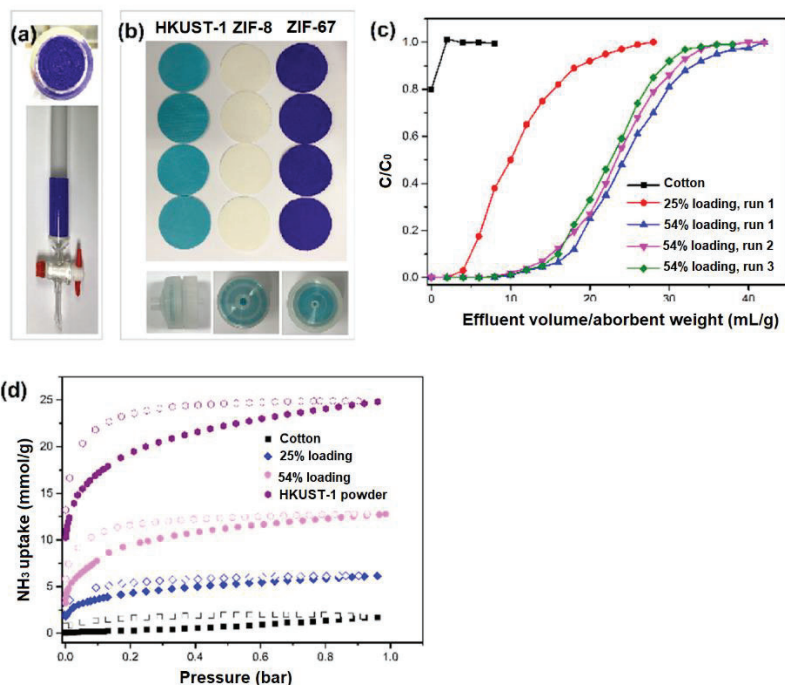


Figure 3.23. (a) Photograph of a glass chromatography column containing a roll of ZIF-67/cotton. Diameter of the column: 3 cm. (b) Photograph of tailored MOF/cotton samples and a syringe filter containing 4 layers of tailored HKUST-1/cotton pieces. Diameter of the tailored samples: 2.5 cm. (c) Breakthrough curves of DBT in *n*-heptane over the tailored samples: 2.5 cm. (d) NH₃ sorption isotherms of HKUST-1/cotton composites at 25 °C up to 1 bar.

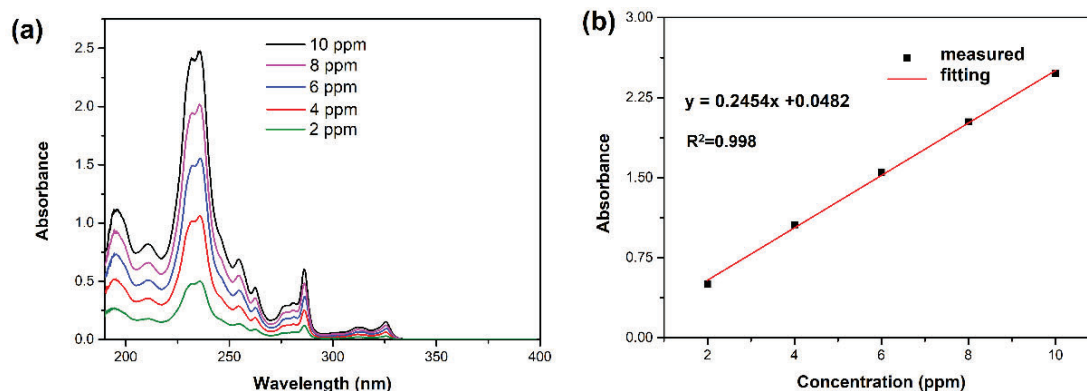


Figure 3.24. UV absorption spectra of DBT in n-heptane with different concentration (a) and the absorbance calibration curve at 232 nm (b).

Table 3.8. Sulfur capacity of HKUST-1/cotton and the HKUST-1 component in different runs

Run	Sulfur capacity of HKUST-1/cotton (mg g^{-1})	Sulfur capacity of the HKUST-1 component (mg g^{-1})
1	20.0	37.0
2	19.7	36.4
3	19.1	35.2

High-performance functional composite fabrics are also highly desirable as alternative ammonia capture filters for personal protection and industrial gas purification on account of the widely produced and toxic nature of ammonia. The ability to tune the MOFs for high uptake capacity and high selectivity toward a target molecule enables MOF-based composites a class of attractive materials for ammonia capture.^{97,98} Thanks to the open Cu sites in HKUST-1, high affinity toward ammonia gas is previously reported in a powder form which renders it attractive for ammonia capture where low concentration of ammonia gas is present. Therefore, we also extended the applicability of the HKUST-1/cotton

composites for ammonia adsorption. The full isotherms of NH_3 at 25 °C up to 1 bar were measured for the cotton, HKUST-1_{25%}/cotton, HKUST-1_{54%}/cotton, and HKUST-1. As illustrated in Figure 2.23d, HKUST-1 shows impressively high ammonia uptake at the very low partial pressures (i.e., 11.04 mmol/g at 0.004 bar) because of open metal sites. Moreover, HKUST-1 crystals on the fiber composite show a comparable NH_3 uptake (at 0.004 bar for HKUST-1_{25%}/cotton and HKUST-1_{54%}/cotton is 2.06 mmol/g and 4.27 mmol/g, respectively) compared to that of the powder form which demonstrates the accessibility of the crystals in the composite material similar to DBT uptake studies. This chapter provides a facile method to grow MOFs on fibers, which can facilitate access to functional fibers for toxic gas removal.

3.4 Conclusions

In summary, a facile, versatile, and scalable coordination replication strategy was developed to prepare MOF/textile composites at room temperature. Sacrificial LHSs were pre-deposited onto a fiber surface and acted as both metal precursors and nucleation sites. We demonstrated the versatility of the methods described here by utilizing different fibers (natural cotton fiber, synthetic PET microfibers, and electrospun polyacrylonitrile nanofibers) and MOFs (HKUST-1, Cu-BDC, ZIF-8, and ZIF-67) where all composite materials exhibited desirable textural properties. The resultant MOF/textiles featured an outstanding stability, tunable loading, and easy processability; therefore, we explored utilization of these composites in contaminant removal and toxic gas capture applications. The facile synthetic strategy described here is expected to improve the scalable and environmentally benign production of MOF-functionalized materials, which could enhance their potential applications in numerous fields.

Chapter 4

Scalable and Template-Free Aqueous Synthesis of Zirconium-Based Metal–Organic Framework Coating on Textile Fiber

Organophosphonate-based nerve agents, such as VX, Sarin (GB), and Soman (GD), are among the most toxic chemicals to humankind. The porous MOFs or their fibrous composite such as described in Chapter 3 could act as promising adsorptive materials to capture the nerve agents, while they may be polluting source with these intact ultra-toxic agents in the pores. So, development of composited materials with dual functions, namely capture and degradation, are highly desired. Recently, zirconium-based metal–organic frameworks (Zr-MOFs) have shown effectively catalytic hydrolysis of these toxic chemicals for diminishing their toxicity. On the other hand, utilizing these materials in powder form is not practical, and developing scalable and economical processes for integrating these materials onto fibers is crucial for protective gear. Chapter 4 reports a scalable, template-free, and aqueous solution-based synthesis strategy for the production of Zr-MOF-coated textiles. Among all MOF/fiber composites reported to date, the MOF-808/polyester fibers exhibit the highest rates of nerve agent hydrolysis. Moreover, such highly porous fiber composites display significantly higher protection time compared to that of its parent fabric for a mustard gas simulant, 2-chloroethyl ethyl sulfide (CEES). A decreased diffusion rate of toxic chemicals through the MOF layer can provide time needed for the destruction of the harmful species.

4.1 Introduction

Nerve agents, extremely toxic organophosphonate-based volatile chemicals, covalently bind to the active site of acetylcholinesterase (AChE), resulting in the loss of muscular control in the body and death by asphyxiation.⁹⁹ Recent reports of the use of toxic phosphonate-based nerve agents have motivated researchers to develop new materials for fast decontamination.¹⁰⁰⁻¹⁰² To this end, metal–organic frameworks (MOFs), composed of a metal node and organic linkers, have emerged as highly effective and versatile heterogeneous catalyst candidates due to their tunable structure.^{3,15,103-105}

Farha's group and others have recently demonstrated that Zr₆-based MOFs can efficiently catalyze the hydrolysis of nerve agents as well as their simulants at ambient temperature.^{17,19,69-71} Rational tuning of the pore aperture,⁷² particle size,¹⁰⁷ linker functionalization,^{108,109} and zirconium node connectivity¹¹⁰ have been demonstrated to be crucial for high catalyst activity. Farha's group have reported that MOF-808, a Zr-based MOF constructed from a 6-connected node and trimesic acid, can degrade dimethyl-4-nitrophenyl phosphate (DMNP), a nerve agent simulant, with a half-life of less than 1 min using <3 mol % catalyst.¹¹⁰ Similarly, Farha's group have also observed that UiO-66-NH₂, another Zr-based MOF with up to a 12-connected node (when no defects present) and 2-aminoterephthalic acid, showed unprecedented catalytic activity toward the hydrolysis of DMNP.¹¹⁹ However, the vast majority of these studies were performed using MOF powders; practical applications for the employment of these materials as protective layers requires integrating these materials on a fabric.

Flexible and air-permeable textiles have been suggested as inexpensive and readily accessible supports for MOFs. Several methods have been developed for the

functionalization of textiles by Zr-MOFs.^{36,37,46,47,50,52,81,111} For example, Parsons and Peterson et al. have reported the functionalization of nanofibers or commercial nonwoven textile substrates with a metal oxide layer using atomic layer deposition (ALD) to serve as nucleation sites for Zr-MOF growth on the fiber.^{36,52} Navarro et al. have integrated Zr-MOF onto nanofibers with electrospinning to form a fibrous mat.⁴⁶ Despite high catalytic efficacy for hydrolysis of the agents by these MOF/fiber composites, the scalability of utilizing such methods that require expensive equipment is challenging. Thus, a straightforward, complementary, and extendible methodology of installing MOF coatings on supports is essential and still sought after for practical and bulk applications.

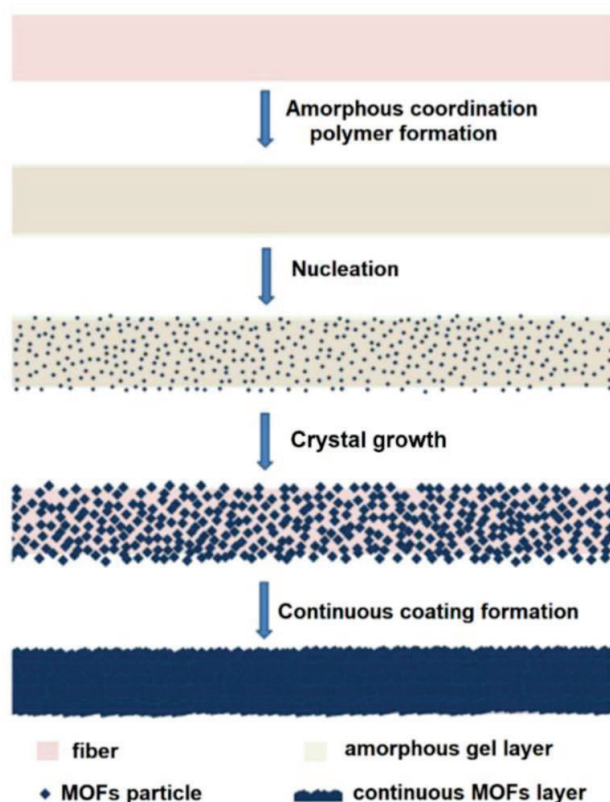


Figure 4.1. Schematic illustration of template-free aqueous synthesis of Zr-MOF coating on fiber.

In this chapter, a facile, scalable, and template-free aqueous solution-based synthesis approach was developed to yield Zr-MOF-coated textiles without the need of prior pretreatment that is applicable across different fiber surfaces (Figure 4. 1). Such MOF-coated textiles exhibited high catalytic activity for the hydrolysis of a highly toxic nerve agent, GD, and its commonly used simulant, DMNP. Additionally, the developed composites provided a protection time significantly higher than that of the parent fabric for CEES, a simulant for the blister agent mustard sulfur. By slowing down CEES diffusion, the MOF layer afforded the necessary contact time for the destruction of the toxic chemicals (Figure 4.2). It can be envisaged that the advantageous method developed herein can realize the practical application of MOFs as protective layers.

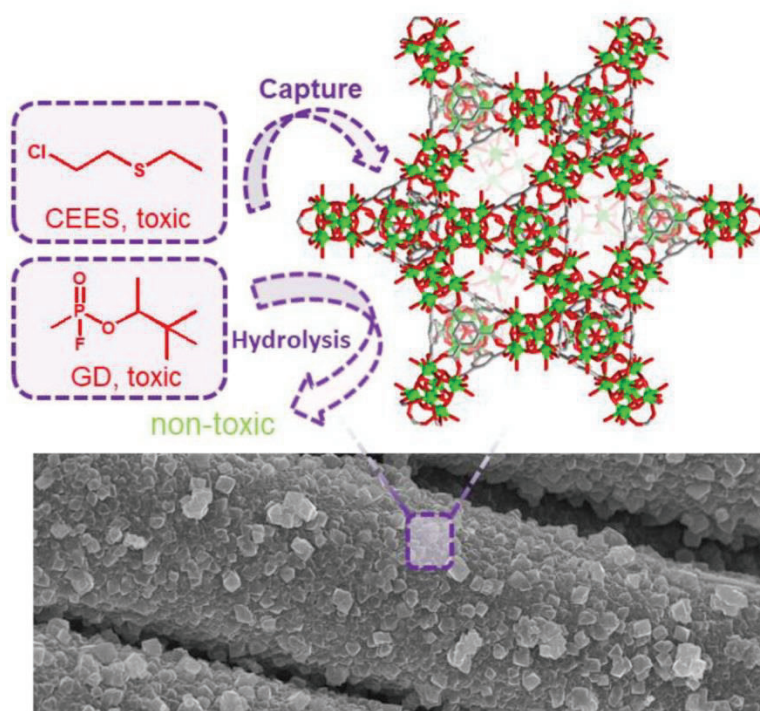


Figure 4.2. Representative Illustration of MOF-Fiber Composites for the 2-Chloroethyl Ethyl Sulfide (CEES) Capture and Soman (GD) Detoxification

4.2 Experimental section

4.2.1 Materials

ZrOCl₂·8H₂O (98%), benzene-1,3,5-tricarboxylic acid (BTCA, 98%), 2-aminoterephthalic acid (H₂BDC-NH₂, 99%), acetic acid, formic acid, and trifluoroacetic acid (99%) were purchased from Sigma-Aldrich. Other chemicals were purchased from Fisher Chemical. Deionized water was used as the water source throughout the experiments. PET fabric (thickness: 120 μm) was provided by China Dyeing Holdings Ltd., Hong Kong. Before using, PET fabric samples were scoured in a 3% NaOH water solution at 90 °C for 20 min to remove impurities, and the NaOH residue on fabric was removed by thorough water washing. Polypropylene (PP) fiber is separated from the inner layer of a 3M N95 mask. Polyacrylonitrile (PAN) nanofiber was prepared by electrospinning at 10 kV with a tip-to-collector distance of 15 cm. A 10% solution of PAN dissolved in N, N-dimethylformamide (DMF) was used as the electrospinning solution.

4.2.2 Instrumentation

Powder X-ray diffraction (PXRD) patterns of fiber substrates and MOFs/fiber composite were recorded at room temperature on a STOE-STADIMP powder diffractometer equipped with an asymmetric curved Germanium monochromator (CuKα1 radiation, $\lambda = 1.54056 \text{ \AA}$) at IMSERC (Integrated Molecular Structure Education and Research Center) of Northwestern University. N₂ adsorption and desorption isotherms of all materials were tested on a Micromeritics Tristar (Micromeritics, Norcross, GA) instrument at 77 K. Scanning electron micrographs (SEM) images of all coatings were taken using a Hitachi SU8030 at the EPIC facility (NUANCE Center-Northwestern University). Before SEM observation, all samples were coated with OsO₄ to ~9 nm thickness in a Denton Desk III

TSC Sputter Coater. Inductively coupled plasma–Optical emission spectroscopy (ICP–OES) was tested using an iCAP™ 7600 ICP-OES Analyzer (Thermo Scientific™) over the 166–847nm spectral range. NMR spectra were collected on 400 MHz Agilent DD MR-400 at IMSERC (Integrated Molecular Structure Education and Research Center) of Northwestern University.

4.2.3 Synthesis of MOF-808 coating on fiber

Four pieces of PET textile (4 cm x 4 cm), BTCA (2 mmol, 0.42 g) and $\text{ZrOCl}_2 \cdot 8\text{H}_2\text{O}$ (4.5 mmol, 1.45 g) were added to a mixture of DI water (20 mL) and TFA (10 mL) in a sealed 80 mL Pyrex Schott bottle. After sonication for 0.5 h, the mixture was placed in an oven at 100 °C for 2 h. After cooling down to room temperature, the obtained fabric samples were immersed in 100 mL hydrochloric acid/acetone solution (volume ratio of 1: 99) for 24 h at 50 °C, and then washed by deionized water (2 x 50 mL), acetone (3 x 50 mL). Finally, the samples were dried at room temperature, and activated at 110 °C for 24 h under vacuum. Caution! Adequate personal protective equipment should be used when handling TFA containing mixtures.

4.2.4 Scale-up synthesis of MOF-808 coating on fiber

One piece of PET textile (10 cm x 120 cm), BTCA (40 mmol, 8.4 g) and $\text{ZrOCl}_2 \cdot 8\text{H}_2\text{O}$ (90 mmol, 29 g) were added to a mixture of DI water (400 mL) and TFA (200 mL) in a sealed 1 L Pyrex Schott bottle. After sonication for 0.5 h, the mixture was placed in an oven at 100 °C for 3 h. After cooling down to room temperature, the obtained fabric samples were immersed in 1 L hydrochloric acid/acetone solution (volume ratio of 1: 99) for 24 h at 50 °C, and then washed by deionized water (2 x 1 L), acetone (3 x 1 L). Finally, the samples were dried at room temperature, and activated at 110 °C for 24 h under vacuum.

Caution! Adequate personal protective equipment should be used when handling TFA containing mixtures.

4.2.5 Synthesis of UiO-66-NH₂ coating on fiber

Four pieces of PET textile (4 cm x 4 cm), BDCA-NH₂ (4.5 mmol, 0.81 g) and ZrOCl₂·8H₂O (3 mmol, 0.97 g) were mixed in DI water (20 mL) and TFA (10 mL) in a sealed 80 mL Pyrex Schott bottle. After sonication for 0.5 h, the mixture was placed in an oven at 100 °C for 4 h. After cooling down to room temperature, the obtained fabric samples were immersed in 100 mL hydrochloric acid/acetone solution (volume ratio of 1:99) for 24 h at 50 °C and then washed by deionized water (2 x 50 mL), acetone (3 x 50 mL). Finally, the samples were dried at room temperature, and activated at 110 °C for 24 h under vacuum. Caution! Adequate personal protective equipment should be used when handling TFA containing mixtures.

4.2.6 Sample digestion for NMR test

Fiber composites (30 mg) were cut into small pieces and put into NMR tube containing 0.95 mL D₂O and 50 mg NaOH. After standing for 24 h, the NMR tube was mounted into equipment for ¹H NMR or ¹⁹F NMR spectrum collection.

4.2.7 Mass loading determination

Mass loadings of Zr-MOFs on fiber were calculated based on ICP-OES analysis. All fibrous samples before ICP-OES test were dried under vacuum oven overnight at 100 °C, and 100 mg of composite was quickly weighted and digested in 10 mL HNO₃. 100 uL of the above solution is diluted into 10 mL using Milli-Q water for testing the Zr concentration using ICP-OES method. The mass loading (ML) is calculated as following equation:

$$ML = (C \times 100 \times 0.01 \text{ L}) / (100 \text{ mg} \times W_{Zr}) \times 100\%$$

where C is the concentration of Zr in the diluted nitric acid solution measured by ICP-OES, mg/L. 100 is the dilution factor, and 0.01 L is the volume of concentrated HNO₃ used in digestion of fiber composite. W_{Zr} is the mass percentage in MOFs: 35.3% for MOF-808 and 32.8% for UiO-66-NH₂.

4.2.8 Catalytic hydrolysis test of DMNP

Catalytic hydrolysis of DMNP experiments were carried out at room temperature and monitored by in situ ³¹P NMR. All activated MOF/textile samples were cut into tiny pieces (0.5 mm x 5 mm) and filled into an NMR tube. For comparison of the catalytic efficiency of fibers with different MOFs loading, all fiber samples containing the same amount (1.5 μmol) of MOFs were added into NMR tube. DMNP (4 μL; 0.025 mmol) was dissolved in 0.4 M *N*-ethylmorpholine solution (1 mL; 0.05 mL *N*-ethylmorpholine, 0.9 mL DI water/0.1 mL D₂O) and transferred into the NMR tube. The tube was vigorously shaken to thoroughly mix the fiber and solution, and rapidly transferred to an NMR equipment and the ³¹P spectrum was immediately collected. The first spectrum was recorded 1.5 min after the start of the catalytic reaction. The extent of the reaction was periodically monitored every 1 min for 1 h (number of scans=16, delay time=28 s). To assess reaction conversions after removal of fiber, an identical reaction mixture was prepared in a 1.5 dram vial, filtered using a 200 nm syringe filter at 1.5 min, and filled in an NMR tube for the measurement of conversion by ³¹P NMR. The catalytic activity of untreated fiber was evaluated under identical conditions and monitored by in situ ³¹P NMR.

4.2.9 Reusability and stability test

To test the reusability, the composite sample (6.5% loading) after catalysis test was washed with 50 mL deionized for 30 min and reused in test without drying. The catalytic activity of composite sample (6.5% loading) after storage for 6 months in air or being stirring (400 rpm) for 24 h in water were also tested to evaluate its durability.

4.2.10 Catalytic hydrolysis test of GD

Caution! GD is extremely toxic. Experiments should be run by trained personnel using appropriate safety procedures. Catalytic hydrolysis of GD tests were carried out at room temperature. MOF-808/PET and UiO-66-NH₂/PET samples, all containing 1.5 μmol MOFs, were filled in a 4-mm glass NMR tube. 1.0 mL of H₂O/D₂O and 50 μL of N-ethylmorpholine were then added to the NMR tube to wet the sample. After, 2.5 μL of GD (1.4 μmol) was added into the NMR tube, the tube was capped immediately and vigorously shaken to mix the GD and fiber thoroughly in solution. The NMR tube was mounted onto a Varian INOVA 400 NB NMR spectrometer to collect ³¹P NMR spectra.

4.2.11 CEES permeation test

CEES permeation testing was conducted in accordance with ASTM F739-12. A 1.5 in by 1.5 in swatch was sealed in a 1 in diameter glass permeation cell. A countercurrent air flow of 300 mL·min⁻¹ at ~2% RH was applied above and below the swatch. CEES was fed to the swatch at a concentration of 300 mg·m⁻³. The feed, retentate, and permeate concentrations were monitored using an Agilent 6890 gas chromatograph with a flame ionization detector. Tests were terminated when steady state was reached and the sum of the retentate and permeation concentrations equaled the feed concentration.

4.3 Results and discussion

To study the growth process of Zr-MOFs on fiber, MOF-808 was selected as a model due to the framework's robust chemical stability¹¹² and high catalytic activity for the hydrolysis of GD and DMNP.^{110,113} To the best of my knowledge, this is the first study investigating the coating of MOF-808 on a fibrous surface. Briefly, the MOF-coated fiber was obtained by heating the textile in an aqueous solution containing the MOF precursors. Polyester fabrics (4 pieces, 4 cm × 4 cm), trimesic acid (2 mmol, 0.42 g), and ZrOCl₂·8H₂O (4.5 mmol, 1.45 g) were added to a mixture of deionized water (20 mL) and trifluoroacetic acid μ (TFA) (10 mL), which was sonicated for 30 min and heated in an oven at 100 °C for 2 h. Systematic characterizations indicated that MOF-808 growth on fiber is via a three-stage process: (1) aggregation of an amorphous coordination polymer on the fibrous surface (0–10 min), (2) formation of MOF-808 nucleation sites (10–20 min), and (3) growth into a continuous MOF coating (>30 min). After 10 min of reaction, a very thin rough layer was observed on the fiber's surface in the scanning electron microscopy (SEM) images (Figure 4.3a,b). It is inferred that this period served as a pseudotemplating period during which reagents were adsorbed on the surface of the fiber and quickly formed an amorphous coordination polymer. The noncrystalline nature of the layer was verified by powder X-ray diffraction (PXRD) measurements, and the presence of Zr in the gel coating was confirmed by energy-dispersive X-ray spectroscopy (EDS) and inductively coupled plasma optical emission spectroscopy (ICP-OES) (Table 4.1).

Proton nuclear magnetic resonance spectroscopy (¹H NMR) of the digested sample indicated the presence of the BTC linker in the gel coating (Figure 4.4). After 20 min, the fiber's surface transitioned from a template site for reagent coverage to a nucleation site

that formed small octahedral MOF particle seeds (Figure 4.3c). The newly formed seeds were identified as MOF-808 by PXRD (Figure 4.5a), and the increased porosity of the coating was evidenced through N₂ sorption isotherm studies (Figure 4.5b,c).¹¹² During the subsequent reaction time, the seeding MOF-808 particles grew larger and interconnected into a continuous layer on the fiber (Figure 4.3b–f). After 2 h reaction, the fiber’s surface was thoroughly covered by intergrown MOF-808 particles. The characteristic elements, such as Ti, O, and C, of the MOF-808 coating were confirmed by EDS mapping analysis (Figure 4.6). SEM images of the fibers’ edges showed a MOF layer thickness of approximately 1 μm (Figure 4.7).

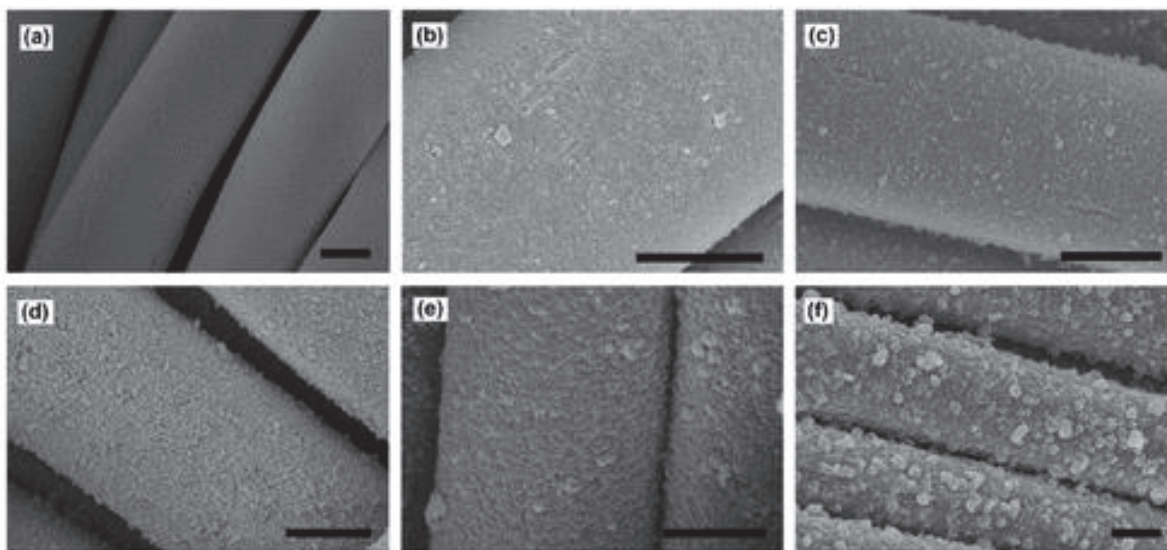


Figure 4.3. SEM images illustrating the PET fiber surface change. Pristine PET fiber (a), after reaction of 10 min (b), 20 min (c), 30 min (d), 60 min (e), and 120 min (f). All scale bars are 5 μm

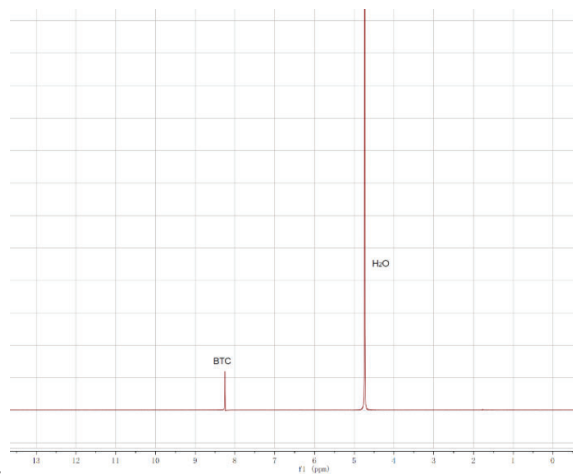


Figure 4.4. ^1H NMR spectrum of sample after 10 min reaction, digested in 5% KOH in D_2O .

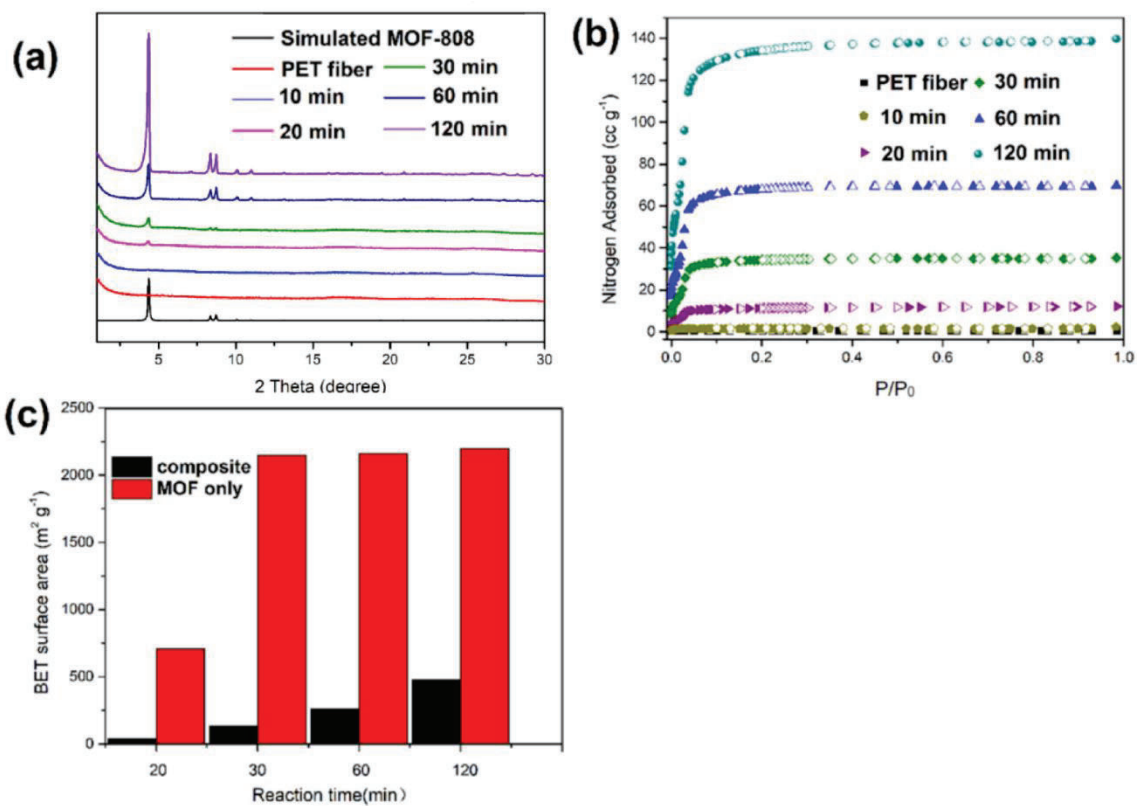


Figure 4.5. (a) PXRD patterns, (b) N_2 sorption isotherms, and (c) BET surface areas of composite materials.

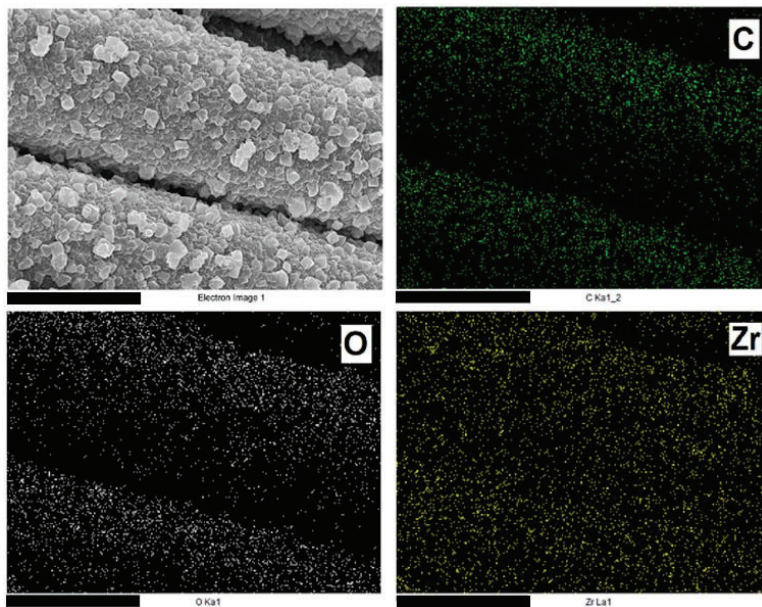


Figure 4.6. EDX mapping of MOF-808/PET sample; all scale bar: 10 μm .

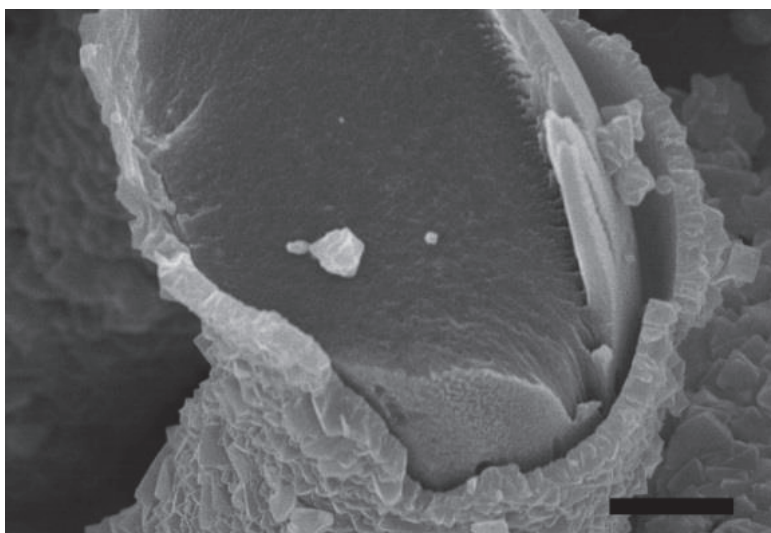


Figure 4.7. SEM image of MOF-808 coated PET on a cutting edge; scale bar: 5 μm .

By controlling the reaction time during the final growth stage, the mass loading of the MOF-808 on fiber was modulated. Zirconium elemental analysis by ICP-OES revealed that mass loadings ranged from 6.5 to 22% when the reaction time was prolonged from 0.5 to 2 h (Table 4.1.). Importantly, these particles were intact even after vigorous washing,

attributed to robust intercrystallite interactions as well as strong binding between crystallites and fiber. Nitrogen adsorption at 77 K confirmed the formation of the highly porous MOF (Figure 4.5b and Figure 4.8); Brunauer–Emmett–Teller (BET) surface area of the composite material increased from 2 to 480 m²/g after 2 h of MOF-808 growth (Table 4.5c and Table 4.1.). Importantly, the normalized BET surface area of the MOF-808 coating is about 2200 m²/g after 0.5 h, in agreement with previously reported values of MOF-808 powders^{110,113} to indicate the high quality of MOF coating obtained.

Table 4.1. Loading and BET surface area summary of the samples

Reaction time (min)	Zr element content (%)	MOF-808 mass loading ^a (%)	BET surface area of the composite (m ² /g)	Normalized BET surface area of MOFs coating ^b (m ² /g)
0	0		2	
10	1.8		6	
20	2.1	5.8	40	710
30	2.4	6.5	130	2150
60	4.5	12	260	2160
120	8.2	22	480	2200

Note: ^a The MOF-808 mass loading is calculated based on the six connected form (FW: 1551). ^bIt is hypothesized that all of the zirconium element is from MOF-808 when calculating the normalized BET surface area of MOFs coating.

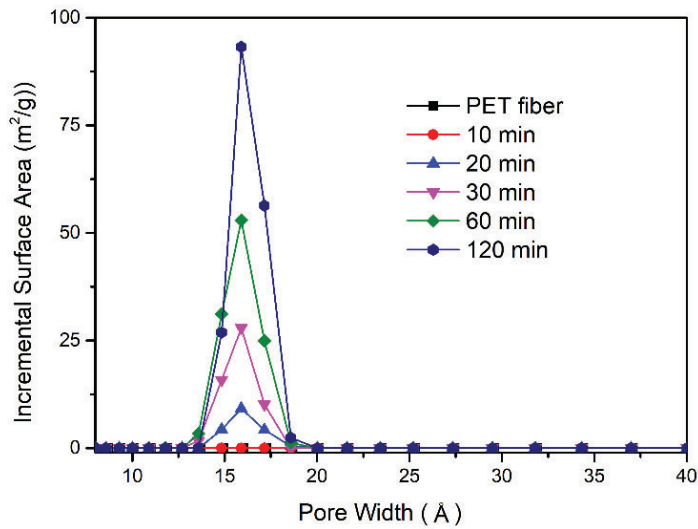


Figure 4.8. Pore size distribution of MOF-808/PET sample from different reaction time.

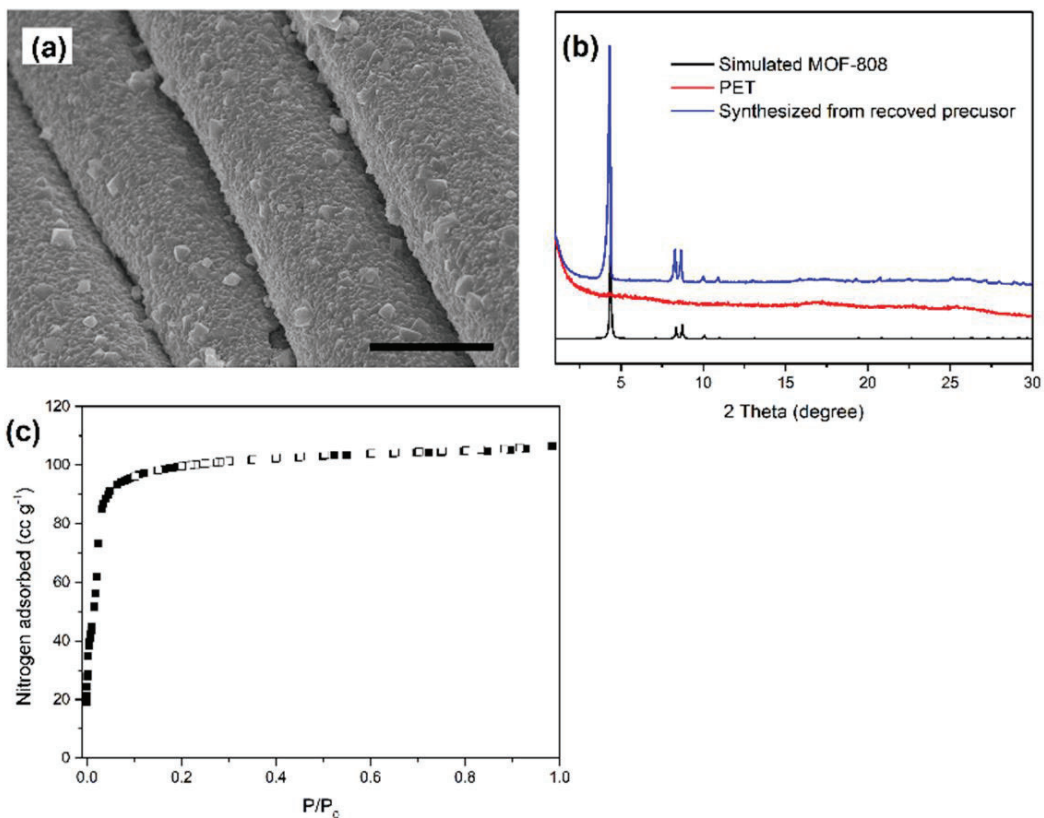


Figure 4.9. SEM image (a), XRD pattern, and nitrogen sorption isotherm (c) of MOF-808 coated PET sample prepared from reused precursor; scale bar: 10 μm .

When MOF–fiber composites are prepared using solvo/hydrothermal methods, the yield of the resulting coating can indicate how much MOF formed on the fiber as opposed to free powder in solution. This protocol showed negligible free MOF particles in solution after the reaction, which implies that MOF-808 nucleation selectively started on the fiber’s surface. This can be attributed to a preconcentration effect because the fiber provides an interface for precursor adsorption during the first growth stage, eliminating the necessity of the surface’s pretreatment prior to MOF growth.¹¹⁴ Following the reaction, the precursor mixture was reused in a new synthesis process, highlighting potential for efficient mass production. A coating with similar morphology and slightly lower loading (18%) was obtained from this reused precursor mixture (Figure 4.9). Previous solvothermal methods of MOF-coated fibers yielded 5–20 times more free MOF particles in reaction media compared with the amount that coated onto the fiber’s surface.⁵² Therefore, the highly efficient method reported here could lower the cost of production and minimize the environmental impact.

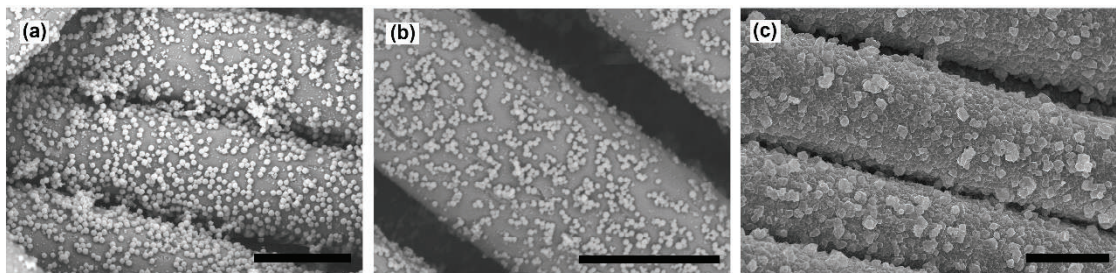


Figure 4.10. SEM images of MOF-808 coating on PET fiber using 33% formic acid (a), 33% acetic acid (b), and 33% trifluoroacetic acid (c); scale bars: (a-c) 10 μm .

The use of TFA as a modulator in the synthesis played a critical role for creating a uniform surface coverage of fibers. Notably, when other organic acids such as acetic acid and formic

acid were used as modulators, aggregated islands of particles were formed on the fiber surface instead of uniform surface coverage achieved by TFA (Figure 4.10). Moreover, crystallization generally occurred in the solvent rather than on the fiber surface when using other modulators. It is hypothesized that the higher acidity of TFA slowed down the crystallization to yield a continuous coating.¹¹⁵ Additionally, TFA volume below 29% prevented total coverage of fiber by the MOF coating, emphasizing the importance of modulator concentration (Figure 4.11). Though both 33 and 50% TFA yielded complete surface coverage, safety and cost considerations render 33% TFA as the selected condition for the reliable growth of MOF-808 on fiber.

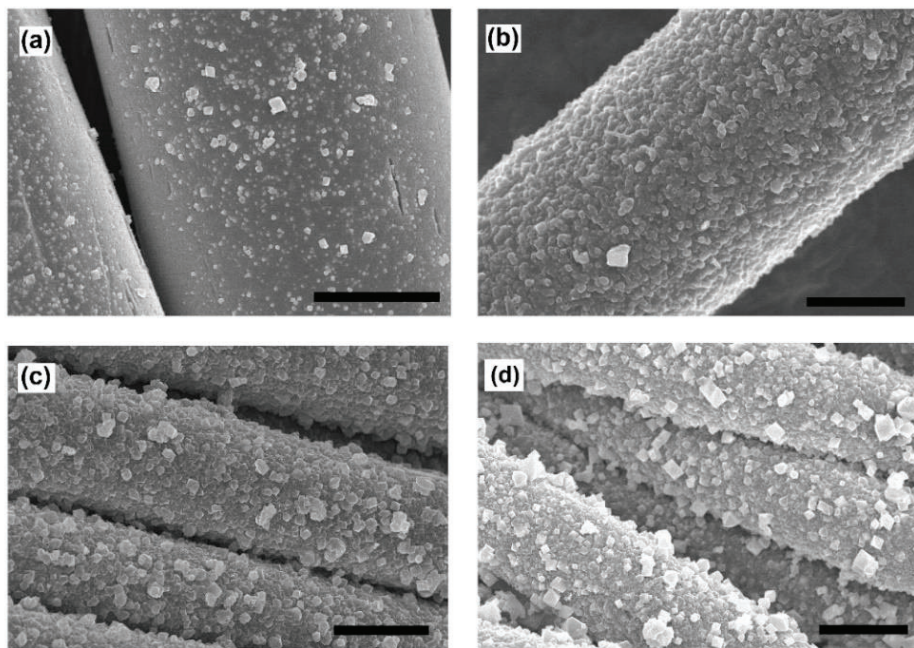


Figure 4.11. SEM images of MOF-808 coating on PET fiber using 25% (a), 29% (b), 33% (c), and 50% (d) trifluoroacetic acid as a modulator; scale bars: (a) and (b) 5 μm , (c) and (d) 10 μm .

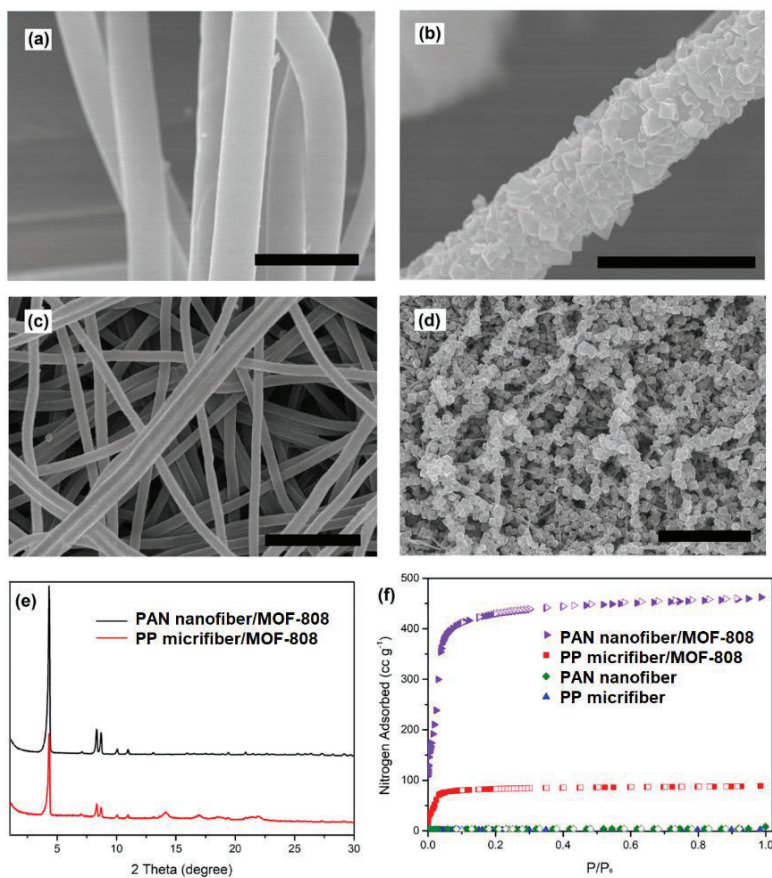


Figure 4.12. SEM images of PP fiber (a), MOF-808 coated PP fiber (b), PAN fiber (c), and MOF-808 coated PAN fiber (d). XRD patterns (e) and N₂ sorption isotherm (f) of related samples. Scale bare: (a) 10 μm , (b) 5 μm , (c) 4 μm , (d) 10 μm .

To ensure that the developed MOF on fiber synthesis is amenable to a variety of final applications, the efficacy of the synthesis with different fibers was studied. Therefore, polyacrylonitrile (PAN, 500 nm) nanofiber and polypropylene (PP, 2 μm) microfibr were also used in coating synthesis in addition to PET fiber. The dense and continuous MOF coating on these fiber substrates was observed via SEM imaging, whereas the high-quality MOF-808 coating was confirmed by PXRD and N₂ sorption of the composite (Figure 4.12). Importantly, the aqueous synthesis method developed here offers unique applicability to

some polymeric fibers, which are soluble in polar organic solvents such as dimethylformamide (DMF). For example, PAN nanofiber dissolved within 5 min in a typical MOF-808 synthetic procedure using DMF as a solvent (Figure 4.13).

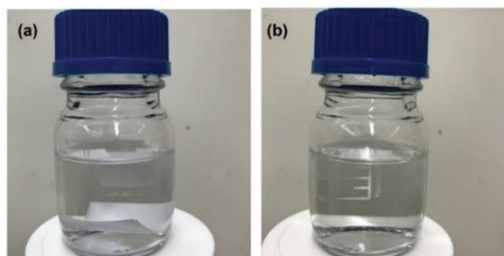


Figure 4.13. Optical photographs of PAN nanofiber membrane before (a) and after (b) heating at 130 °C for 5 min in a typical MOF-808 synthesis system using DMF as the solvent. The PAN nanofiber mat is totally dissolved in the precursor solution.

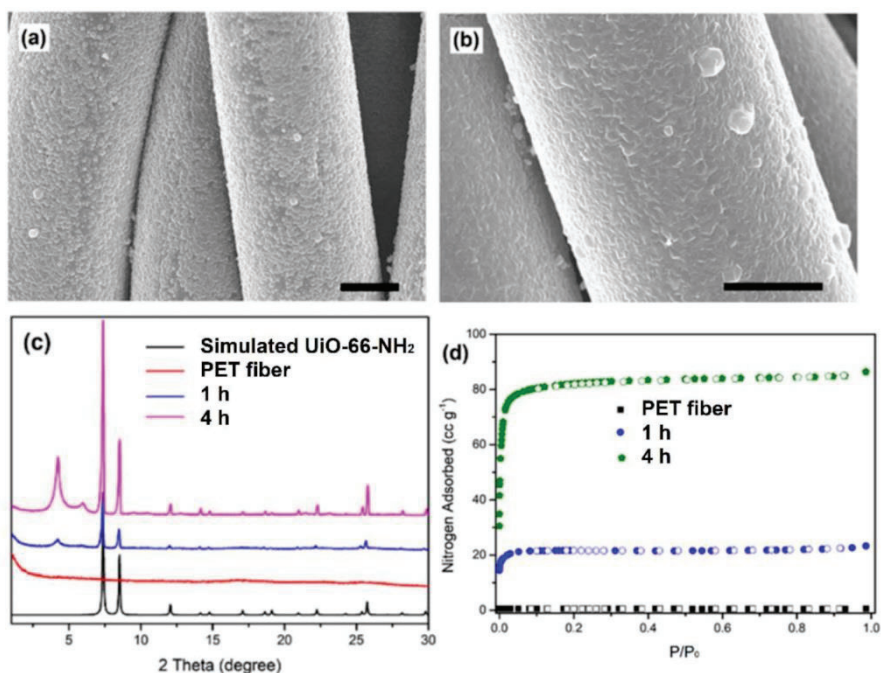


Figure 4.14. SEM images of UiO-66-NH₂ coating on fiber after reaction of 1 h (a) and 4 h (b). Scale bars: 5 µm. PXRD patterns (c) and N₂ sorption isotherms (d) of related samples.

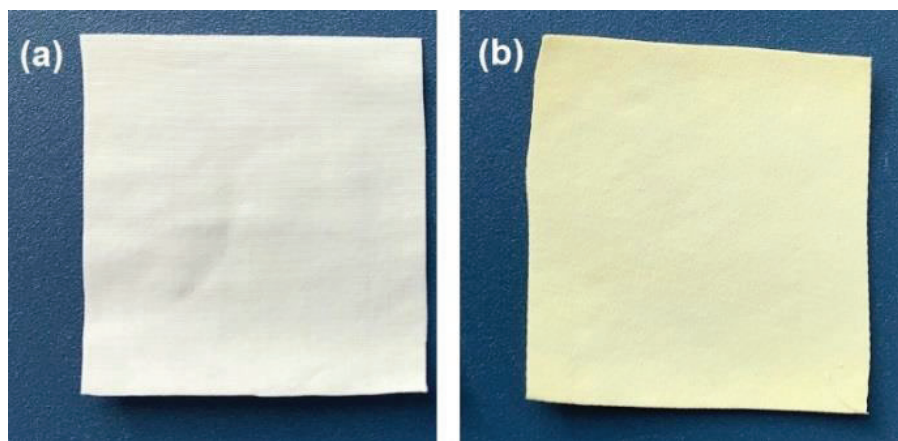


Figure 4.15. Optical photographs of PET fabric before (a) and after (b) UiO-66-NH₂ coating.

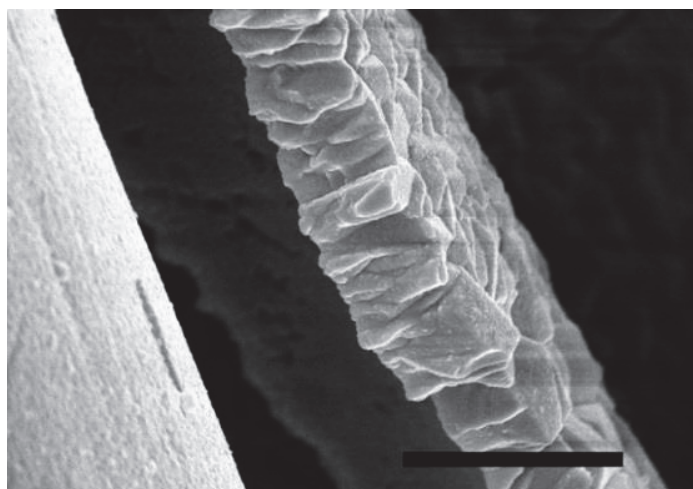


Figure 4.16. SEM image of UiO-66-NH₂ coated PET at the cutting edge; scale bar: 3 μ m.

In order to demonstrate the compatibility of the current method with other MOF systems, PET fiber was also coated with UiO-66-NH₂, another Zr-based MOF that previously achieved exceptionally high hydrolysis rates of nerve agents. After 4 h reaction, a coating with continuous morphology was observed on the UiO-66-NH₂/PET composite with SEM imaging, and PXRD indicated good agreement of the composite material crystallinity with

simulated UiO-66-NH₂ (Figure 4.14). PXRD patterns suggested the presence of missing cluster defects that form an 8-connected reotopology. Such defects have been shown to increase catalytic activity by increasing substrate diffusion inside the crystals as well as exposing more Zr active sites.^{116,117} High porosity of the UiO-66-NH₂ coatings was verified with a N₂ sorption test (Figure 4.12d). An observed color change of the white pristine fabric to a pale yellow after reaction completion (Figure 4.14) was rationalized as a visual indication of UiO-66-NH₂ deposition. ICP-OES determined the MOF mass loading on the fiber as 8 and 27% after 1 and 4 h reactions, respectively, and the thickness of the coating after a 4 h reaction is about 1.5 μm (Figure 4.16)

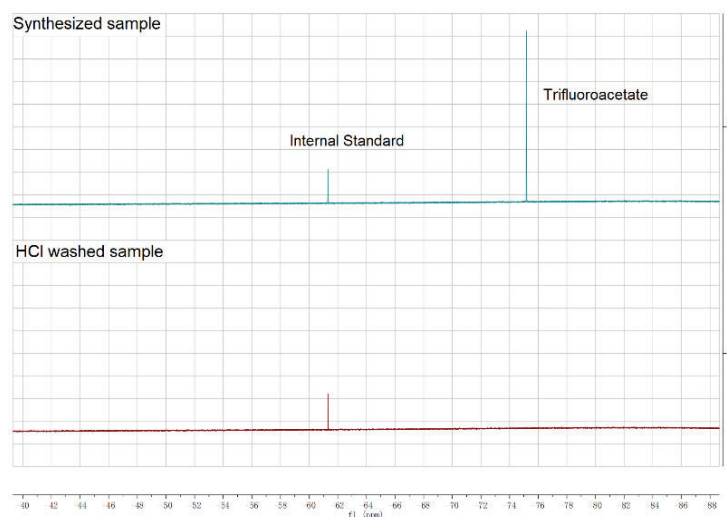


Figure 4.17. ¹⁹F NMR spectra of alkaline-digested MOF-808/fiber-TFA before and after HCl washing. Sample was digested in 5% KOH in D₂O, and 1,3-bis(trifluoromethyl)-5-bromobenzene was used an internal standard.

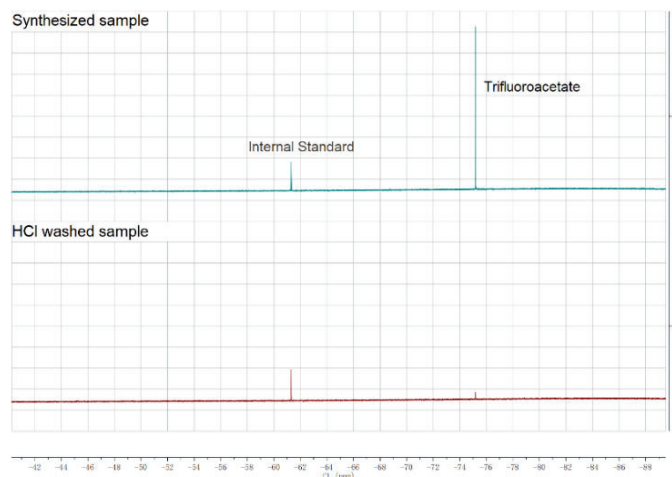


Figure 4.18. ^{19}F NMR spectra of alkaline-digested UiO-66-NH₂/fiber-TFA before and after HCl washing. Sample was digested in 5% KOH in D₂O, and 1,3-bis(trifluoromethyl)-5-bromobenzene (BTB) was used as an internal standard.

The as-synthesized Zr-MOF coating contained coordinated organic acid modulators on the Zr node, confirmed by the NMR spectra of the digested samples. After the composite material was treated with diluted HCl in acetone solution (0.12 M), the peak corresponding to trifluoroacetic acid nearly vanished, revealing the successful removal of the residual modulator bound to the Zr cluster (Figure 4.17 and Figure 4.18).¹¹⁸ The crystallinity and porosity of the MOF coating was still retained after the treatment.

In addition to illustrating the generality of the current protocol by varying the identity of fibers and/or MOFs, the scalability was probed through a larger proof of concept synthesis. A piece of PET fabric (about 10 cm × 120 cm) was coated with MOF-808, and the representative larger composite featured surface morphology and loading (20%) comparable to that previously obtained with smaller pieces of fabrics (Figure 4.19). The BET area of the MOF-808 layer coated on fiber was approximately 2200 m²/g, demonstrating the high porosity of MOF-808 coating obtained from the scaled-up synthesis.

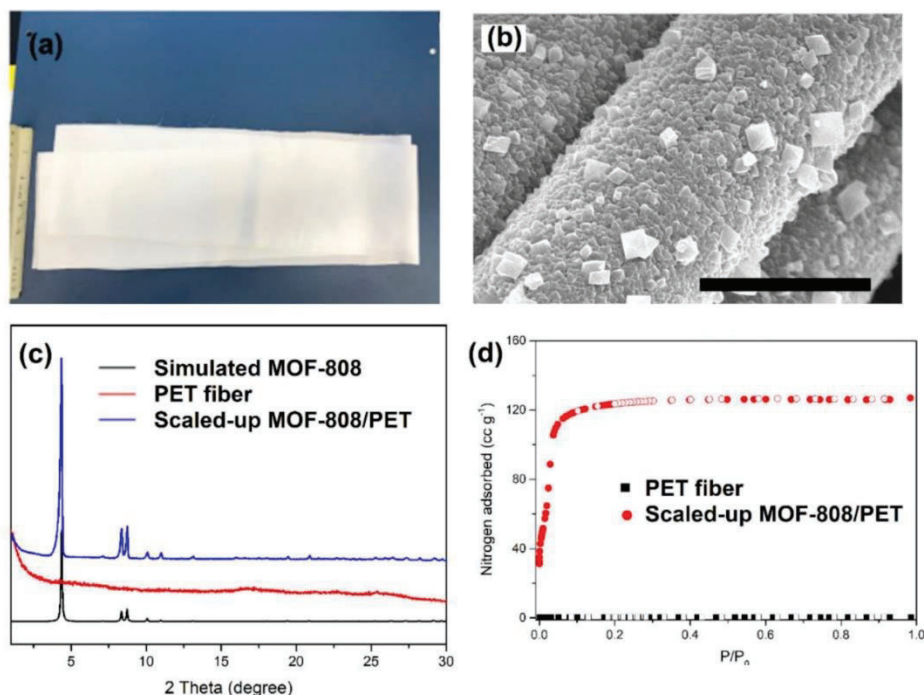


Figure 4.19. Optical photograph (a), SEM image (b), PXRD patterns (c), and N₂ sorption isotherm (d) of samples from scale-up PET fabric coating (about 10 cm × 120 cm). Scale bar: 10 μm.

After the high quality of Zr-MOF coatings on the PET fiber was confirmed, the catalytic hydrolysis of the nerve agent simulant DMNP was first tested in aqueous *N*-ethylmorpholine buffer (0.45 M, pH 10) media. Reaction conversion was monitored by ³¹P NMR spectroscopy by comparing the integration of the ³¹P peak for DMNP ($\delta = -4.4$ ppm) and that of the hydrolysis product, dimethyl phosphate anion ($\delta = 2.8$ ppm).¹¹⁰ MOF-808/PET composites with MOF loadings of 6.5, 12, and 22%, denoted as MOF-808_{6.5%}/PET, MOF-808_{12%}/PET, and MOF-808_{22%}/PET, were probed for their catalytic activity, and the same amount of MOF-808 was used in all catalytic tests (normalized based on Zr amount in the composite).

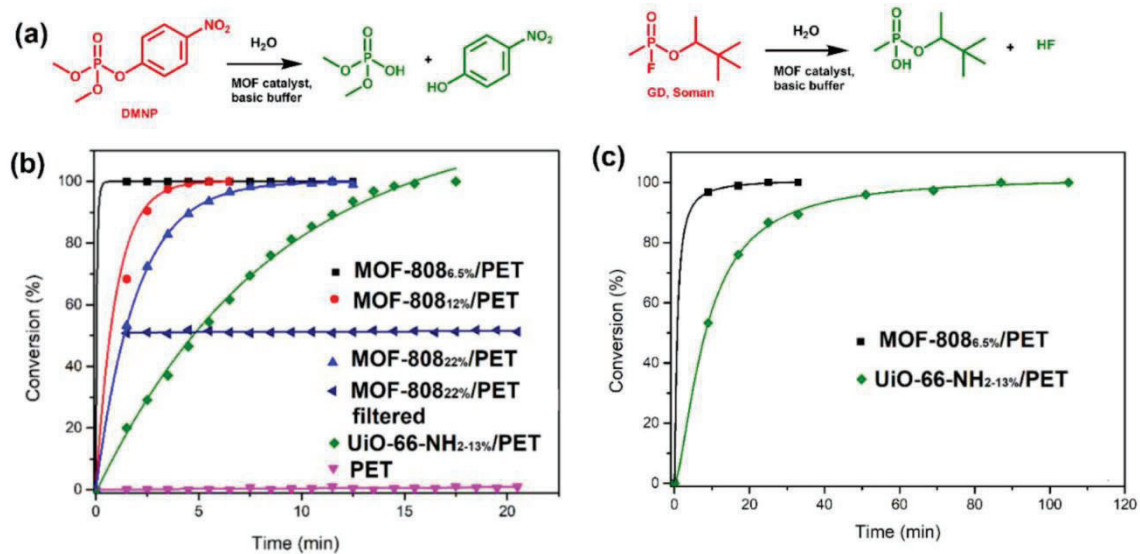


Figure 4.20. (a) Catalytic reaction of DMNP and GD hydrolysis. Kinetic profiles for hydrolysis of (b) DMNP and (c) GD using MOF-coated fibers as the catalyst: 1.5 μmol of catalyst; 25 μmol of reagent.

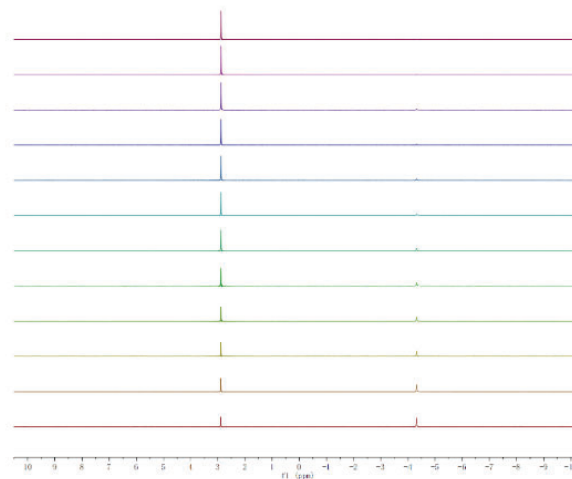


Figure 4.21. *In-situ* ³¹P NMR spectra showing the progress of hydrolysis of DMNP (-4.4 ppm) to dimethoxy phosphate anion (2.8 ppm) in the presence of 10.6 mg of MOF-808_{22%}/PET. The first spectrum was recorded in 1.5 min, and the interval of each spectrum was 1 min.

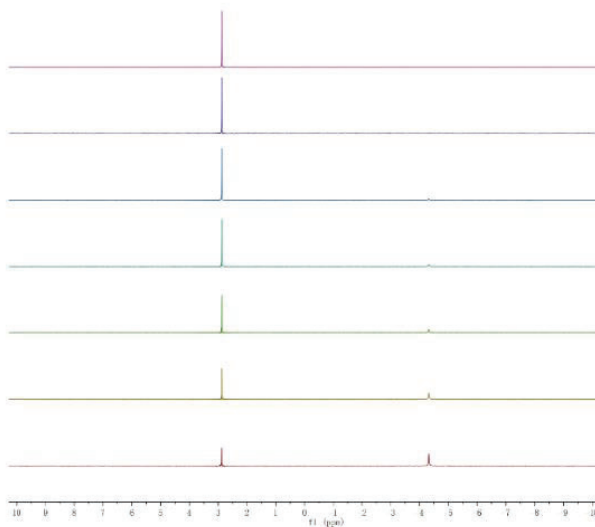


Figure 4.22. *In-situ* ^{31}P NMR spectra showing the progress of hydrolysis of DMNP in the presence of 19.4 mg of MOF-808_{12%}/PET. The first spectrum was recorded in 1.5 min, and the interval of each spectrum was 1 min.

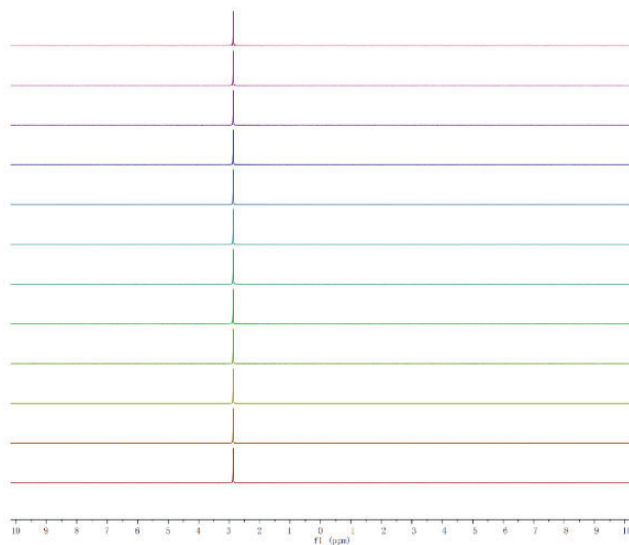


Figure 4.23. *In-situ* ^{31}P NMR spectra showing the progress of hydrolysis of DMNP in the presence of 35.8 mg of MOF-808_{6.5%}/PET. The first spectrum was recorded in 1.5 min, and the interval of each spectrum was 1 min.

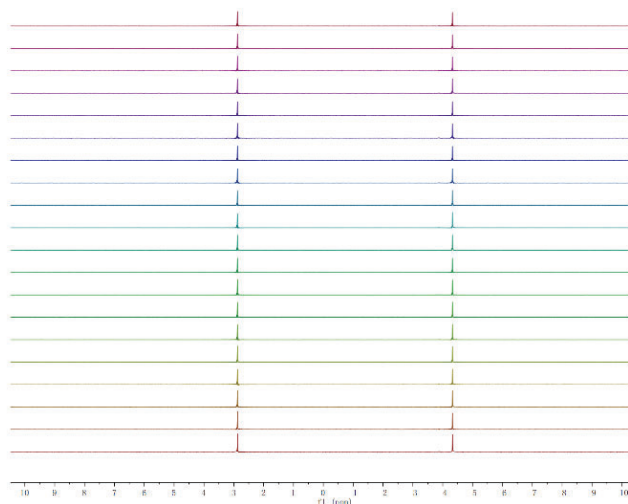


Figure 4.24. *In-situ* ^{31}P NMR spectra showing the progress of hydrolysis of DMNP after filtering the MOF-808_{22%}/PET catalysis. The first spectrum was recorded in 1.5 min, and the interval of each spectrum was 1 min.

The corresponding initial half-lives for MOF-808_{6.5%}/PET, MOF-808_{12%}/PET, and MOF-808_{22%}/PET are <0.5, <1, and 3 min, respectively. Total conversion of DMNP is achieved after approximately 1.5 min for MOF-808_{6.5%}/PET, 5 min for MOF-808_{12%}/PET, and 10 min for MOF-808_{22%}/PET (Figure 4.20a, Figure 4.21- 4.24, and Table 4.2). Significantly enhanced hydrolysis rates with lower MOF loading compared to higher loadings was attributed to the accessibility of Zr_6 node active sites (1.5 μmol in total).¹¹⁹ It was found that the reaction immediately stopped after the removal of the MOF/fiber composite from the reaction mixture, confirming the heterogeneous nature of the reaction (Figure 4.20b and Figure 4.24). After catalysis, SEM and PXRD indicated the adhesion of the MOF layer to the polyester fiber, and its catalytic activity was fully recovered after being washed with water (Figure 4.25-4.26). Moreover, the catalytic activity remained unchanged after 6 months of air exposure or 24 h of stirring (400 rpm) in water (Figure 4.27), demonstrating

the excellent durability of the composite material. Additionally, the catalytic reaction was studied with UiO-66-NH₂/PET, with a MOF loading of 8%, which demonstrated a half-life of 5 min (Figure 4.20b and Figure 4.28). The faster reaction rate in the case of the MOF-808/fiber was attributed to the lower connectivity on the Zr node (6-connected), which affords more open Zr sites available for the reaction, in agreement with the previous findings with free MOF.¹¹⁰ As a control, the background reaction of DMNP hydrolysis with fiber only in the buffer solution showed negligible conversion over 20 min (Figure 4.20b and Figure 4.29).

Encouraged by the high catalytic activity of the MOF/fiber composite for hydrolysis of DMNP, the catalytic activity of these composite materials was explored for the hydrolysis of an actual nerve agent, GD (Figure 4.20 and Table 4.2). MOF-808/fiber and UiO-66-NH₂/fiber composites efficiently degraded GD with respective half-lives of 2 and 8 min, similar to those achieved by powders (Figure 4.20c). Remarkably, the MOF-808/fiber composite exhibited the highest catalytic activity for DMNP and GD hydrolysis as compared with that of the previously reported composite materials (Table 4.2).

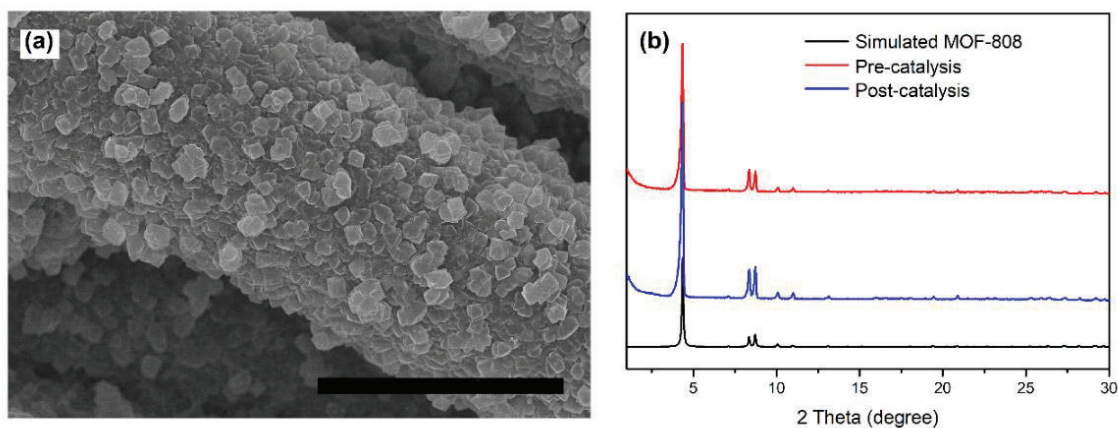


Figure 4.25. SEM image (a), XRD patterns (b) of the sample after catalysis.

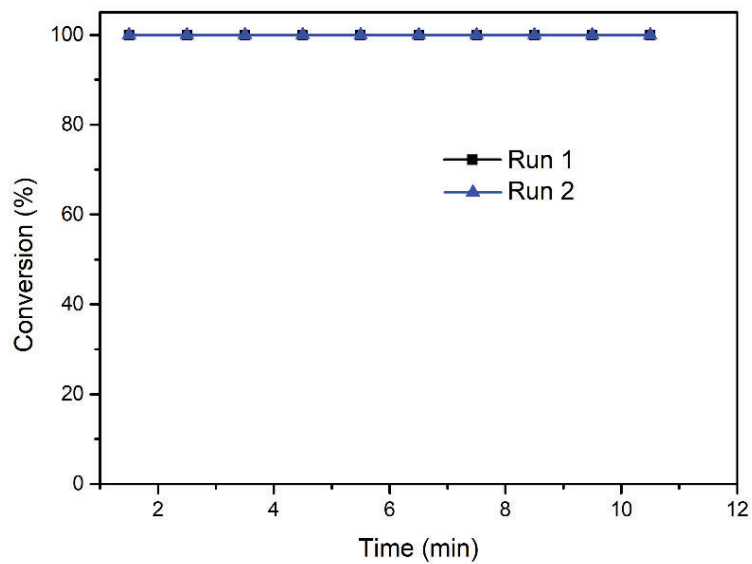


Figure 4.26. The reusability of the MOF-808_{6.5%}/PET catalyst.

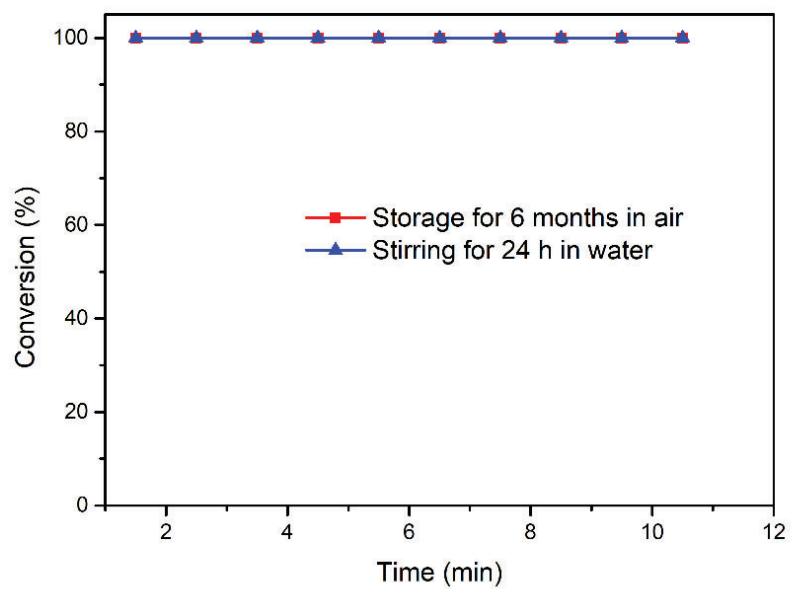


Figure 4.27. The durability of the MOF-808_{6.5%}/PET catalyst after storage and stirring test.

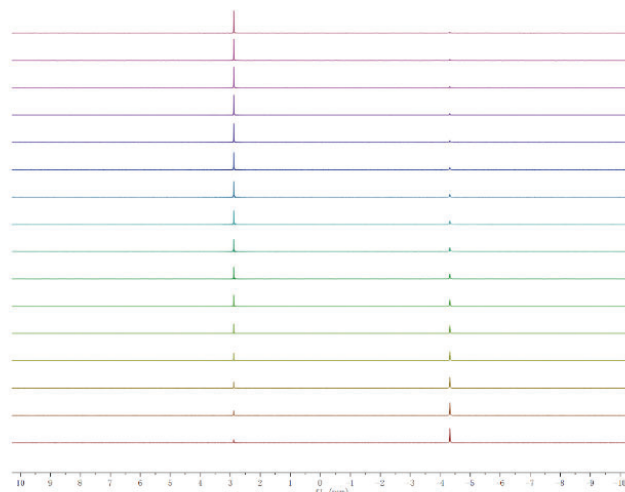


Figure 4.28. *In-situ* ^{31}P NMR spectra showing the progress of hydrolysis of DMNP in the presence of 31.5 mg of UiO-66-NH₂-8%PET. The first spectrum was recorded in 1.5 min, and the interval of each spectrum was 1 min.

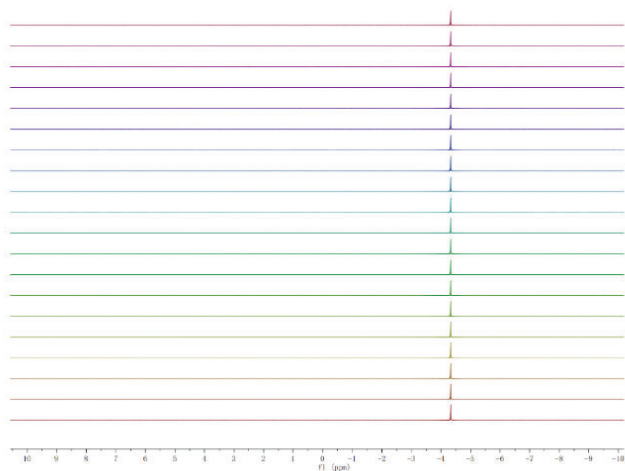


Figure 4.29. *In-situ* ^{31}P NMR spectra showing the progress of hydrolysis of DMNP in the presence of 40 mg uncoated PET fiber. The first spectrum was recorded in 1.5 min, and the interval of each spectrum was 1 min.

Table 4.2. Comparison of materials fabrication methods, properties and catalytic performance of DMNP and GD between this chapter and recent reported works.

Materials	Synthesis method	Mass loading (%)	BET surface (m ² /g)	Half-lives of NMNP (min)	Half-lives of GD (min)	Ref.
MOF-808/PET	template-free, aqueous synthesis	6.5	130	< 0.5	2	This chapter
		12	260	<1		
		22	480	3		
UiO-66-NH ₂ /PET		8	95	5	8	
PA-6@TiO ₂ @UiO-66	ALD oxides templated growth in DMF	8.8	144	135	3	36
PA-6@TiO ₂ @UiO-67		14.7	356	7	3.7	
PA-6@TiO ₂ @UiO-66-NH ₂		15.4	206	7.3	2.3	
PP/ZnO + UiO-66-NH ₂	ALD oxide assisted assembly in DMF	30.7	211	6.5		50
PP@ZnO@UiO-66-NH ₂	ALD oxides templated growth in DMF	15	145	10		52
MOFabric UiO-66-NH ₂	Impregnation during electrospinning	33	225	12		41

The diffusion of reactants and products through porous materials is an integral component of their catalytic activity.¹²⁰⁻¹²² Ideally, high retention time (contact time) of an agent is

desired to facilitate ample time for the agent to react with the catalyst. In order to demonstrate the barrier properties of the MOF coating layer, the permeation rates of the prepared Zr-MOF/PET composite materials were measured using CEES as an analyte in accordance with ASTM F739-12, where 300 mg/m³ CEES was fed across a fabric swatch (1 in. in diameter) at a flow rate of 300 mL min⁻¹. The exiting air streams were monitored using an Agilent 6890 gas chromatograph equipped with a flame ionization detector. The results indicated that full permeation of CEES through the uncoated PET sample occurred immediately, suggesting minimal blocking/adsorption capabilities from the pristine PET fabric (Figure 4.30). According to ASTM F739-12 standard, protective clothing has effective protection function when the permeation rate of chemicals is under 0.1 μg min⁻¹ cm⁻².¹²³ Strikingly, UiO-66-NH₂/PET (loading 27%) and MOF-808/PET (loading 22%) showed negligible (<0.1 μg min⁻¹ cm⁻²) permeation over a considerably long time. According to ASTM F739-12 standard, UiO-66-NH₂/PET and MOF-808/PET had effective protection over 50 and 126 min, respectively.

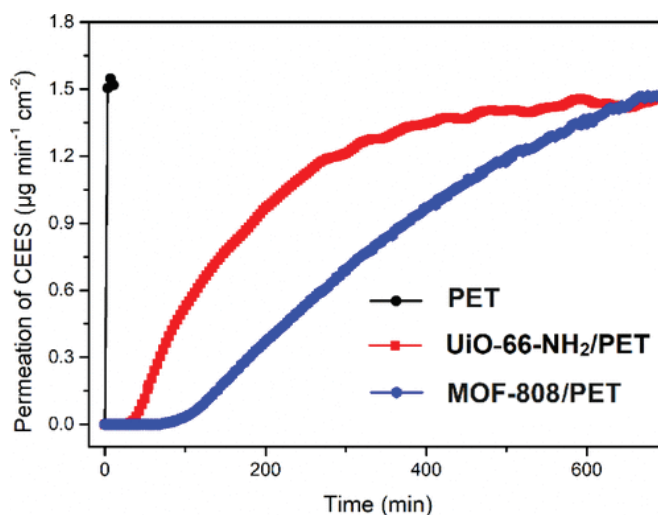


Figure 4.30. CEES permeation through MOF/fiber materials.

4.4 Conclusion

Toward the practical implementation of MOF-based chemical warfare agent (CWA) catalysts, a facile, high yielding, low cost, scalable, template-free, and aqueous synthesis strategy was developed for the preparation of a continuous Zr-MOF coating on textile supports. A three-phase growth mechanism for MOF growth on fibers was optimized to yield high porosity composite materials with uniform coverage. These MOF-coated textiles exhibited the highest to date catalytic activity among composite materials for the hydrolysis of a nerve agent simulant DMNP and a nerve agent GD. Moreover, the highly porous MOF/fiber composite showed excellent capture performance for a mustard simulant, CEES, where the composite material exhibited considerable protection for over 2 h, implying a nearly defect-free surface coverage of the fiber, which is crucial for the current application. Importantly, these flexible MOF/textile composites could be conveniently tailored into different shapes, promising great potential for these materials to be incorporated into suits and masks as protective layers. Both the high catalytic activity and adsorption capacity of the MOF/fiber material observed herein invite further engineering to implement these materials as next-generation protective gear against multiple CWA contaminants.

Chapter 5

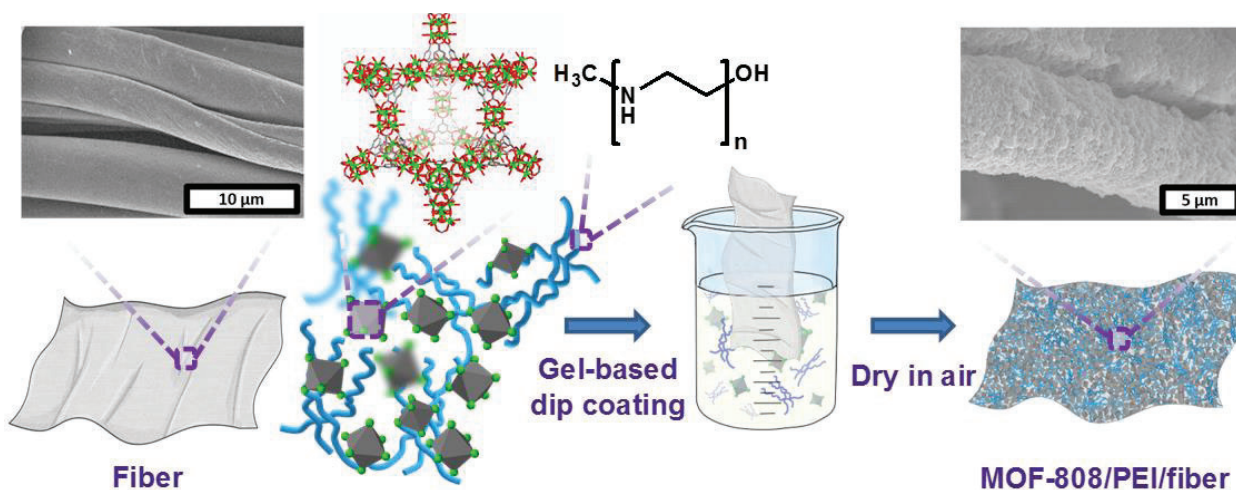
Dip-Coating Method for Fabrication of Metal-Organic Frameworks/Polymeric Buffer/Fiber Composite for Catalytic Hydrolysis of Nerve Agents under Ambient Conditions

As shown in Chapter 4, zirconium-based metal–organic frameworks (Zr-MOFs)/fiber composites are promising catalysts for the hydrolysis degradation of nerve agents and their simulants, while liquid water and volatile bases fiber are required for hydrolysis with these Zr-MOF/fiber catalysts, preventing real-world application. In Chapter 5, a much more practical and scalable gel-based dip-coating approach was developed for integrating Zr-MOF nanoparticles, non-volatile polymeric polyethyleneimine (PEI) buffer base, and textile fibers substrate into a Zr-MOF/PEI/fiber composite for nerve agent catalytic hydrolysis. Surprisingly, the Zr-MOF/PEI/fiber composite material showed similar catalytic efficiency under ambient conditions compared to the well-dispersed MOFs nanoparticle catalysts in aqueous alkaline buffer solution, which indicate this an important step toward the practical application of Zr-MOF/fiber composite in human protection against nerve agent threat.

5.1 Introduction

Human protection against chemical warfare agents (CWAs) still is a serious challenge nowadays.¹³⁴ Because of their ultra-high acute toxicity, organophosphonate-based nerve agents, are one of the most serious threat to human safety.¹³⁴ Thus, the chemical degradation of these harmful compounds to nontoxic and innocuous chemicals is crucial, and the development of high-efficient personal protective gears against the nerve agents is highly desirable. Current widely used gas mask filtration systems are composed of fibers filter for particulate capture and activated carbon for toxic vapor uptake.¹²⁵⁻¹²⁷ However, protective gears contain activated carbon that suffers from slow degradation efficiency of these captured nerve agents. Farha's group and others¹⁰⁷⁻¹¹¹ have explored zirconium-based metal-organic frameworks (Zr-MOFs) as promising candidate catalysts for the catalytic hydrolysis of organophosphonate-based nerve agents and their simulants.

Nevertheless, the need for liquid water and/or volatile bases brings the limitations to their utility as a fielded protective gear. Luckily, MOFs, including Zr-MOFs, could capture water from air at low humidity at room temperature.^{122,128-131} The water capture behaviour of Zr-MOFs brings great possibility and practicality in catalytic hydrolysis of nerve agents under ambient humidity by using the water captured in MOF pores, rather than liquid water. Chapter 5 shows the integration of MOFs and non-volatile base buffer polyethylenimine (PEI), and fiber substrate into a functional Zr-MOF/PEI/fiber composite material for the catalytic hydrolysis of organophosphonate-based nerve agents, such as GD and VX, and their simulant, dimethyl 4-nitrophenyl phosphonate (DMNP) under ambient conditions (Scheme 5.1). This is a significant step accessing a efficient catalytically active MOF/fiber composite for the facile and practical production of gear protection.



Scheme 5.1. Schematic illustration of the fabrication procedure of MOF-808/PEI/fiber composite.

5.2 Experimental section

5.2.1 Materials

ZrOCl₂·8H₂O (98%), benzene-1,3,5-tricarboxylic acid (BTCA, 98%), terephthalic acid (BDCA, 99%), 2-aminoterephthalic acid (BDCA-NH₂, 99%), acetic acid, formic acid, and trifluoroacetic acid (99%) were purchased from Sigma-Aldrich. Other chemicals were purchase Fisher Chemical. Deionized water was used as the water source throughout the experiments. Cotton fabric was provided by China Dyeing holdings Ltd., Hong Kong. Before using, cotton fabric samples were washed in surfactant water solution at 90 °C for 20 min to remove impurities, and the surfactant residue on fabric was removed by thorough water washing.

5.2.2 Instrumentation

Powder X-ray diffraction (PXRD) patterns of fiber substrates and MOFs/fiber composite were recorded at room temperature on a STOE-STADIMP powder diffractometer equipped with an asymmetric curved Germanium monochromator (CuK α 1 radiation, $\lambda = 1.54056 \text{ \AA}$) at IMSERC (Integrated Molecular Structure Education and Research Center) of Northwestern University. N₂ adsorption and desorption isotherms of all materials were tested on a Micromeritics Tristar (Micromeritics, Norcross, GA) instrument at 77 K. Scanning electron micrographs (SEM) images of all coating were taken using a Hitachi SU8030 at the EPIC facility (NUANCE Center-Northwestern University). Before SEM observation, all samples were coated with OsO₄ to ~9 nm thickness in a Denton Desk III TSC Sputter Coater. Inductively coupled plasma–Optical emission spectroscopy (ICP–OES) was tested using an iCAP™ 7600 ICP-OES Analyzer (Thermo Scientific™) over the 166–847nm spectral range. For DNMP hydrolysis, ³¹P NMR spectra were collected on 400 MHz Agilent DD MR-400 at IMSERC (Integrated Molecular Structure Education and Research Center) of Northwestern University. For the GD and VX hydrolysis, the ³¹P NMR measurements were conducted on a 400 MHz Varian NMR spectrometer using H₃PO₄ as in internal standard. Water isotherms were measured on a Micromeritics 3Flex, and the water uptake in g g⁻¹ units is calculated as [(adsorbed amount of water)/(amount of adsorbent)]. Prior to the water adsorption measurements, water (analyte) was degassed by freeze-pump-thaw cycling using liquid nitrogen until the saturation pressure of water at a given temperature was achieved. The temperature of the sample tube was controlled with a Micromeritics Isocontroller. Activation of MOFs was performed under a dynamic vacuum for 12 h on SVP at 120 °C (2 °C/min).

5.2.3 Synthesis of NU-1000

NU-1000 was prepared according to a reported protocol with slight modification¹³²: ZrOCl₂·8H₂O (98 mg, 0.30 mmol) and benzoic acid (2 g, 16.38 mmol) were ultrasonically dissolved in 8 mL of DMF in an 8-dram. The DMF solution was heated in an oven at 100 °C for 1 h. After cooling down to room temperature, 40 mg (0.06 mmol) of 1,3,6,8-tetrakis(p-benzoic acid)pyrene (H₄TBAPy) linker and trifluoroacetic acid (TFA) modulator (40 μL, 0.52 mmol) were added. After sonication for 10 min, the mixture was incubated at a 100 °C oven for 18 h. After the vial was cooled to room temperature, obtained yellow powder material was isolated by centrifugation for 5 min at 7500 rpm and washed with 15 mL of *N,N*-dimethylformamide (DMF) three times by soaking ~1 h between each wash cycle. An HCl activation step was performed to remove coordinated benzoic acid modulator from the Zr₆ node by heating the powder in a mixture of 12 mL DMF and 0.5 mL of 8 M aqueous HCl in an oven at 100 °C for 18 h. After the vial was cooled to room temperature, the yellow powder was centrifugated and washed with 15 mL of DMF three times and 15 mL of acetone three times. In each washing cycle, the powder was soaked for 1 h in the solvent. The NU-1000 powder was centrifugated and dried in a vacuum oven at 80 °C overnight, and then heated at Micromeritics Smart VacPrep under vacuum at 120 °C for 18 h to remove the captured solvents.

5.2.4 Synthesis of UiO-66

UiO-66 was prepared according to a reported procedure with slight modification¹³³: ZrCl₄ (125 mg, 0.54 mmol), 1,4-benzene dicarboxylic acid (123 mg, 0.75 mmol) dissolved in 15 ml of DMF under sonication. 1 mL of concentrated HCl (12 M) was added to above precursor solution and then mixed by sonication for another 5 min. The obtained solution

was heated at 80 °C in oven for 18 h. After cooling down to room temperature, the white powder was collected by centrifugation, and washed with 15 mL of DMF for three time and 15 mL of acetone for three time and finally soaked in 15 mL of acetone overnight. The obtained powder was dried in a vacuum oven at 80 °C overnight and activated according to the method described above.

5.2.5 Synthesis of UiO-66-NH₂

UiO-66-NH₂ was prepared according to a reported procedure with slight modification¹³⁴. ZrCl₄ (0.27mmol, 67 mg), 2-aminoterephthalic acid (0.38 mmol; 69 mg) and 15 mL DMF, were added in a 8-dram vial and sonicated to get a clear solution, then 0.5 mL of concentrated HCl was added to the precursor solution and sonicated for several minutes. The above solution was heated at 80 °C for 18h in a preheated oven. The resulting powder was then centrifuged and washed first with fresh DMF and then with fresh ethanol and finally soaked in ethanol overnight to exchange residual DMF. The obtained powder was dried in a vacuum oven at 80 °C overnight and activated according to the method described above.

5.2.6 Synthesis of MOF-808 microcrystals

MOF-808 was synthesized according to a previous procedure with slight modifications.¹³⁵ ZrOCl₂·8H₂O (2 g, 6.2 mmol) and 1,3,5-benzenetricarboxylic acid (BTCA; 1.5 g, 7.1 mmol) were dissolved under sonication in a mixture of 284 mL of DMF and 284 mL of formic acid in a 2-L screw-capped glass jar. The glass gar was then heated at 120 °C for 48 hours in a preheated oven. After cooling to room temperature, the obtained white powder was collected by centrifugation, and washed with fresh DMF for three and the solvent was exchanged by fresh acetone overnight. The powder was then washed with large amounts

of fresh acetone. After centrifugation, obtained powder was then dried in a vacuum oven at 85 °C for two hours, and then soaked in 284 mL of aqueous hydrochloric acid solution (0.1 M) at room temperature overnight to remove the formic acid coordinated on zirconium nodes. The obtained white powder was then washed with large amounts of deionized water was acetone for three times and soaked in acetone overnight. The obtained white powder then initially dried in a preheated vacuum oven at 85 °C and activated according to the method described above.

5.2.7 Synthesis of MOF-808 nanoparticles

MOF-808 nanoparticles used in gel-based dipping-coating were prepared using a published procedure with slight modifications.¹³⁶ BTCA (4.2 g, 20 mmol) and $\text{ZrOCl}_2 \cdot 8\text{H}_2\text{O}$ (6.4 g, 20 mmol) were dissolved in DMF/formic acid (300 mL/300 mL) and placed in a 2-L screw-capped glass jar, which was heated to 120 °C for 24 h. White powder was collected by centrifugation (8000 rpm for 10 min) and washed three times with 200 mL of fresh DMF three times and with 200 mL of fresh acetone three times. As-synthesized MOF-808 nanoparticles were then immersed in 200 mL of anhydrous acetone for three days, during which time the acetone was replaced every day. The acetone-washed sample was then evacuated at 80 °C for 24 h and activated according to the method described above.

5.2.8 Preparation of PEI/fiber composite as control.

1 g of PEI powder was dissolved in 10 mL methanol under stirring to get a clear solution. A piece of cotton fabric (5 cm x 5 cm) was immersed into the solution for 10 min while stirring, and then it was taken out from suspension to rest on aluminum foil overnight inside the fume hood to dry.

5.2.9 Preparation of MOF-808/fiber composite as control.

1 g of MOF-808 was added into 20 mL methanol, which was stirred for 10 h to get a uniform suspension. A piece of cotton fabric (5 cm x 5 cm) was immersed into the suspension for 10 min while stirring, and then it was taken out from suspension to rest on aluminum foil overnight inside the fume hood to dry.

5.2.10 Hydrolysis of DMNP with MOFs/PEI composite under ambient humidity.

Hydrolysis experiments were carried out at room temperature under different relative humidity (RH) controlled by a humidified chamber. MOF catalyst (1.5 μmol ; corresponds to 6 mol% catalyst) and 17 mg PEI transferred into a 2-dram vial. The MOFs/PEI composite are formed via vortex-mixing for 15 seconds. DMNP (4 μL) was carefully added onto the composite with multiple contacted spots and then swirled via vortex-mixing for 15 sec. The uncapped vial was led in the humidified chamber under specific RH for recorded time before conduction digestion. To digest the sample for NMR, 0.7 mL of $\text{D}_2\text{SO}_4/\text{DMSO-D}_6$ (15/100 V/V) was added into the vial. The vial was sealed, whirled by vortex for 1 min, and was then transferred to an NMR tube for ^{31}P NMR measurement.

5.2.11 Preparation of MOF-808/PEI/fiber composite. 5 g of PEI powder was dissolved in 50 mL methanol under stirring to get a clear solution. 2.5 g of MOF-808 nanoparticle was added into above PEI solution, which was stirred for 10 h to get a uniform suspension. A piece of cotton fabric (5 cm x 5 cm) was dipped into the suspension for 10 min under stirring, and then it was taken out from suspension and placed on aluminum foil overnight inside the fume hood to remove the solvent by evaporation. This stock suspension can be reused for preparation of 15 pieces of the MOF-808/PEI/fiber composite (5 cm x 5 cm).

5.2.12 Hydrolysis of DMNP with MOF-808/PEI/fiber under ambient humidity.

Hydrolysis experiments on MOF-808/PEI/fiber were carried out similar to MOF/PEI composite at room temperature under different RH controlled by a humidified chamber. DMNP (4 μL) was carefully added onto the center of MOF-808/PEI/fiber composite (1 cm x 1 cm) in an uncapped vial, and then put the chamber at 50% humidity for recorded time. The sample digestion and ^{31}P NMR measurement were same to these on MOF-808/PEI composite.

5.2.13 Hydrolysis of Soman (GD) with MOF-808/PEI/fiber under ambient humidity.

Caution! Experiments should be run by trained personnel using appropriate safety procedures. Hydrolysis experiments were carried out on composite materials at room temperature using a procedure similar to DMNP experiments. Samples were prehumidified at 50% RH for ~ 16 h after which 2.4 μL of GD were added dropwise to the composite. After 15, 30, and 60 min, 900 μL of DMSO- D_6 were added followed by vortexing. Immediately after vortexing, 100 μL of 50% HF was added to the solution. After 30 min, the solution was vortexed and transferred to the NMR reaction tube and monitored for GD and PMPA using ^{31}P NMR on a 400 MHz Varian NMR spectrometer using H_3PO_4 as in internal standard. Background data were collected by first digesting the MOF-808/PEI/cotton composite in HF/DMSO- D_6 followed by GD spiking to ensure no homogeneous reactivity occurred in solution between digestion and NMR analysis.

5.2.14 Stability test on MOF-808/PEI/fiber composite.

To test the catalytic performance of sample under CO_2 and simulated gasoline atmosphere, 50 mg of dry ice or 100 μL of octane was added in the incubation chamber. After standing for 1 h to gasify the dry ice and octane, MOF-808/PEI/fiber composite (1 cm x 1 cm) loaded

with DMNP (4 μ L) was put the chamber at 50% humidity for recorded time. The sample digestion and ^{31}P NMR measurement was sample to these on MOF-808/PEI/fiber. To test the catalytic performance of sample after perspiration exposure, 10 μ L of artificial perspiration (pH = 4.5) was added in the center of MOF-808/PEI/fiber composite (1 cm x 1cm), and DMNP (4 μ L) was dropped in the center of MOF-808/PEI/fiber composite for catalytic test. Dried sample after perspiration addition was also tested using the same method. MOF-808/PEI/cotton after storage in air for 100 days or after agitation in water in a beaker for 24 h with or without drying in air also tested in solid state hydrolysis.

5.2.15 Scaled up coating MOF-808/PEI composite layer on fiber.

20 g of PEI powder was added in 200 mL of methanol under stirring to get a clear solution. 10 g of MOF-808 nanoparticle was added into PEI solution, which was stirred for 10 h to get a uniform suspension. A pieces of cotton fabric (30 cm x 30 cm) was immersed into the suspension for 10 min, and then taken out from suspension. The cotton fabric with about 200% liquid pick-up was carefully placed on an aluminium foil and dried in a hood overnight.

5.3 Results and discussions

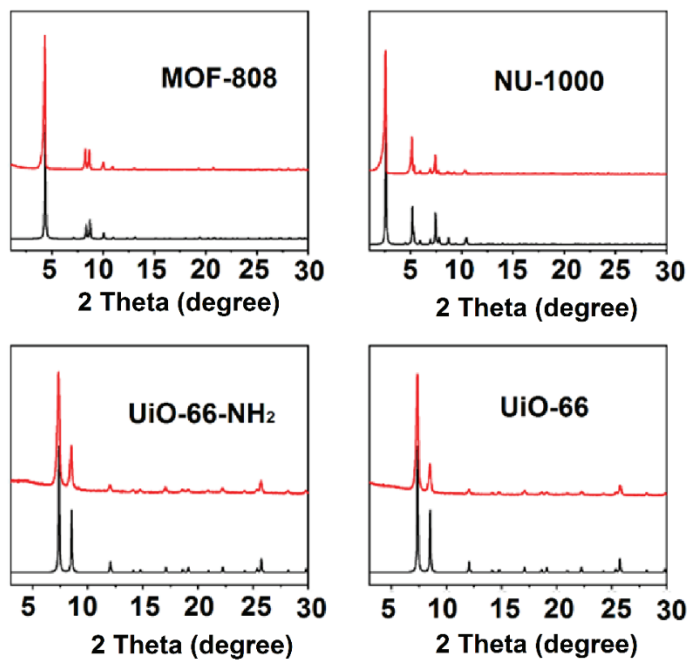


Figure 5.1. PXRD patterns of MOF-808, NU-1000, UiO-66-NH₂ and UiO-66.

Red: synthesized; black: simulated.

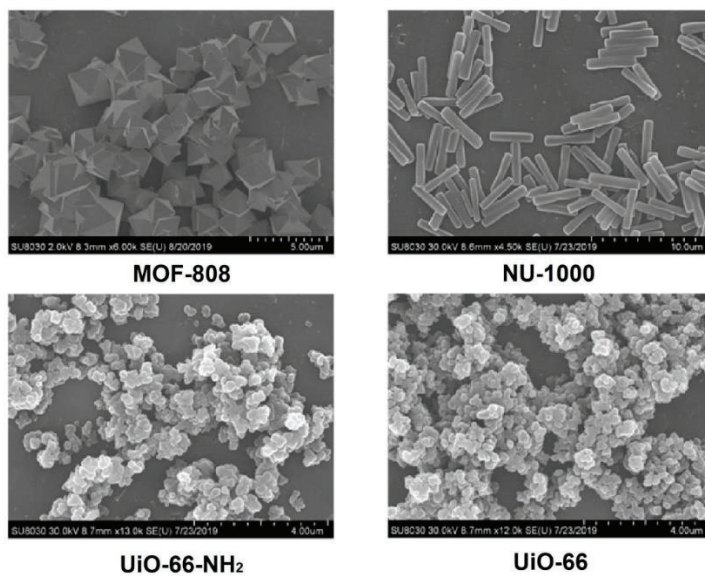


Figure 5.2. SEM images of MOF-808, NU-1000, UiO-66-NH₂ and UiO-66.

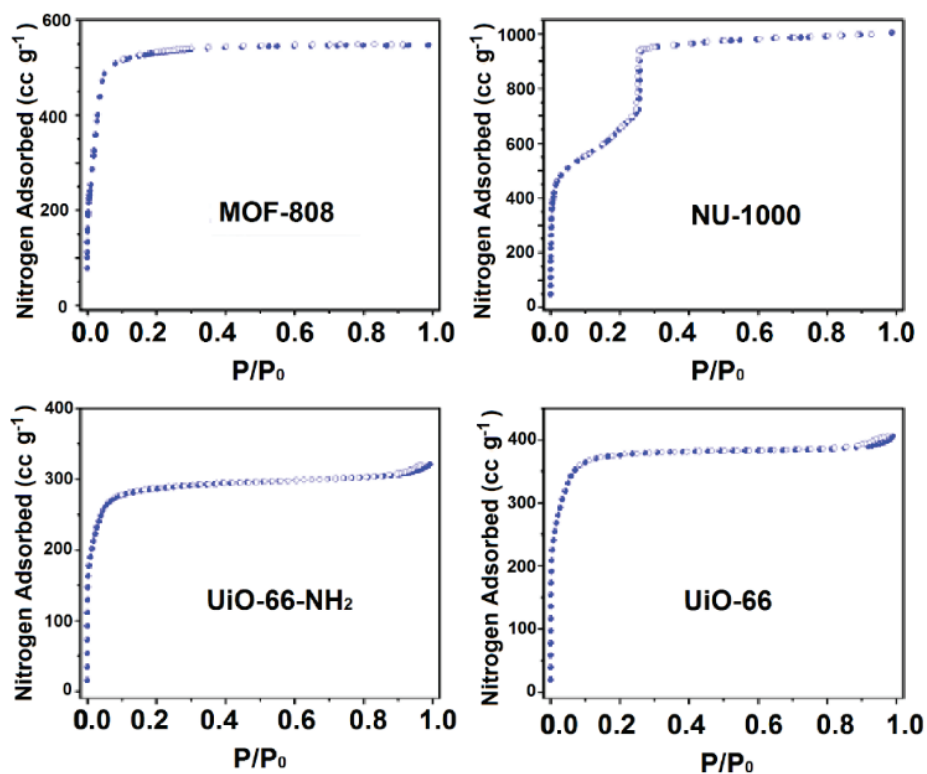


Figure 5.3. N₂ sorption isotherms of MOF-808, NU-1000, UiO-66-NH₂ and UiO-66.

Four Zr-MOFs, namely UiO-66, UiO-66-NH₂, MOF-808, NU-1000, were synthesized according to reported protocols, and the phase purity, morphology and porosity of these materials were consistent to reported works (Figure 5.1-Figure 5.3).¹³²⁻¹³⁵ The water vapor adsorption isotherms of these Zr-MOFs were tested, and the results were summarized in Figure 5.4. From the water adsorption isotherms, the pores of UiO-66, UiO-66-NH₂ and MOF-808 can be saturated with water at RH = 40% at 25 °C while NU-1000 reaches its saturation at RH = 70% at 25 °C. These data indicate the possibility to use UiO-66, UiO-66-NH₂ and MOF-808 in catalytic hydrolysis of nerve agents and their simulant under ambient humidity (~50%) since the essential water molecules for the hydrolysis of nerve agents and the simulant were captured inside the pores of these Zr-MOFs.

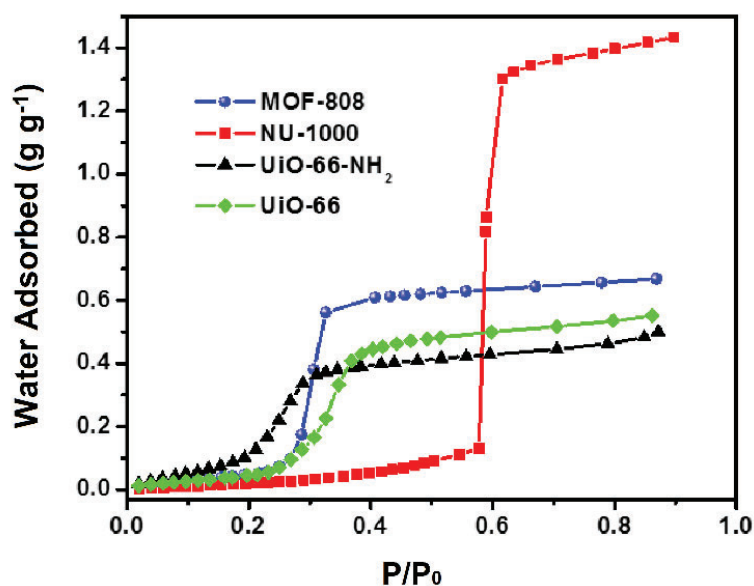


Figure 5.4. Water adsorption isotherms of UiO-66, UiO-66-NH₂, MOF-808, and NU-1000 at 298K.

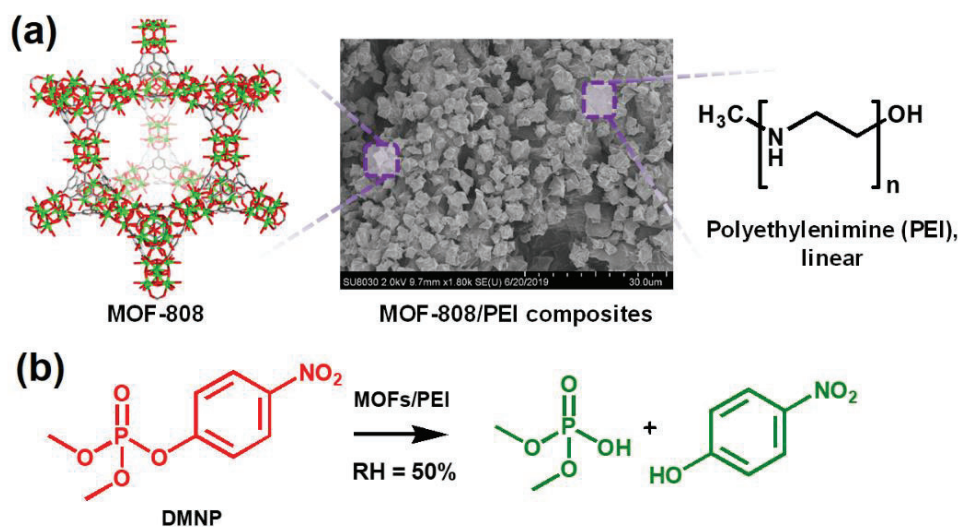


Figure 5.5. (a) Illustration of MOF-808/PEI composites from vortex mixing of MOFs and PEI particles. Atom color scheme of MOF-808 structure: C, grey; Zr, green; O, red. H atoms are omitted for the sake of clarity. (b) Catalytic hydrolysis reaction of DMNP with MOFs/PEI composites under RH = 50%.

Table 5.1. The result of the solid-state hydrolysis of DMNP with MOFs, MOFs/PEI powdered catalysts (6%), or PEI at 50% humidity.

Catalysts	Conversion (%)
MOF-808	14
MOF-808/PEI	65
UiO-66	5
UiO-66/PEI	25
UiO-66-NH ₂	6
UiO-66-NH ₂ /PEI	22
NU-1000	5
NU-1000/PEI	23
PEI	12

Recently, Farha's group have reported the replacement of volatile organic small molecular bases, as used in hydrolysis experiment in Chapter 4, with involatile polymeric buffer bases, namely linear polyethyleneimine (PEI), to achieve more practical degradation of nerve agents.^{137,138} Thus, polymeric PEI was chosen as the buffer was chosen to regenerate Lewis acidic Zr sites during the solid state catalysis in this chapter. The powdered heterogeneous MOF/PEI composite catalyst catalysts were synthesized by a simple vortex mixing of MOF powders and PEI particles (Figure 5.5a).

A solid-state hydrolysis of a nerve agent simulant, dimethyl 4-nitrophenyl phosphonate (DMNP), experiment was designed to probe the catalytic performance of this powdered catalysts under ambient humidity (RH = 50%) as described in the Experiments part. It demonstrated the efficacy of MOFs/PEI composite catalysts for the hydrolysis of phosphate ester bonds of DMNP at RH = 50%. Among all studies using MOFs, MOFs/PEI

powdered catalysts (6%), or PEI, MOF-808/PEI composite showed the best catalytic activity in degrading DMNP (Table 5.1). It can be attributed to three main reasons as following: (i) the large pore size of MOF-808 allows facile diffusion of DMNP to the Zr node catalytic sites; (ii) 6-connected Zr_6 node of MOF-808, as opposed to higher connectivities in the other Zr-MOFs, offering more active sites for reaction; (iii) the good water adsorption performance at the RH = 50%.

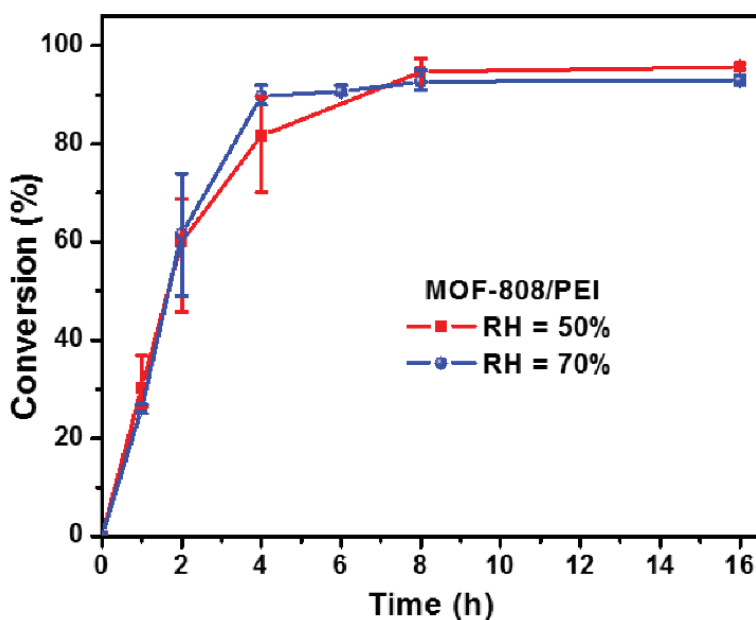


Figure 5.6. Solid state hydrolysis profile of DMNP with MOF-808/PEI composite using 6 mol% catalyst loading under RH = 50% and RH = 70%.

Kinetic studies revealed an initial half-life of $t_{1/2} = \sim 1.6$ h for hydrolysis of DMNP in the presence of MOF-808/PEI composite (6 mol% catalyst loading) under RH = 50% as shown in Figure 5.6. It is important to note that it is not all of MOF particles contacting with DMNP due to the high viscosity of DMNP liquid, which may lead to a slight underestimating of the catalytic activity of the powdered heterogeneous catalyst. In

addition, it is found that the effect of increasing humidity on the catalytic activity of the MOF-808/PEI composite is limited after the pore filling RH is reached. For example, only a slightly enhanced performance was observed for MOF-808/PEI composites in the catalytic hydrolysis of DMNP under RH = 70% with $t_{1/2} = \sim 1.2$ h.

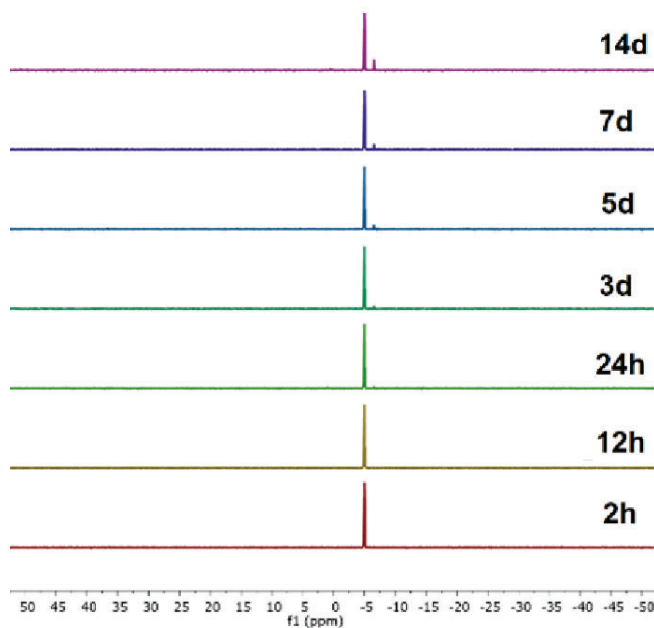


Figure 5.7. Control experiments for testing the background hydrolysis reaction under MOF digestion conditions.

To exclude the possibility of hydrolysis of NMDP caused by the digestion solvent. A background study of the digestion using $\text{D}_2\text{SO}_4/\text{DMSO-D}_6$ was conducted. 0.6 mL of $\text{D}_2\text{SO}_4/\text{DMSO-D}_6$ (15/100 V/V) was added into the vial containing DMNP (4 μL ; 25 μmol), and then transferred to an NMR tube. ^{31}P NMR was measured at different times, and, no conversion was detected after 2 h and about 14% conversion of DMNP to M4NP was observed after 14 days as shown in Figure 5.7. Since the typical NMR measurements were performed in less than 2 hours after the digestion, the contribution of the background reaction was immeasurably low.

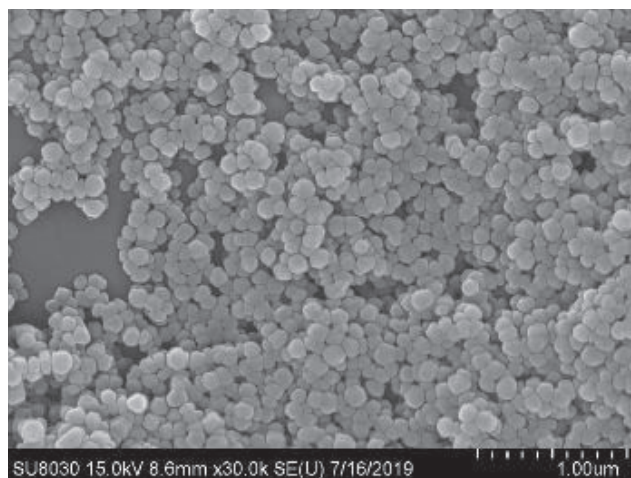


Figure 5.8. A SEM image of MOF-808 nanoparticles used for MOF-808/PEI/cotton fiber composite using gel-based coating methods.

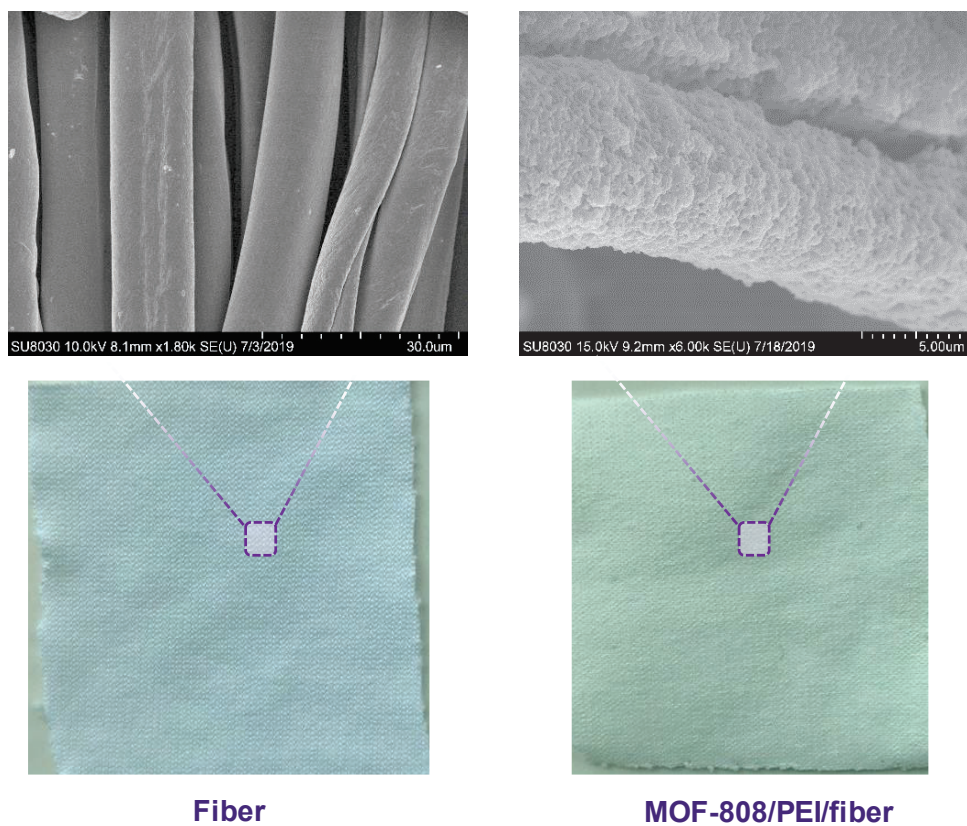


Figure 5.9. SEM and optical images of cotton fiber and MOF-808/PEI/fiber.

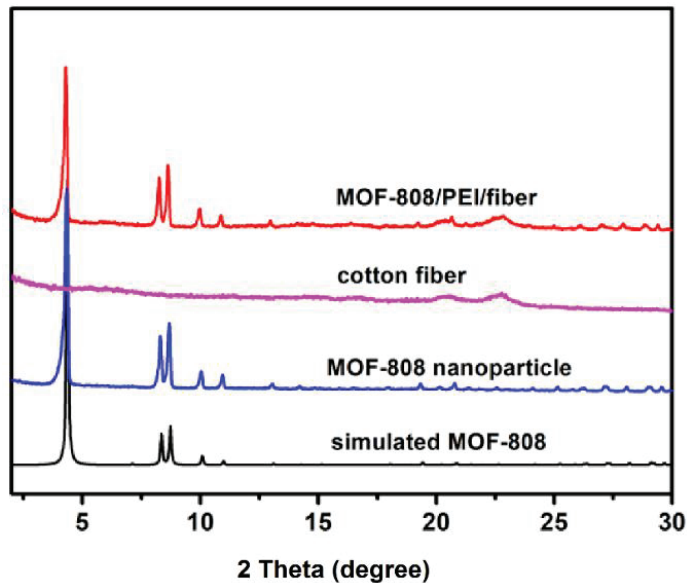


Figure 5.10. PXRD pattern of MOF-808 nanoparticles, cotton fiber, and MOF-808/PEI/cotton fiber composite.

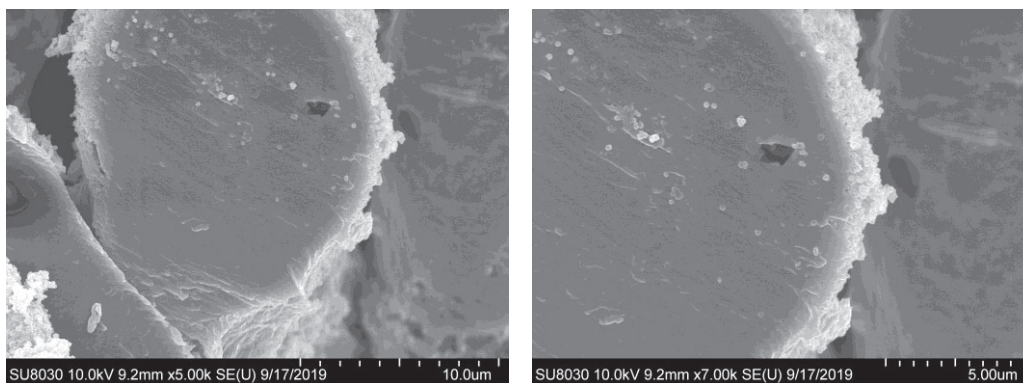


Figure 5.11. SEM images of MOF-808/PEI/fiber composite on a cutting edge.

While the powdered MOFs/PEI composite showed efficient catalytic activity towards DMNP catalytic hydrolysis, their practical application as protective gear requires the combination of the powdered catalysts with supporting materials. Inexpensive, flexible, and permeable cotton textile was employed as readily accessible supporting materials for MOF/PEI composites in this chapter. A gel-based dip-coating method¹³⁹, for the first time, was developed to prepare a MOF-808/PEI/cotton fiber composite. Briefly, MOF-808

nanoparticles with particles sized below 200 nm were synthesized¹³⁶ (Figure 5.8) and dispersed in a PEI solution in methanol, which was used as the stock suspension for dipping-coating. After a dipping-drying process at room temperature as described in experimental section 5.2.11, a dense and continuous MOF-808/PEI composite coating (as shown in Figure 5.9) was obtained on the cotton fiber with a mass loading of 12%. The crystallinity of MOF-808 component was maintained after coating onto cotton fiber (Figure 5.10). The thickness of the coating is approximately 1-2 μm based on observation of the in the SEM image of the cross section as shown in Figure 5.11.

It is worth noting that the coating method in this chapter is very facile and scalable compared to previous reported methods of MOF/fiber composite production.^{36,52,140} The kinetic studies of the catalytic hydrolysis of DMNP with MOF/PEI/cotton composite under RH = 50% revealed a half-life of 0.4 h (Figure 5.12- 5.13), which is close to the catalytic activity of some well dispersed Zr-MOFs nanoparticle catalyst in the aqueous solution of volatile organic buffer base.⁷¹ The improved catalytic performance of MOF/PEI/cotton fiber composite compared to MOF/PEI powder should be attributed to the better blending and dispersion of the MOF/PEI coating with a thickness only 1-2 μm on the fiber surface, exposing more catalytic activity sites and better exploit wicking effects of simulant compared to bulk powdered MOF/PEI catalysts.

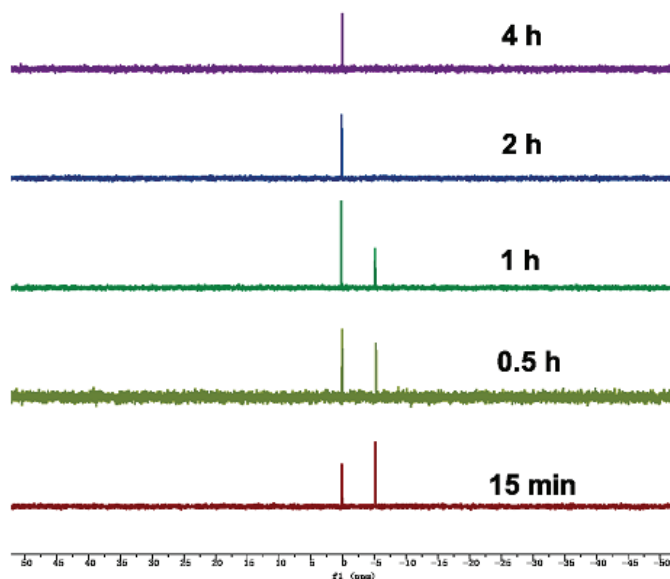


Figure 5.12. The representative ^{31}P NMR spectra of using MOF-808/PEI/fiber composites in solid state hydrolysis at different time points (at 50 % humidity).

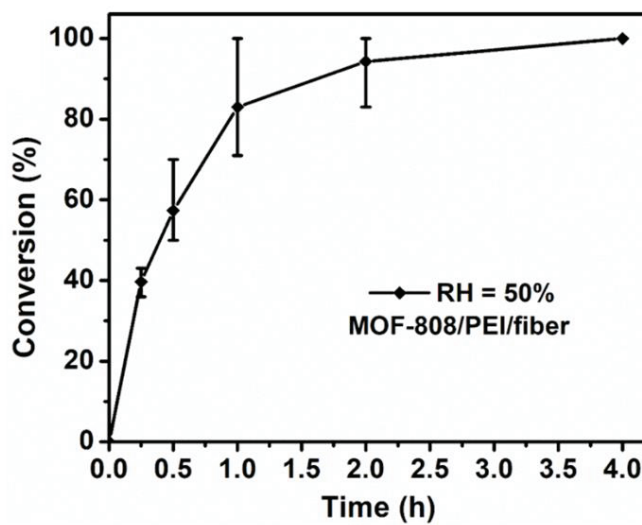


Figure 5.13. Solid state DMNP hydrolysis reaction conversion profile using MOF-808/PEI/fiber composite catalyst (1 cm x 1 cm) at 50 % humidity.

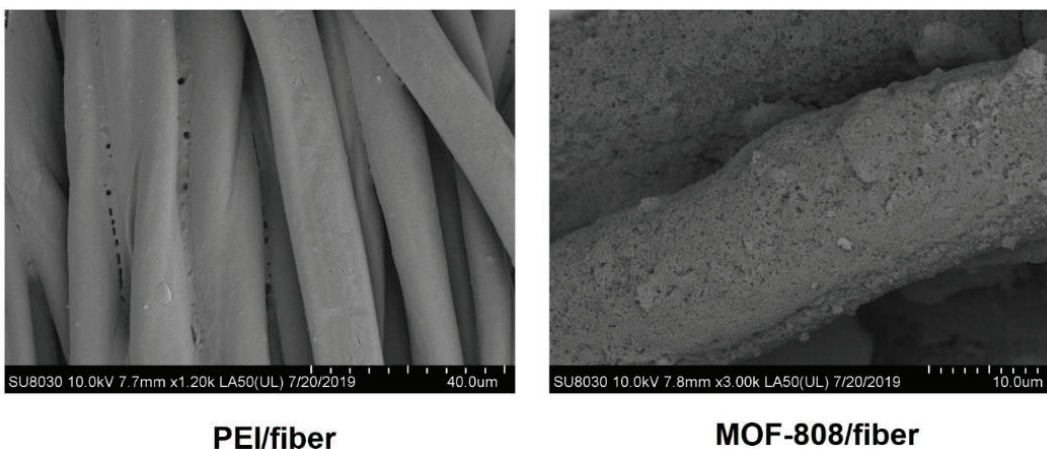


Figure 5.14. SEM images of PEI coated cotton fiber (PEI/fiber) and MOF-808 coated fiber (MOF-808/fiber) for control experiments.

MOF-808 nanoparticle and PEI polymer coated cotton fibers were also prepared and used in control catalysis tests, as well with pure cotton fiber (Figure 5.14-Figure 5.15). After 0.5 h reaction, negligible conversion obtained when pure cotton fiber, PEI coated cotton fiber, and MOF-808 coated cotton fiber were used as catalyst, which revealed the importance of the synergistic effect of the ternary components in our prepared composite catalyst. Despite the use of aqueous solution of volatile *N*-ethylmorpholine in the recently reported works about MOFs/fiber composite,^{36,52,140} the prepared MOF-808/PEI/fiber composite tested without liquid water showed comparable reactivity toward hydrolysis of DMNP ($t_{1/2} = \sim 24$ min vs. ~ 12 -210 min).

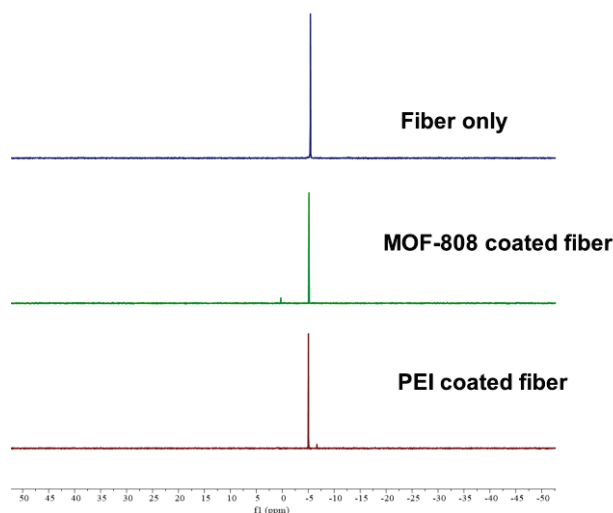


Figure 5.15. Control test using fiber, MOF-808 coated fiber, and PEI coated fiber in solid state hydrolysis (50 % humidity, 0.5 h).

High robustness and stability of the MOF coating on fiber substrate is critical in practical applications, as the peeling MOF particles from the fiber could reduce the lifespan of a protective textile. The adhesion of the MOF/PEI composite coating to cotton fiber was evaluated through agitation test on the sample in water for 24 h. No notable loss on crystallinity of the composite sample was observed (Figure 5.16) and quantitative zirconium analysis by ICP-OES showed that Zr content was nearly unchanged after agitation test in water (before:12% vs after:11.8%). More importantly, the MOF-808/PEI/fiber composite's catalytic activity keeps intact after direct drying in air at room temperature. The stability of the MOF-808/PEI/fiber composite should be attributed to the low solubility of the PEI polymer in water which can act as a binder between MOF and cotton fiber surface. Shelf-life of the MOF-808/PEI/fiber composite was also investigated. Strikingly, after storage in air for 100 days, the catalytic performance for DMNP hydrolysis

was within the experimental error (conversion at 0.5 h: fresh: ~57 % vs. after storage: ~68 %).

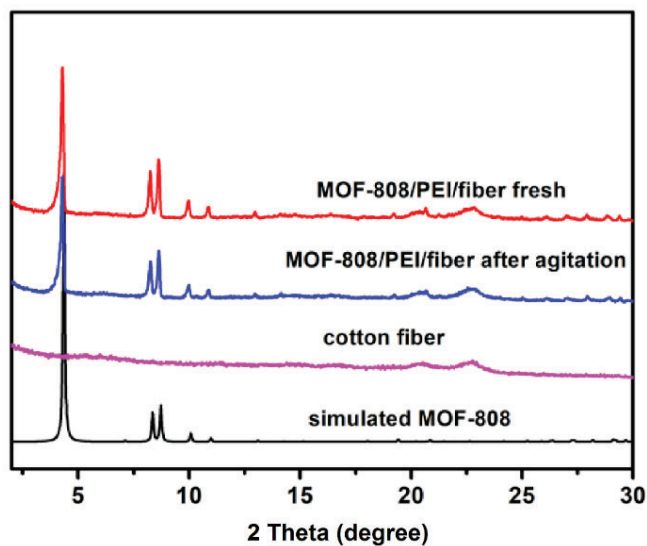


Figure 5.16. PXRD pattern of MOF-808/PEI/cotton fiber composite after agitation of the sample in water for 24 h.

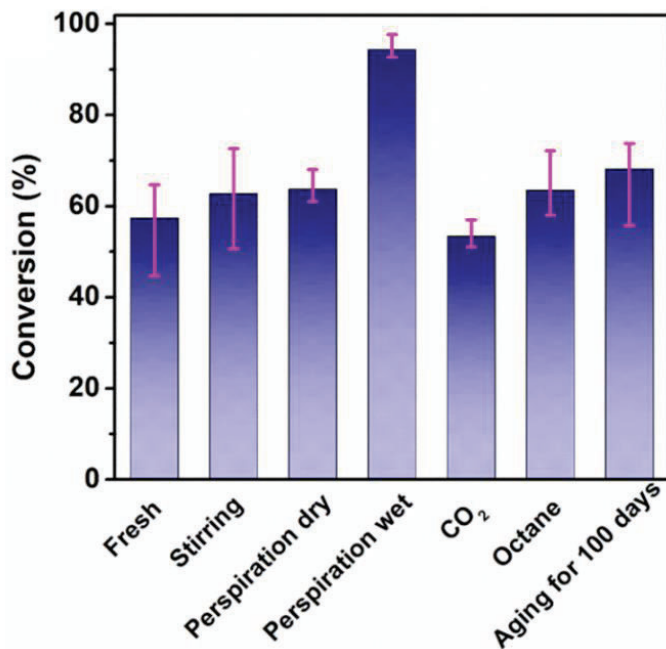


Figure 5.17. MOF-808/PEI/fiber catalyst's tolerance performance to surrounds.

In real application, the protective gear was exposed to numerous other conditions as well as humidity, including perspiration, atmospheric CO₂, and organic contaminants (i.e. octane) from vehicles. The performance of the MOF-808/PEI/fiber composite was evaluated under simulated conditions, including after exposure to perspiration, simulated CO₂-rich atmosphere, simulated gasoline-rich atmosphere, and after exposure to air for 100 days as shown in Figure 5.17. After wetting MOF-808/PEI/fiber composite (1 cm x 1 cm) by 10 uL of artificial perspiration (pH = 4.5), the catalytic conversion of DMNP at 0.5 h improved from 57% to 94% (Figure 5.16), which could be attribute to the sufficient water supply in perspiration benefiting the hydrolysis reaction. Interesting, after drying the sweated composites in air, the catalytic performance was comparable to that of freshly prepared composite sample. In addition, MOF-808/PEI/fiber composite retained its catalytic efficiency after exposure to CO₂-rich and simulated gasoline atmosphere (Figure 5.16). The scalability of the dipping-coating method was also demonstrated using a large piece of cotton textile (30 cm x 30 cm) as fiber substrate, and the resulting MOF-808/PEI/fiber composite showed similarly mass loading (13%), crystallinity (Figure 5.18) and high catalytic activity (with a conversion of DMNP about 60% at 0.5 h). It is interesting to note that the MOF-808 nanoparticle in the fibrous composite could be recoverable by removing the PEI polymer in methanol. The BET surface areas of recovered MOF-808 nanoparticle was 1720 m²/g, similar to that of fresh nanoparticles (2150 m²/g) as shown in Figure 5.19.

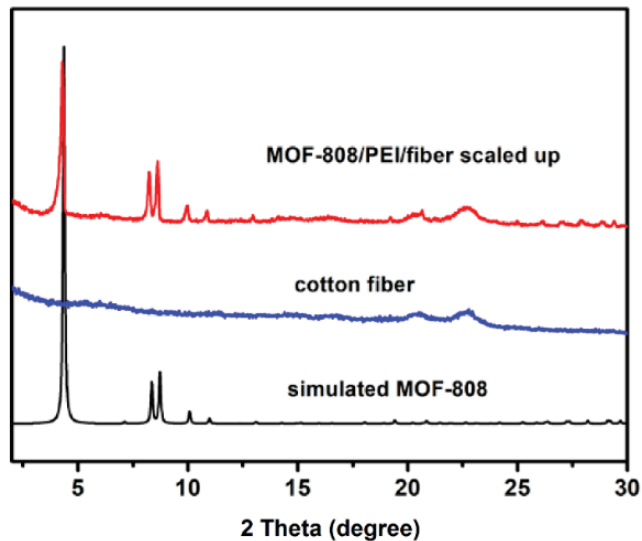


Figure 5.18. PXRD pattern of cotton fiber, and MOF-808/PEI/cotton fiber composite.

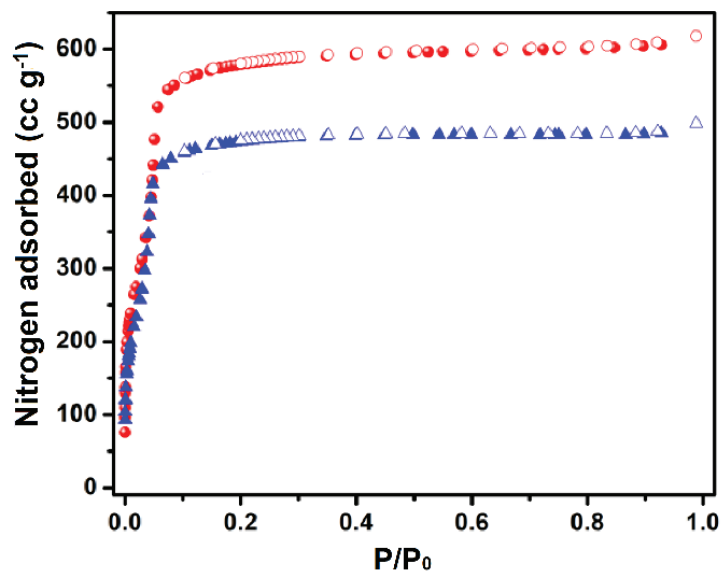


Figure 5.19. Isotherms of MOF-808 nanoparticle (red) and MOF-808 nanoparticle recovered from MOF-808/PEI/cotton composite (blue).

With these attractive simulant degradation results, solid state catalytic hydrolysis tests using the MOF-808/PEI/fiber composite were also conducted on the nerve agent soman

(GD) (Figure 5.20-Figure 5.21). Notably, the MOF-808/PEI/fiber composite was much more reactive towards the real nerve agent (GD) than the simulant (DMNP), showing a half-life of only 12 min, while former reported method using MOF powder only achieved a half-life over 2 h. High toxic GD was almost totally hydrolyzed into non-toxic pinacolyl methylphosphonic acid (PMPA) after only 1 h reaction.¹⁴¹ In addition, the acid solution used in digestion didn't show obvious degradation of GD under experiment conditions (Figure 5.22).

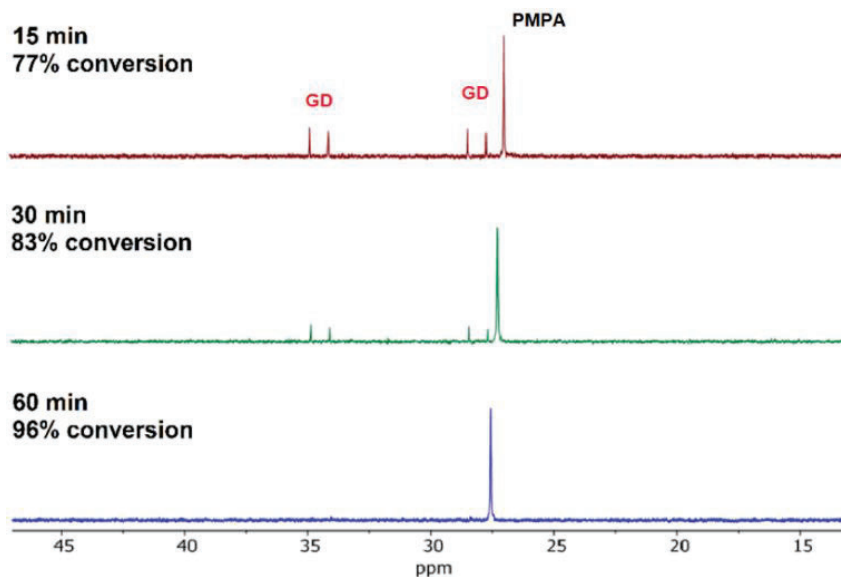


Figure 5.20. ³¹P NMR spectra of using MOF-808/PEI/fiber composites in solid state hydrolysis of GD at different time points. 100 uL HF and 900 uL DMSO-D₆ were used as digestion solvent.

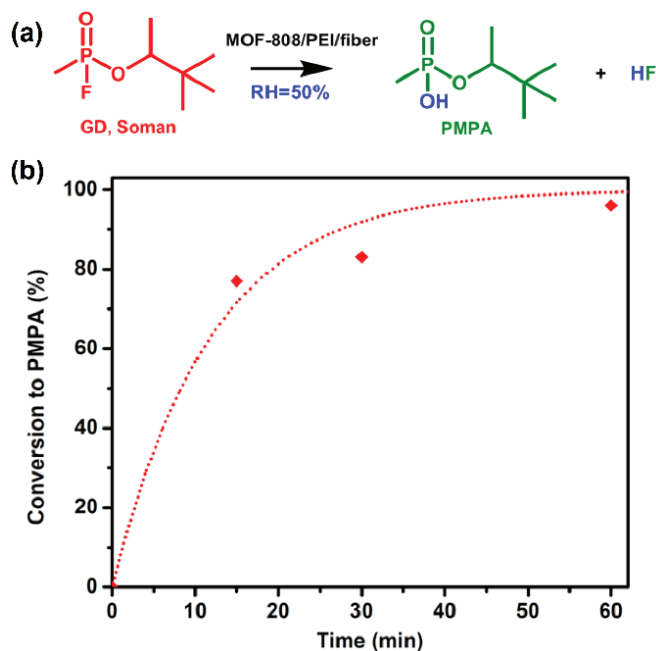


Figure 5.21. (a) Hydrolysis reaction of soman (GD) with MOF-808/PEI/fiber composites. (b) Solid state conversion profile for the hydrolysis of soman under ambient condition. Dotted lines correspond to first-order fits.

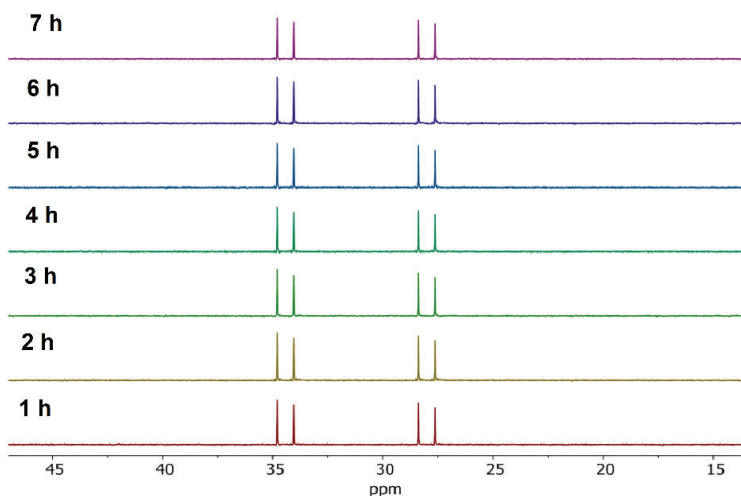


Figure 5.22. The background study of the digestion step using HF/DMSO- D_6 (1/9 V/V). MOF-808/PEI fabric was incubated with HF/DMSO- D_6 for about 30 min. Then GD was added, and ^{31}P NMR measurement was monitored overtime.

Moreover, another high toxic nerve agent, VX (O-ethyl S-[2-(diisopropylamino)ethyl] methylphosphonothioate), was also totally degraded into the nontoxic compounds, namely EMPA (ethyl methyl phosphonic acid) and DESH [2-(diisopropylamino)ethanethiol] (Figure 5.23) after only 1 h under the same condition. This result demonstrated the generality of this MOF-808/PEI/fiber for hydrolyzing both P-F and P-S bonds in different nerve agents under ambient conditions.¹⁴¹

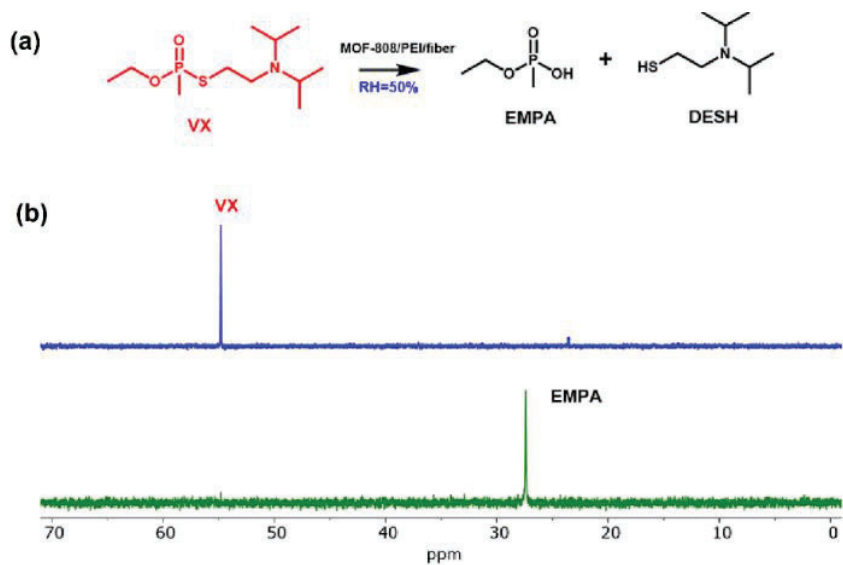


Figure 5.23. (a) Hydrolysis reaction of VX with MOF-808/PEI/fiber composites. (b) NMR spectra VX and its product after 1 h of solid-state hydrolysis using MOF-808/PEI/fiber composites. 100 μ L HF + 900 μ L DMSO-D6 was used as digestion solvents.

5.4 Conclusion

This chapter demonstrated the fabrication of a ternary MOF-808/PEI/fiber composite using a gel-based dip-coating method which showed high catalytic activity for the hydrolysis of a nerve agent under relevant conditions. Encouragingly, just utilizing only the moisture

water in air, the MOF-808/PEI/fiber composite showed excellent catalytic activity for the hydrolysis of nerve agents and their simulant compared to previously reported Zr-MOFs catalysts using volatile organic base buffer in water solution. Durability tests verified the robustness of MOF-808/PEI/fiber composite under real application atmospheres and conditions, demonstrating their practicality as protective textile against CWAs. This facile processing method could be easily scaled up using common equipment in textile industry, which could boost the application of MOF-808/PEI/fiber composite in protective gear production.

Chapter 6

Conclusions and Suggestions for Future Work

6.1 Conclusions

In this thesis, a study has been presented on the fabrication of MOFs/fiber composites integrating the processibility of textile fiber substrates and functionalities of MOF coatings. Two in-situ growth method and an ex-situ coating method were developed to synthesize MOF coatings on polymer fibers and explore related applications. Mechanism insights into the MOF growth on fiber surface during the in-situ coating methods have been revealed.

The conclusions of this thesis are summarized as follows. Firstly, the fabrication of a facile MOF/fiber composite through a room temperature coordination method has been presented. The prepared MOF/fiber composite shows tunable mass loading, good stability, high porosity and crystallinity, and excellent processability which makes it a promising candidate in gasoline desulfurization and toxic industrial gas removal. As reported, the method has good generality to different MOFs (HKUST-1, Cu-BDC, ZIF-8 and ZIF-67) and fiber substrates (nature fiber and synthetic fiber). Also, benefiting from the facile fabrication conditions of this method, it could be easily scaled up onto large pieces of fiber substrates. Secondly, an eco-friendly aqueous media synthesis method was developed to deposit MOF-808 and UiO-66-NH₂ on commercially available textile. Importantly, this method does not require pre-treatment of fibers with atomic layer deposition to install a metal-oxide template layer, and still results in a high MOF loading. Based on systematic characterization techniques, a three-stage MOF growth mechanism was revealed. Furthermore, when deposited on the fibers, the MOF maintained the high crystallinity and

porosity, as well as the high catalytic activity towards detoxification of high toxic organophosphate-based nerve agent. At the same time, the flexible porous MOF/fiber composite showed durable barrier performance against a mustard gas simulant. Finally, a cost-effective room temperature dipping coating method without expensive equipment has been developed to prepare Zr-MOF/buffer polymer/cotton fiber composite. The resulted composite could be used for ultrafast solid-state catalytic degradation of nerve agent in air without the assistant from alkaline buffer solution. Besides, due to the facile operation conditions of the dipping coating method, it is very ease to be scaled-up to industrial production of large pieces of MOF/fiber composite. This dipping coating method may provide solution to develop efficient protective gear in the real application conditions.

Green solvent such as water or alcohol was used the media in processing, and no chemical modification or atomic layer deposition (ALD) precoating on fiber surface were necessary as a nucleation layer for MOF growth. The reported three methods had high utilization of precursors, while previously reported solvothermal methods for MOF/fibers composite fabrication yielding 5–20 times free MOF particles in reaction solvent compared with these coated on the fiber substrate. Therefore, the practical and efficient methods reported in this thesis could reduce the cost in production and lower the impact to environment. The scalable and facile MOF/fiber composite fabrication techniques in this thesis can shed light on the future exploration of inexpensive, multifunctional, and durable materials that may be extended to energy and environmental application fields.

6.2 Suggestions for future work

Fabrication of MOF/fiber composite is critical toward practical industrial applications, such as functional filter, heterogeneous catalyst, sensor, and protective gear. Although great research progress in small batch scale has been made in developing functional MOF/fiber composites, the scaled up industrial production and the application of MOF/fiber composites in relevant condition only stays in primary stage. So, facile and scaled-up fabrication of MOF/fiber composites with excellent performance is an essential step to industrial processing. Also, design of the multicomponent MOF/fiber composites is important to multitask system. Based on the results in fabrication of MOF/fiber composite for pollutant removal and human protection against warfare agent, several suggestions for future work are outlined as follows.

- (1) For the coordination replication coating method reported in chapter 3, further exploration of the generality is necessary to other metal containing MOF, such as iron-based MOF, aluminum-based MOF, and zirconium-based MOF, to extend the application areas.
- (2) The aqueous synthesis procedure for Zr-MOF/fiber composite entails near reflux temperatures which hinders its use for coating MOF for nature cellulose fiber, such as cotton. Therefore, the facile methods should be further explored to prepare MOF/fiber composites at room temperature in aqueous media, a process which will be very useful for coating MOF on widely used thermal sensitive fiber.

- (3) For the aqueous synthesis method reported in chapter 4, microwave assisted heating may be useful to shorten the reaction time to get highly recovered MOF coating on fiber surface.
- (4) The prepared MOF/fiber composite showed excellent barrier function materials using mustard gas simulant CEES as an analyte. While the diffusion of real warfare agent such as mustard gas and GD through porous the composite should be further investigated, because their difference in molecular size and hydrophobicity. Also, the real protection efficiency of the composite against mixed warfare agents should be studied.
- (5) The pyrene-based NU-1000 or porphyrin-based PCN-222 MOF powder has been developed as a photocatalyst for the degradation of a mustard gas simulant, 2-chloroethyl ethyl sulfide (CEES). Under ultraviolet (UV) light irradiation, reactive singlet oxygen ($^1\text{O}_2$) is generated by MOF coating and selectively oxidizes CEES to the nontoxic product. While, the coating of photocatalytic MOF on fiber is unexplored. Future works on this field is necessary to prepare protective cloth against mustard gas.
- (6) The room temperature dipping coating method reported method in Chapter 5 is inexpensive and efficient. Further scaling-up production using common industrial roll-to-roll equipment should be promising for the bulk production.
- (7) The prepared MOF/fiber composites with high porosity and crystallinity may be extended to various application fields, such as drug delivery, continuous catalysis, sensor, water purification, and air cleaning.

References

1. Furukawa, H.; Cordova, K. E.; O’Keeffe, M.; Yaghi, O. M. The Chemistry and Applications of Metal-Organic Frameworks. *Science* **2013**, *341* (6149), 1230444.
2. Li, H.; Eddaoudi, M.; O’Keeffe, M.; Yaghi, O. M. Design and synthesis of an exceptionally stable and highly porous metal-organic framework. *Nature* 1999, *402*, 276-279.
3. Zhou, H.-C.; Kitagawa, S., Metal-Organic Frameworks (MOFs). *Chem. Soc. Rev.* **2014**, *43* (16), 5415-5418.
4. Park, K. S.; Ni, Z.; Côté, A. P.; Choi, J. Y.; Huang, R.; Uribe-Romo, F. J.; Chae, H. K.; O’Keeffe, M.; Yaghi, O. M. Exceptional Chemical and Thermal Stability of Zeolitic Imidazolate Frameworks. *Proc. Natl. Acad. Sci.* **2006**, *103* (27), 10186-10191.
5. James, S. L. Metal-Organic Frameworks. *Chem. Soc. Rev.* **2003**, *32* (5), 276-288.
6. Farha, O. K.; Eryazici, I.; Jeong, N. C.; Hauser, B. G.; Wilmer, C. E.; Sarjeant, A. A.; Snurr, R. Q.; Nguyen, S. T.; Yazaydin, A. Ö.; Hupp, J. T. Metal–Organic Framework Materials with Ultrahigh Surface Areas: Is the Sky the Limit? *J. Am. Chem. Soc.* **2012**, *134* (36), 15016-15021.
7. Rosi, N. L.; Eckert, J.; Eddaoudi, M.; Vodak, D. T.; Kim, J.; O’Keeffe, M.; Yaghi, O. M. Hydrogen Storage in Microporous Metal-Organic Frameworks. *Science* **2003**, *300* (5622), 1127-1129.
8. Li, J.-R.; Kuppler, R. J.; Zhou, H.-C. Selective Gas Adsorption and Separation in Metal-Organic Frameworks. *Chem. Soc. Rev.* **2009**, *38* (5), 1477-1504.

9. Pan, L.; Olson, D. H.; Ciemmolonski, L. R.; Heddy, R.; Li, J. Separation of Hydrocarbons with a Microporous Metal–Organic Framework. *Angew. Chem. Int. Ed.* **2006**, *45* (4), 616-619.
10. Sumida, K.; Rogow, D. L.; Mason, J. A.; McDonald, T. M.; Bloch, E. D.; Herm, Z. R.; Bae, T.-H.; Long, J. R. Carbon Dioxide Capture in Metal-Organic Frameworks. *Chem. Rev.* **2012**, *112* (2), 724-781.
11. Couck, S.; Denayer, J. F. M.; Baron, G. V.; Remy, T.; Gascon, J.; Kapteijn, F. An Amine-Functionalized MIL-53 Metal-Organic Framework with Large Separation Power for CO₂ and CH₄. *J. Am. Chem. Soc.* **2009**, *131* (18), 6326-6327.
12. Murray, L. J.; Dinca, M.; Long, J. R. Hydrogen Storage in Metal-Organic Frameworks. *Chem. Soc. Rev.* **2009**, *38* (5), 1294-1314.
13. Corma, A.; García, H.; Llabrés Xamena, F. X. Engineering Metal Organic Frameworks for Heterogeneous Catalysis. *Chem. Rev.* **2010**, *110* (5), 4606- 4655.
14. Xiao, J.-D.; Jiang, H.-L. Metal–Organic Frameworks for Photocatalysis and Photothermal Catalysis. *Acc. Chem. Res.* **2019**, *52* (2), 356-366.
15. Lee, J.; Farha, O. K.; Roberts, J.; Scheidt, K. A.; Nguyen, S. T.; Hupp, J. T. Metal-organic framework materials as catalysts. *Chem. Soc. Rev.* **2009**, *38* (5), 1450-1459.
16. Wang, C.; Xie, Z.; deKrafft, K. E.; Lin, W. Doping Metal-Organic Frameworks for Water Oxidation, Carbon Dioxide Reduction, and Organic Photocatalysis. *J. Am. Chem. Soc.* **2011**, *133* (34), 13445-13454.
17. DeCoste, J. B.; Peterson, G. W., Metal–Organic Frameworks for Air Purification of Toxic Chemicals. *Chem. Rev.* **2014**, *114* (11), 5695-5727.

18. Britt, D.; Tranchemontagne, D.; Yaghi, O. M. Metal-Organic Frameworks with High Capacity and Selectivity for Harmful Gases. *Proc. Natl. Acad. Sci. U. S. A.* **2008**, *105* (33), 11623-11627.
19. Barea, E.; Montoro, C.; Navarro, J. A., Toxic Gas Removal–Metal–Organic Frameworks for the Capture and Degradation of Toxic Gases and Vapours. *Chem. Soc. Rev.* **2014**, *43* (16), 5419-5430.
20. Li, J.; Wang, X.; Zhao, G.; Chen, C.; Chai, Z.; Alsaedi, A.; Hayat, T.; Wang, X. Metal–Organic Framework-Based Materials: Superior Adsorbents for the Capture of Toxic and Radioactive Metal Ions. *Chem. Soc. Rev.* **2018**, *47*, 2322-2356.
21. Lu, G.; Hupp, J. T. Metal-Organic Frameworks as Sensors: A ZIF-8 Based Fabry-Perot Device as a Selective Sensor for Chemical Vapors and Gases. *J. Am. Chem. Soc.* **2010**, *132* (23), 7832-7833.
22. Liu, X.; Fu, W.; Bouwman, E. One-step Growth of Lanthanoid Metal–Organic Framework (MOF) Films under Solvothermal Conditions for Temperature Sensing. *Chem. Commun.* **2016**, *52*, 6926-6929.
23. Kreno, L. E.; Leong, K.; Farha, O. K.; Allendorf, M.; Van Duyne, R. P.; Hupp, J. T. Metal-Organic Framework Materials as Chemical Sensors. *Chem. Rev.* **2012**, *112* (2), 1105-1125.
24. Shekhah, O.; Liu, J.; Fischer, R. A.; Wöll, C. MOF Thin Films: Existing and Future Applications. *Chem. Soc. Rev.* **2011**, *40* (2), 1081- 1106.
25. Kitao, T.; Zhang, Y.; Kitagawa, S.; Wang, B.; Uemura, T. Hybridization of MOFs and Polymers. *Chem. Soc. Rev.* **2017**, *46* (11), 3108-3133.

26. Bradshaw, D.; Garai, A.; Huo, J. Metal-Organic Framework Growth at Functional Interfaces: Thin Films and Composites for Diverse Applications. *Chem. Soc. Rev.* **2012**, *41* (6), 2344-2381.
27. Li, S.; Huo, F. Metal-Organic Framework Composites: From Fundamentals to Applications. *Nanoscale* **2015**, *7* (17), 7482–7501.
28. Gregory W. Peterson, Matthew A. Browe, Erin M. Durke, Thomas H. Epps, III. Flexible SIS/HKUST-1 Mixed Matrix Composites as Protective Barriers against Chemical Warfare Agent Simulants. *ACS Appl. Mater. Interfaces* **2018**, *10* (49), 43080-43087.
29. Mao, Y. Y.; Li, G. R.; Guo, Y.; Li, Z. P.; Liang, C. D.; Peng, X. S.; Lin, Z. Foldable Interpenetrated Metal-Organic Frameworks/Carbon Nanotubes Thin Film for Lithium-Sulfur Batteries. *Nat. Commun.* **2017**, *8*, 14628.
30. Zhuang, J.-L.; Ar, D.; Yu, X.-J.; Liu, J.-X.; Terfort, A. Patterned Deposition of Metal-Organic Frameworks onto Plastic, Paper, and Textile Substrates by Inkjet Printing of a Precursor Solution. *Adv. Mater.* **2013**, *25* (33), 4631-4635.
31. M. L. Pinto, S. Dias and J. Pires, Composite MOF Foams: The Example of UiO-66/Polyurethane, *ACS Appl. Mater. Interfaces* **2013**, *5* (7), 2360-2363.
32. S. Aguado, J. Canivet and D. Farrusseng, Facile Shaping of an Imidazolate-Based MOF on Ceramic Beads for Adsorption and Catalytic Applications, *Chem. Commun.* **2010**, *46* (42), 7999-8001.
33. Hermes, S.; Schröder, F.; Chelmoski, R.; Wöll, C.; Fischer, R. A. Selective Nucleation and Growth of Metal–Organic Open Framework Thin Films on

- Patterned COOH/CF₃-Terminated Self-Assembled Monolayers on Au (111). *J. Am. Chem. Soc.* **2005**, *127* (40), 13744-13745.
34. Pinto, M. da S.; Augusto Sierra-Avila, C.; Hinestroza, J. P. In Situ Synthesis of A Cu-BTC Metal-Organic Framework (MOF 199) onto Cellulosic Fibrous Substrates: Cotton. *Cellulose* **2012**, *19* (5), 1771-1779.
35. Abbasi, A. R.; Akhbari, K.; Morsali, A. Dense Coating of Surface Mounted Cubtc Metal-Organic Framework Nanostructures on Silk Fibers, Prepared by Layer-By-Layer Method under Ultrasound Irradiation with Antibacterial Activity. *Ultrason. Sonochem.* **2012**, *19* (4), 846-852.
36. Zhao, J.; Lee, D. T.; Yaga, R. W.; Hall, M. G.; Barton, H. F.; Woodward, I. R.; Oldham, C. J.; Walls, H. J.; Peterson, G. W.; Parsons, G. N., Ultra-Fast Degradation of Chemical Warfare Agents Using MOF-Nanofiber Kebabs. *Angew. Chem. Int. Ed.* **2016**, *55* (42), 13224-13228.
37. Kalaj, M.; Denny Jr, M. S.; Bentz, K. C.; Palomba, J. M.; Cohen, S. M., Nylon–MOF Composites through Postsynthetic Polymerization. *Angew. Chem. Int. Ed.* **2019**, *58* (8), 2336-2340.
38. Meilikhov, M.; Yusenko, K.; Schollmeyer, E.; Mayer, C.; Buschmann, H.-J.; Fischer, R. A. Stepwise Deposition of Metal Organic Frameworks on Flexible Synthetic Polymer Surfaces. *Dalton Trans.* **2011**, *40* (18), 4838-4841.
39. Zhao, J.; Losego, M. D.; Lemaire, P. C.; Williams, P. S.; Gong, B.; Atanasov, S. E.; Blevins, T. M.; Oldham, C. J.; Walls, H. J.; Shepherd, S. D.; et al. Highly Adsorptive, MOF-Functionalized Nonwoven Fiber Mats for Hazardous Gas

- Capture Enabled by Atomic Layer Deposition. *Adv. Mater. Interfaces* **2014**, *1* (4), 1400040.
40. Bechelany, M.; Drobek, M.; Vallicari, C.; Chaaya, A. A.; Julbe, A.; Miele, P. Highly Crystalline MOF-Based Materials Grown on Electrospun Nanofibers. *Nanoscale* **2015**, *7* (13), 5794-5802.
41. Zhang, Y.; Yuan, S.; Feng, X.; Li, H.; Zhou, J.; Wang, B. Preparation of Nanofibrous Metal–Organic Framework Filters for Efficient Air Pollution Control. *J. Am. Chem. Soc.* **2016**, *138* (18), 5785-5788.
42. Zhao, J.; Gong, B.; Nunn, W. T.; Lemaire, P. C.; Stevens, E. C.; Sidi, F. I.; Williams, P. S.; Oldham, C. J.; Walls, H. J.; Shepherd, S. D.; et al. Conformal and Highly Adsorptive Metal–Organic Framework Thin Films via Layer-By-Layer Growth on ALD-Coated Fiber Mats. *J. Mater. Chem. A* **2015**, *3* (4), 1458-1464.
43. Zhao, J.; Nunn, W. T.; Lemaire, P. C.; Lin, Y.; Dickey, M. D.; Oldham, C. J.; Walls, H. J.; Peterson, G. W.; Losego, M. D.; Parsons, G. N. Facile Conversion of Hydroxy Double Salts to Metal-Organic Frameworks Using Metal Oxide Particles and Atomic Layer Deposition Thin-Film Templates. *J. Am. Chem. Soc.* **2015**, *137* (43), 13756-13759.
44. Li, Z.; Zhou, G.; Dai, H.; Yang, M.; Fu, Y.; Ying, Y.; Li, Y. Biomimetic Preparation of Hybrid Membranes with Ultra-High Loading of Pristine Metal-Organic Frameworks Grown on Silk Nanofibers for Hazard Collection in Water. *J. Mater. Chem. A* **2018**, *6* (8), 3402-3413.

45. Chen, Y.; Li, S.; Pei, X.; Zhou, J.; Feng, X.; Zhang, S.; Cheng, Y.; Li, H.; Han, R.; Wang, B. A Solvent-Free Hot-Pressing Method for Preparing Metal-Organic-Framework Coatings. *Angew. Chem., Int. Ed.* **2016**, *55* (10), 3419-3423.
46. López-Maya, E.; Montoro, C.; Rodríguez-Albelo, L. M.; Aznar Cervantes, S. D.; Lozano-Pérez, A. A.; Cenís, J. L.; Barea, E.; Navarro, J. A. R. Textile/Metal–Organic-Framework Composites as Self-Detoxifying Filters for Chemical-Warfare Agents. *Angew. Chem. Int. Ed.* **2015**, *54* (23), 6790-6794.
47. Lu, A. X.; McEntee, M.; Browe, M. A.; Hall, M. G.; DeCoste, J. B.; Peterson, G. W., MOFabric: Electrospun Nanofiber Mats from PVDF/UiO-66-NH₂ for Chemical Protection and Decontamination. *ACS Appl. Mater. Inter.* **2017**, *9* (15), 13632-13636.
48. Neufeld, M. J.; Harding, J. L.; Reynolds, M. M. Immobilization of Metal–Organic Framework Copper (II) Benzene-1,3,5-tricarboxylate (CuBTC) onto Cotton Fabric as a Nitric Oxide Release Catalyst. *ACS Appl. Mater. Interfaces* **2015**, *7* (48), 26742-26750.
49. Yu, M.; Li, W. X.; Wang, Z. Q.; Zhang, B. W.; Ma, H. J.; Li, L. F.; Li, J. Y. Covalent Immobilization of Metal-Organic Frameworks onto the Surface of Nylon—a New Approach to the Functionalization and Coloration of Textiles. *Sci. Rep.* **2016**, *6*, 22796.
50. Lee, D. T.; Zhao, J.; Peterson, G. W.; Parsons, G. N., Catalytic “MOF-Cloth” Formed via Directed Supramolecular Assembly of UiO-66-NH₂ Crystals on Atomic Layer Deposition-coated Textiles for Rapid Degradation of Chemical Warfare Agent Simulants. *Chemistry of Materials* **2017**, *29* (11), 4894-4903.

51. Boehringer, B.; Fischer, R.; Lohe, M. R.; Rose, M.; Kaskel, S.; Küsgens, P. *MOF Shaping and Immobilization*; Farrusseng, D., Ed.; Wiley-V C H Verlag GmbH: Weinheim, **2011**.
52. Lee, D.; Zhao, J.; Oldham, C.; Peterson, G.; Parsons, G., UiO-66-NH₂ MOF Nucleation on TiO₂, ZnO, and Al₂O₃ ALD-Treated Polymer Fibers: Role of Metal Oxide on MOF Growth and Catalytic Hydrolysis of Chemical Warfare Agent Simulants. *ACS Appl. Mater. Interfaces* **2017**, *9* (51), 44847-44855.
53. Rose, M.; Boehringer, B.; Jolly, M.; Fischer, R.; Kaskel, S. MOF Processing by Electrospinning for Functional Textiles. *Adv. Eng. Mater.* **2011**, *13* (4), 356-360.
54. Liu, C.; Wu, Y. N.; Morlay, C.; Gu, Y. F.; Gebremariam, B.; Yuan, X.; Li, F. T. General Deposition of Metal-Organic Frameworks on Highly Adaptive Organic-Inorganic Hybrid Electrospun Fibrous Substrates. *ACS Appl. Mater. Interfaces* **2016**, *8* (4), 2552–2561.
55. Reboul, J.; Furukawa, S.; Horike, N.; Tsotsalas, M.; Hirai, K.; Uehara, H.; Kondo, M.; Louvain, N.; Sakata, O.; Kitagawa, S. Mesoscopic Architectures of Porous Coordination Polymers Fabricated by Pseudomorphic Replication. *Nat. Mater.* **2012**, *11*, 717-723.
56. Nakahama, M.; Reboul, J.; Kamei, K.-i.; Kitagawa, S.; Furukawa, S. Fibrous Architectures of Porous Coordination Polymers-Alumina Composites Fabricated by Coordination Replication *Chem. Lett.* **2014**, *43* (7), 1052-1054.
57. Majano, G.; Pérez-Ramírez, J. Scalable Room-Temperature Conversion of Copper (II) Hydroxide into HKUST-1 (Cu₃(btc)₂). *Adv. Mater.* **2013**, *25* (7), 1052- 1057.

58. Okada, K.; Ricco, R.; Tokudome, Y.; Styles, M. J.; Hill, A. J.; Takahashi, M.; Falcaro, P. Copper Conversion into Cu(OH)₂ Nanotubes for Positioning Cu₃(BTC)₂ MOF Crystals: Controlling the Growth on Flat Plates, 3D Architectures, and as Patterns *Adv. Funct. Mater.* **2014**, *24* (14), 1969-1977.
59. Stavila, V.; Volponi, J.; Katzenmeyer, A. M.; Dixon, M. C.; Allendorf, M. D. Kinetics and Mechanism of Metal-Organic Framework Thin Film Growth: Systematic Investigation of HKUST-1 Deposition on QCM Electrodes. *Chem. Sci.* **2012**, *3* (5), 1531-1540.
60. Lemaire, P. C.; Zhao, J. J.; Williams, P. S.; Walls, H. J.; Shepherd, S. D.; Losego, M. D.; Peterson, G. W.; Parsons, G. N. Copper Benzenetricarboxylate Metal-Organic Framework Nucleation Mechanisms on Metal Oxide Powders and Thin Films Formed by Atomic Layer Deposition. *ACS Appl. Mater. Interfaces* **2016**, *8*, 9514–9522.
61. Khanjani, S.; Morsali, A. Ultrasound-Promoted Coating Of MOF-5 on Silk Fiber and Study of Adsorptive Removal and Recovery of Hazardous Anionic Dye “Congo Red.” *Ultrason. Sonochem.* **2014**, *21* (4), 1424-1429.
62. Biemmi, E.; Scherb, C.; Bein, T. Oriented Growth of the Metal Organic Framework Cu₃(BTC)₂(H₂O)₃·xH₂O Tunable with Functionalized Self-Assembled Monolayers *J. Am. Chem. Soc.* **2007**, *129* (26), 8054-8055.
63. Li, P.; Li, J.; Feng, X.; Li, J.; Hao, Y.; Zhang, J.; Wang, H.; Yin, A.; Zhou, J.; Ma, X.; Wang, B. Metal-Organic Frameworks with Photocatalytic Bactericidal Activity for Integrated Air Cleaning. *Nat. Commun.* **2019**, *10*, 2177.

64. Chen, Y.; Zhang, S.; Cao, S.; Li, S.; Chen, F.; Yuan, S.; Xu, C.; Zhou, J.; Feng, X.; Ma, X.; Wang, B. Roll-to-Roll Production of Metal-Organic Framework Coatings for Particulate Matter Removal. *Adv. Mater.* **2017**, *29*, 1606221.
65. Ma, X.; Chai, Y.; Li, P.; Wang, B. Metal–Organic Framework Films and Their Potential Applications in Environmental Pollution Control. *Acc. Chem. Res.* **2019**, *52*, 1461–1470.
66. Zhuang, J.-L.; Ceglarek, D.; Pethuraj, S.; Terfort, A. Rapid Room-Temperature Synthesis of Metal–Organic Framework HKUST-1 Crystals in Bulk and as Oriented and Patterned Thin Films. *Adv. Funct. Mater.* **2011**, *21* (8), 1442-1447.
67. Ameloot, R.; Gobechiya, E.; Uji-i, H.; Martens, J. A.; Hofkens, J.; Alaerts, L.; Sels, B. F.; De Vos, D. E. Direct Patterning of Oriented Metal-Organic Framework Crystals via Control over Crystallization Kinetics in Clear Precursor Solutions. *Adv. Mater.* **2010**, *22* (24), 2685-2688.
68. Wang, H.; Rassu, P.; Wang, X.; Li, H.; Wang, X.; Wang, X.; Feng, X.; Yin, A.; Li, P.; Jin, X.; Chen, S.-L.; Ma, X.; Wang, B. An Iron-Containing Metal–Organic Framework as a Highly Efficient Catalyst for Ozone Decomposition. *Angew. Chem., Int. Ed.* **2018**, *57*, 16416-16420.
69. Plonka, A. M.; Wang, Q.; Gordon, W. O.; Balboa, A.; Troya, D.; Guo, W.; Sharp, C. H.; Senanayake, S. D.; Morris, J. R.; Hill, C. L.; et al. In situ Probes of Capture and Decomposition of Chemical Warfare Agent Simulants by Zr-based Metal Organic Frameworks. *J. Am. Chem. Soc.* **2017**, *139* (2), 599–602.
70. Mondloch, J. E.; Katz, M. J.; Isley III, W. C.; Ghosh, P.; Liao, P.; Bury, W.; Wagner, G. W.; Hall, M. G.; DeCoste, J. B.; Peterson, G. W., Destruction of

- Chemical Warfare Agents Using Metal–Organic Frameworks. *Nat. Mater.* **2015**, *14* (5), 512.
71. Katz, M. J.; Mondloch, J. E.; Totten, R. K.; Park, J. K.; Nguyen, S. T.; Farha, O. K.; Hupp, J. T., Simple and Compelling Biomimetic Metal–Organic Framework Catalyst for the Degradation of Nerve Agent Simulants. *Angew. Chem. Int. Ed.* **2014**, *53* (2), 497-501.
72. Peterson, G. W.; Moon, S.-Y.; Wagner, G. W.; Hall, M. G.; DeCoste, J. B.; Hupp, J. T.; Farha, O. K., Tailoring the Pore Size and Functionality of UiO-type Metal–Organic Frameworks for Optimal Nerve Agent Destruction. *Inorg. Chem.* **2015**, *54* (20), 9684-9686.
73. Zhu, H.; Ka, B.; Murad, F. Nitric Oxide Accelerates the Recovery from Burn Wounds *World J. Surg.* **2007**, *31* (4) 624-631.
74. Wu, Y.; Zhou, Z.; Meyerhoff, M. E. In vitro Platelet Adhesion on Polymeric Surfaces with Varying Fluxes of Continuous Nitric Oxide Release. *J. Biomed. Mater. Res., Part A* **2007**, *81* (4) 956-963.
75. Al-Sa'doni, H. H.; Ferro, A. S-Nitrosothiols as Nitric Oxide-Donors: Chemistry, Biology and Possible Future Therapeutic Applications. *Curr. Med. Chem.* **2004**, *11* (20) 2679-2690.
76. Harding, J. L.; Reynolds, M. M. Metal Organic Frameworks as Nitric Oxide Catalysts. *J. Am. Chem. Soc.* **2012**, *134* (7), 3330-3333.
77. Ahmed, I.; Jhung, S. H., Composites of Metal–Organic Frameworks: Preparation and Application in Adsorption. *Mater. Today* **2014**, *17*, 136-146.

78. Liu, J.; Wöll, C., Surface-Supported Metal–Organic Framework Thin Films: Fabrication Methods, Applications, and Challenges. *Chem. Soc. Rev.* **2017**, *46*, 5730-5770.
79. Falcaro, P.; Ricco, R.; Doherty, C. M.; Liang, K.; Hill, A. J.; Styles, M. J., MOF Positioning Technology and Device Fabrication. *Chem. Soc. Rev.* **2014**, *43*, 5513-5560.
80. Schelling, M.; Kim, M.; Otal, E.; Hinestroza, J., Decoration of Cotton Fibers with a Water-Stable Metal–Organic Framework (UiO-66) for the Decomposition and Enhanced Adsorption of Micropollutants in Water. *Bioengineering* **2018**, *5*, 14.
81. Bunge, M. A.; Davis, A. B.; West, K. N.; West, C. W.; Glover, T. G., Synthesis and Characterization of UiO-66-NH₂ Metal–Organic Framework Cotton Composite Textiles. *Ind. Eng. Chem. Res.* **2018**, *57* (28), 9151-9161.
82. Guo, H.; Zhu, G.; Hewitt, I. J.; Qiu, S., “Twin Copper Source” Growth of Metal–Organic Framework Membrane: Cu₃(BTC)₂ with High Permeability and Selectivity for Recycling H₂. *J. Am. Chem. Soc.* **2009**, *131*, 1646-1647.
83. Kang, Z.; Xue, M.; Fan, L.; Huang, L.; Guo, L.; Wei, G.; Chen, B.; Qiu, S., Highly Selective Sieving of Small Gas Molecules by Using an Ultra-microporous Metal–Organic Framework Membrane. *Energy Environ. Sci.* **2014**, *7*, 4053-4060.
84. Park, S.-H.; Kim, H. J., Unidirectionally Aligned Copper Hydroxide Crystalline Nanorods from Two-dimensional Copper Hydroxy Nitrate. *J. Am. Chem. Soc.* **2004**, *126*, 14368-14369.

85. Campagnol, N.; Van Assche, T. R.; Li, M.; Stappers, L.; Dincă, M.; Denayer, J. F.; Binnemans, K.; De Vos, D. E.; Fransaer, J., On the Electrochemical Deposition of Metal–Organic Frameworks. *J. Mater. Chem. A* **2016**, *4*, 3914-3925.
86. Ameloot, R.; Vermoortele, F.; Vanhove, W.; Roeffaers, M. B.; Sels, B. F.; De Vos, D. E., Interfacial Synthesis of Hollow Metal–Organic Framework Capsules Demonstrating Selective Permeability. *Nat. Chem.* **2011**, *3*, 382-387.
87. Zhan, W.; Kuang, Q.; Zhou, J.; Kong, X.; Xie, Z.; Zheng, L., Semiconductor@Metal–Organic Framework Core–Shell Heterostructures: A Case of ZnO@ZIF-8 Nanorods with Selective Photoelectrochemical Response. *J. Am. Chem. Soc.* **2013**, *135*, 1926-1933.
88. Khaletskaya, K.; Reboul, J.; Meilikhov, M.; Nakahama, M.; Diring, S. p.; Tsujimoto, M.; Isoda, S.; Kim, F.; Kamei, K.-i.; Fischer, R. A., Integration of Porous Coordination Polymers and Gold Nanorods into Core–Shell Mesoscopic Composites toward Light-Induced Molecular Release. *J. Am. Chem. Soc.* **2013**, *135*, 10998-11005.
89. Falcaro, P.; Okada, K.; Hara, T.; Ikigaki, K.; Tokudome, Y.; Thornton, A. W.; Hill, A. J.; Williams, T.; Doonan, C.; Takahashi, M., Centimetre-scale Micropore Alignment in Oriented Polycrystalline Metal–Organic Framework Films via Heteroepitaxial Growth. *Nat. Mater.* **2017**, *16*, 342-348.
90. Puthiaraj, P.; Suresh, P.; Pitchumani, K. J., Aerobic Homocoupling of Arylboronic Acids Catalysed by Copper Terephthalate Metal–Organic Frameworks. *Green Chem.* **2014**, *16*, 2865-2875.

91. Schlur, L.; Carton, A.; Pourroy, G., A New Zinc Hydroxy Acetate Hydrogen Carbonate Lamellar Phase for Growing Large and Clean ZnO Nanorod Arrays. *Chem. Comm.* **2015**, *51*, 3367-3370.
92. Kandare, E.; Hossenlopp, J. M., Hydroxy Double Salt Anion Exchange Kinetics: Effects of Precursor Structure and Anion Size. *J. Phys. Chem. B* **2005**, *109* (17), 8469-8475.
93. Hu, Y.; Kazemian, H.; Rohani, S.; Huang, Y.; Song, Y., In Situ High Pressure Study of ZIF-8 by FTIR Spectroscopy. *Chem. Comm.* **2011**, *47*, 12694-12696.
94. Xu, R.; Zeng, H. C., Dimensional Control of Cobalt-hydroxide-carbonate Nanorods and Their Thermal Conversion to One-Dimensional Arrays of Co₃O₄ Nanoparticles. *J. Phys. Chem. B* **2003**, *107*, 12643-12649.
95. Cychoz, K. A.; Wong-Foy, A. G.; Matzger, A. J., Liquid Phase Adsorption by Microporous Coordination Polymers: Removal of Organosulfur Compounds. *J. Am. Chem. Soc.* **2008**, *130*, 6938-6939.
96. Cychoz, K. A.; Wong-Foy, A. G.; Matzger, A. J., Enabling Cleaner Fuels: Desulfurization by Adsorption to Microporous Coordination Polymers. *J. Am. Chem. Soc.* **2009**, *131*, 14538-14543.
97. Peterson, G. W.; DeCoste, J. B.; Fatollahi-Fard, F.; Britt, D. K., Engineering UiO-66-NH₂ for Toxic Gas Removal. *Ind. Eng. Chem. Res.* **2014**, *53*, 701-707.
98. Rieth, A. J.; Dincă, M., Controlled Gas Uptake in Metal–Organic Frameworks with Record Ammonia Sorption. *J. Am. Chem. Soc.* **2018**, *140*, 3461-3466.

99. Colovic, M. B.; Krstic, D. Z.; Lazarevic-Pasti, T. D.; Bondzic, A. M.; Vasic, V. M., Acetylcholinesterase Inhibitors: Pharmacology and Toxicology. *Curr. Neuropharmacol.* **2013**, *11* (3), 315-335.
100. Mercey, G.; Verdelet, T.; Renou, J.; Kliachyna, M.; Baati, R.; Nachon, F.; Jean, L.; Renard, P.-Y., Reactivators of Acetylcholinesterase Inhibited by Organophosphorus Nerve Agents. *Acc. Chem. Res.* **2012**, *45* (5), 756-766.
101. Yang, Y.-C., Chemical Detoxification of Nerve Agent VX. *Acc. Chem. Res.* **1999**, *32* (2), 109-115.
102. Dong, J.; Hu, J.; Chi, Y.; Lin, Z.; Zou, B.; Yang, S.; Hill, C. L.; Hu, C., A Polyoxoniobate–Polyoxovanadate Double-Anion Catalyst for Simultaneous Oxidative and Hydrolytic Decontamination of Chemical Warfare Agent Simulants. *Angew. Chem. Int. Ed.* **2017**, *56* (16), 4473-4477.
103. Trickett, C. A.; Popp, T. M. O.; Su, J.; Yan, C.; Weisberg, J.; Huq, A.; Urban, P.; Jiang, J.; Kalmutzki, M. J.; Liu, Q., Identification of the Strong Brønsted Acid Site in a Metal–Organic Framework Solid Acid Catalyst. *Nat. Chem.* **2019**, *11* (2), 170.
104. Meng, L.; Cheng, Q.; Kim, C.; Gao, W. Y.; Wojtas, L.; Chen, Y. S.; Zaworotko, M. J.; Zhang, X. P.; Ma, S., Crystal Engineering of a Microporous, Catalytically Active fcu Topology MOF Using a Custom-Designed Metalloporphyrin Linker. *Angew. Chem. Int. Ed.* **2012**, *51* (40), 10082-10085.
105. Zhou, H.-C.; Long, J. R.; Yaghi, O. M., Introduction to Metal–Organic Frameworks. *Chem. Rev.* **2012**, *112*(2), 673-674
106. Diercks, C. S.; Liu, Y.; Cordova, K. E.; Yaghi, O. M., The Role of Reticular Chemistry in the Design of CO₂ Reduction Catalysts. *Nat. Mater.* **2018**, *17* (4), 301.

107. Cho, K. Y.; Seo, J. Y.; Kim, H.-J.; Pai, S. J.; Do, X. H.; Yoon, H. G.; Hwang, S. S.; Han, S. S.; Baek, K.-Y., Facile Control of Defect Site Density and Particle Size of UiO-66 for Enhanced Hydrolysis Rates: Insights into Feasibility of Zr (IV)-based Metal-Organic Framework (MOF) Catalysts. *Appl. Catal., B-Environ.* **2019**, *245*, 635-647.
108. Islamoglu, T.; Ortuño, M. A.; Prousaloglou, E.; Howarth, A. J.; Vermeulen, N. A.; Atilgan, A.; Asiri, A. M.; Cramer, C. J.; Farha, O. K., Presence versus Proximity: the Role of Pendant Amines in the Catalytic Hydrolysis of a Nerve Agent Simulant. *Angew. Chem. Int. Ed.* **2018**, *57* (7), 1949-1953.
109. Katz, M. J.; Moon, S.-Y.; Mondloch, J. E.; Beyzavi, M. H.; Stephenson, C. J.; Hupp, J. T.; Farha, O. K., Exploiting Parameter Space in MOFs: a 20-fold Enhancement of Phosphate-ester Hydrolysis with UiO-66-NH₂. *Chem. Sci.* **2015**, *6* (4), 2286-2291.
110. Moon, S. Y.; Liu, Y.; Hupp, J. T.; Farha, O. K., Instantaneous Hydrolysis of Nerve-Agent Simulants with a Six-Connected Zirconium-Based Metal–Organic Framework. *Angew. Chem. Int. Ed.* **2015**, *54* (23), 6795-6799.
111. Dwyer, D. B.; Dugan, N.; Hoffman, N.; Cooke, D. J.; Hall, M. G.; Tovar, T. M.; Bernier, W. E.; DeCoste, J.; Pomerantz, N. L.; Jones Jr, W. E., Chemical Protective Textiles of UiO-66-Integrated PVDF Composite Fibers with Rapid Heterogeneous Decontamination of Toxic Organophosphates. *ACS Appl. Mater. Inter.* **2018**, *10* (40), 34585-34591.

112. Furukawa, H.; Gándara, F.; Zhang, Y.-B.; Jiang, J.; Queen, W. L.; Hudson, M. R.; Yaghi, O. M., Water Adsorption in Porous Metal–Organic Frameworks and Related Materials. *J. Am. Chem. Soc.* **2014**, *136* (11), 4369-4381.
113. de Koning, M. C.; van Grol, M.; Breijaert, T., Degradation of Paraoxon and the Chemical Warfare Agents VX, Tabun, and Soman by the Metal–Organic Frameworks UiO-66-NH₂, MOF-808, NU-1000, and PCN-777. *Inorg. Chem.* **2017**, *56* (19), 11804-11809.
114. Liu, X.; Wang, C.; Wang, B.; Li, K., Novel Organic-Dehydration Membranes Prepared from Zirconium Metal-Organic Frameworks. *Adv. Funct. Mater.* **2017**, *27* (3), 1604311.
115. Morris, W.; Wang, S.; Cho, D.; Auyeung, E.; Li, P.; Farha, O. K.; Mirkin, C. A., Role of Modulators in Controlling the Colloidal Stability and Polydispersity of the UiO-66 Metal–Organic Framework. *ACS Appl. Mater. Inter.* **2017**, *9* (39), 33413-33418.
116. Cliffe, M. J.; Wan, W.; Zou, X.; Chater, P. A.; Kleppe, A. K.; Tucker, M. G.; Wilhelm, H.; Funnell, N. P.; Coudert, F.-X.; Goodwin, A. L., Correlated Defect Nanoregions in a Metal–Organic Framework. *Nat. Commun.* **2014**, *5*, 4176.
117. Liu, L.; Chen, Z.; Wang, J.; Zhang, D.; Zhu, Y.; Ling, S.; Huang, K.; Belmabkhout, Y.; Adil, K.; Zhang, Y., Imaging Defects and their Evolution in a Metal-Organic Framework at Sub-unit-cell Resolution. *Nat. Chem.* **2019**, *11*, 622.
118. Li, K.; Lin, S.; Li, Y.; Zhuang, Q.; Gu, J., Aqueous-Phase Synthesis of Mesoporous Zr-Based MOFs Templated by Amphoteric Surfactants. *Angew. Chem. Int. Ed.* **2018**, *130* (13), 3497-3501.

119. The composite with lower loadings had a thinner MOF coating on the fiber while the composite with higher loading had a thicker MOF coating on the fiber. Since the same amount of MOF-808 was used in all catalytic tests (normalized based on Zr amount in the composite), the composite with thinner layer had more surface particles. The results showed that the thinner the MOF layer, the faster the catalytic activity since accessibility to the MOF crystals in the innerlayers is controlled by the diffusion of the simulant.
120. Matito-Martos, I.; Moghadam, P. Z.; Li, A.; Colombo, V.; Navarro, J. A.; Calero, S.; Fairen-Jimenez, D., Discovery of an Optimal Porous Crystalline Material for the Capture of Chemical Warfare Agents. *Chem. Mater.* **2018**, *30* (14), 4571-4579.
121. Peterson, G. W.; Lu, A. X.; Hall, M. G.; Browe, M. A.; Tovar, T.; Epps III, T. H., MOFwich: Sandwiched Metal–Organic Framework-Containing Mixed Matrix Composites for Chemical Warfare Agent Removal. *ACS Appl. Mater. Inter.* **2018**, *10* (8), 6820-6824.
122. Montoro, C.; Linares, F.; Quartapelle Procopio, E.; Senkovska, I.; Kaskel, S.; Galli, S.; Masciocchi, N.; Barea, E.; Navarro, J. A., Capture of Nerve Agents and Mustard Gas Analogues by Hydrophobic Robust MOF-5 type Metal–Organic Frameworks. *J. Am. Chem. Soc.* **2011**, *133* (31), 11888-11891.
123. ASTM F739-12, Standard Test Method for Permeation of Liquids and Gases through Protective Clothing Materials under Conditions of Continuous Contact, ASTM International, West Conshohocken, PA, **2012**, www.astm.org. DOI: 10.1520/F0739-12, accessed 9 July 2019.

124. Raushel, F. M. Chemical biology: Catalytic detoxification. *Nature* **2011**, 469, 310-311.
125. OPCW Issues Fact-Finding Mission Report on Chemical Weapons Use Allegation in Douma, Syria, in **2018**, Organisation for the Prohibition of Chemical Weapons, March 1, **2019**.
126. Yang, Y. C.; Baker, J. A.; Ward, J. R. Decontamination of Chemical Warfare Agents. *Chem. Rev.* **1992**, 92 (8), 1729-1743.
127. Marrs, T. T.; Maynard, R. L.; Sidell, F., Chemical Warfare Agents: Toxicology and Treatment. John Wiley & Sons: **2007**.
128. Rieth, A. J.; Yang, S.; Wang, E. N.; Dincă, M. Record Atmospheric Fresh Water Capture and Heat Transfer with A Material Operating at the Water Uptake Reversibility Limit. *ACS Cent. Sci.* **2017**, 3 (6), 668-672.
129. Wang, S.; Lee, J. S.; Wahiduzzaman, M.; Park, J.; Muschi, M.; Martineau-Corcoss, C.; Tissot, A.; Cho, K. H.; Marrot, J.; Shepard, W.; Maurin, G.; Chang, J.-S.; Serre, C. A Robust Large-Pore Zirconium Carboxylate Metal–Organic Framework For Energy-Efficient Water-Sorption-Driven Refrigeration. *Nat. Energy* **2018**, 3, 985-993.
130. Towsif Abtab, S. M.; Alezi, D.; Bhatt, P. M.; Shkurenko, A.; Belmabkhout, Y.; Aggarwal, H.; Weseliński, Ł. J.; Alsadun, N.; Samin, U.; Hedhili, M. N.; Eddaoudi, M. Reticular Chemistry in Action: A Hydrolytically Stable MOF Capturing Twice Its Weight in Adsorbed Water. *Chem* **2018**, 4 (1), 94-105.

131. Chen, Z.; Li, P.; Zhang, X.; Li, P.; Wasson, M. C.; Islamoglu, T.; Stoddart, J. F.; Farha, O. K. Reticular Access to Highly Porous acs-Mofs with Rigid Trigonal Prismatic Linkers for Water Sorption. *J. Am. Chem. Soc.* **2019**, *141* (7), 2900-2905.
132. Islamoglu, T.; Otake, K.-i.; Li, P.; Buru, C. T.; Peters, A. W.; Akpınar, I.; Garibay, S. J.; Farha, O. K. Revisiting the Structural Homogeneity Of NU-1000, a Zr-Based Metal–Organic Framework. *CrystEngComm* **2018**, *20* (39), 5913-5918.
133. Islamoglu, T.; Ray, D.; Li, P.; Majewski, M. B.; Akpınar, I.; Zhang, X.; Cramer, C. J.; Gagliardi, L.; Farha, O. K. From Transition Metals to Lanthanides to Actinides: Metal-Mediated Tuning of Electronic Properties of Isostructural Metal–Organic Frameworks. *Inorg. Chem.* **2018**, *57* (21), 13246-13251.
134. Islamoglu, T.; Ortuño, M. A.; Proussaloglou, E.; Howarth, A. J.; Vermeulen, N. A.; Atilgan, A.; Asiri, A. M.; Cramer, C. J.; Farha, O. K. Presence Versus Proximity: The Role Of Pendant Amines in The Catalytic Hydrolysis of a Nerve Agent Simulant. *Angew. Chem. Int. Ed.* **2018**, *57* (7), 1949-1953
135. Drout, R. J.; Howarth, A. J.; Otake, K.-i.; Islamoglu, T.; Farha, O. K. Efficient Extraction of Inorganic Selenium from Water by a Zr Metal–Organic Framework: Investigation of Volumetric Uptake Capacity and Binding Motifs. *CrystEngComm* **2018**, *20* (40), 6140-6145.
136. Jiang, J.; Gándara, F.; Zhang, Y.-B.; Na, K.; Yaghi, O. M.; Klemperer, W. G. Superacidity in Sulfated Metal–Organic Framework-808. *J. Am. Chem. Soc.* **2013**, *136* (37), 12844-12847.
137. Moon, S.-Y.; Proussaloglou, E.; Peterson, G. W.; DeCoste, J. B.; Hall, M. G.; Howarth, A. J.; Hupp, J. T.; Farha, O. K. Detoxification of Chemical Warfare

- Agents Using a Zr₆-Based Metal–Organic Framework/Polymer Mixture. *Chem. Eur. J.* **2016**, *22* (42), 14864-14868.
138. Chen, Z.; Islamoglu, T.; Farha, O. K. Toward Base Heterogenization: A Zirconium Metal–Organic Framework/Dendrimer or Polymer Mixture for Rapid Hydrolysis of a Nerve-Agent Simulant. *ACS Appl. Nano Mater.* **2019**, *2* (2), 1005-1008.
139. Lu, Y.; Sathasivam, S.; Song, J.; Crick, C. R.; Carmalt, C. J.; Parkin, I. P. Robust Self-Cleaning Surfaces That Function When Exposed to Either Air or Oil. *Science* **2015**, *347* (6226), 1132.
140. Ma, K.; Islamoglu, T.; Chen, Z.; Li, P.; Wasson, M. C.; Chen, Y.; Wang, Y.; Peterson, G. W.; Xin, J. H.; Farha, O. K. Scalable and Template-Free Aqueous Synthesis of Zirconium-Based Metal–Organic Framework Coating on Textile Fiber. *J. Am. Chem. Soc.* **2019**, *141* (39), 15626-15633.
141. Wang, H.; Mahle, J. J.; Tovar, T. M.; Peterson, G. W.; Hall, M. G.; DeCoste, J. B.; Buchanan, J. H.; Karwacki, C. J. Solid-Phase Detoxification of Chemical Warfare Agents Using Zirconium-Based Metal Organic Frameworks and The Moisture Effects: Analyze Via Digestion. *ACS Appl. Mater. Interfaces* **2019**, *11* (23), 21109-21116.